Experimental Modelling of Surface Roughness and Dynamic Friction Coefficient of Diamond Like Carbon Coated Shafts

By

Sergio Mordo

Thesis submitted in partial fulfilment of the requirements for the degree of

Master of Applied Science

in

Automotive Engineering

Faculty of Engineering and Applied Science

University of Ontario Institute of Technology

December, 2013

Abstract

Companies that coat their products with DLC often have strict surface roughness and friction coefficient goals. This research investigates the surface roughness and friction coefficient properties of uncoated and DLC coated specimens in an effort to satisfy two particular requirements of the industry.

The first requirement is to know what uncoated surface roughness is needed to obtain a certain DLC coated surface roughness. Therefore, a model describing the relationship between uncoated and DLC coated surface roughness is needed. If this relationship can be estimated, the cost of surface finishing can be minimized by avoiding any unnecessary processes.

The second requirement is to know what uncoated surface roughness is needed to reach a specific friction coefficient after the DLC coating process. Therefore, a model describing the relationship between uncoated surface roughness and DLC coated friction coefficient is needed. This will also help minimize surface finishing costs.

This research focuses on DLC coating of steel. A total of 7, 1045 steel specimens were tested before and after coating process with a non-contact surface roughness measurement microscope and a specifically designed and built friction measurement machine.

An experimental methodology was described for applying the findings to other coating methods and materials as the mathematical relationships found in this study are specific to the coating process and materials used.

Keywords: Diamond Like Carbon Coating, Surface Roughness, Friction Coefficient

Acknowledgements

Firstly, I would like to express my sincere gratitude to my advisor Dr. Ahmad Barari. From the days as his student in my undergraduate years to doing research with him in my graduate years, he has always been supportive and understanding, motivating me to do better and better each day.

Furthermore, I would also like to thank Dr. Valery Popravko for showing me all there is to know about diamond like carbon coating technology and letting me work in his facility to combine theoretical knowledge with hands on experience. His extensive knowledge and help made this research possible. All the coating processes were conducted based on the optimized procedures available at Intellectual Alliance Inc. and were completed at their facility in Concord, Ontario.

Also, I would like to thank my friends, especially Mert, along with members of Limoneka and my girlfriend Carolina for encouraging me to do better.

Furthermore, I would like to thank my uncle Yonti, for instilling a love of cars in me and starting this journey along with my aunt Julia for believing in me and supporting me.

I would also like to thank my cousins Miriam and Rifat for making it possible for me to be where I am today and friends Ida and Roger for all the help.

Most importantly, I would like to thank my parents Aleksandro and Meri. The education they gave me is much more precious than anything I can learn by studying. I would also like to thank my brother Aldo, his wife Emel and my nephew Semi, for always supporting me. Finally, I would like to thank my grandpa, for being an inspiration.

Table of Contents

List of Figures

List of Tables

Notations

a_0	Constant parameter for Brenner potential
B	Constant based on experiment
B_{ij}	Many-body coupling
$\bar{B}_{ij}$	Empirical bond order function
c	First order constant
c_0	Constant parameter for Brenner potential
d	Diameter (m)
d_0	Constant parameter for Brenner potential
D_{ij}	Constant parameter for Brenner potential
F_{ext}	External force
F_f	Tangential Friction Force (N)
G_c	Function that describes angles between bonds i-j and i-k
i	Atom number i
i	Cycle number
I	Current (Amp)
I_0	Current usage during free rotation
I_{load}	Current usage during rotation with load applied
j	Atom number j
k	Point that reading is taken
N	Normal force (N)
N	Total number of free sites
N_c	Number of sites on the surface that have bonded with absorbate

$N_i^{(C)}$	Number of carbon atoms bonded to atom i
$N_i^{(H)}$	Number of hydrogen atoms bonded to atom i
$N_i^{(t)}$	Total number of neighbours of atom i or j
p	Constant that depends on the specimen used
p_0	Specific attractive force
P	Power (W)
P_0	Power usage during free rotation (W)
P_f	Power lost to friction from the normal force being applied (W)
P_{tot}	Total power usage during rotation with load applied (W)
r	Constant parameter for Lennard-Jones potential
r	Constant parameter for Brenner potential
r_{ij}	Constant parameter for Brenner potential
R_{ij}	Constant parameter for Brenner potential
S	Contact area of two surfaces
S_a	Average surface roughness
S_q	Root mean square roughness
S_{sk}	Skewness
S_{ku}	Kurtosis
S_v	Valley depth
S_p	Peak height
S_t	Total roughness
S_z	Averaged total roughness
S_{ij}	Constant parameter for Brenner potential
t	Time

T	Torque (Nm)
T_f	Friction torque due to the normal force being applied (Nm)
V	Voltage (V)
V_A	Attractive interaction
V_R	Repulsive interaction
$\nabla_n V_s$	Gradient of the surface potential
α	Constant based on experiment
β_{ij}	Constant parameter for Brenner potential
ε	Constant parameter for Lennard-Jones potential
μ	Friction coefficient
μ_{mech}	Friction due to mechanical effects
$\mu_{mol,1}$	Friction due to interatomic interactions
$\mu_{mol,2}$	Friction due to molecular effects
ϕ_{LJ}	Lennard-Jones potential
σ	Custom parameter for Lennard-Jones potential
θ	Fractional coverage of absorbate
ω	Angular speed (rad/s)

Abbreviations

a-C	Amorphous Carbon
a-C:F	Flourinated Amorphous Carbon
a-C:H	Hydrogenated Amorphous Carbon
a-C:N	Amorphous Carbon Nitride
AFM	Atomic Force Microscopy
CF	Coated Friction Coefficient
CR	Coated Surface Roughness
CVD	Chemical Vapor Diposition
DBD	Dialectric Barier Discharge
DLC	Diamond like Carbon
PCAD	Pulsed Cathodic Arc Deposition
PDF	Probability Density Function
RPM	Revolutions per Minute
RRE	Roughness Reduction Efficiency
ta-C	Tetrahedral Amorphous Carbon
ta-C-H	Hydrogenated Tetrahedral Amorphous Carbon
UF	Uncoated Friction Coefficient
UR	Uncoated Surface Roughness

Chapter 1: Introduction

Coatings are thin films applied to a surface to improve its chemical, mechanical or aesthetic properties. (Athey, 2010) This research focuses on improvement of mechanical properties, in particular, friction coefficient and surface roughness. In general, coatings can be categorized as soft coatings and hard coatings. Soft coatings are polymers and soft metals that have relatively low friction coefficient but can wear easily. On the other hand, hard coatings are ceramics, carbides, nitrides and other similar materials which have high wear resistance but usually have high friction coefficient.

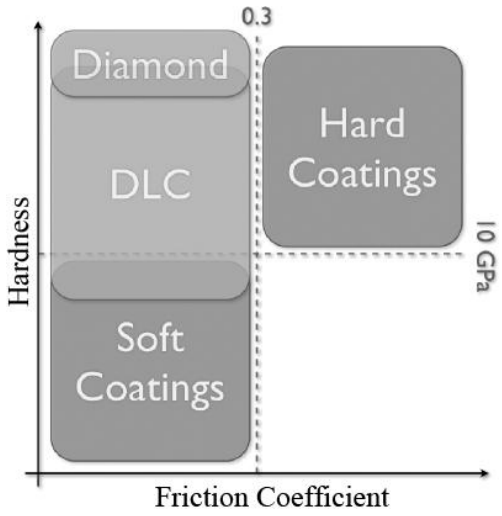

Figure 1-1: Hardness and friction coefficient of different types of coatings (Fontaine, Donnet & Erdemir, 2008)

In this research, the mechanical properties, specifically friction coefficient and surface roughness, of diamond like carbon (DLC) coatings are studied. Diamond like carbon combines mechanical properties of both soft and hard coatings. DLC is a thin film made from amorphous carbon with high concentration of sp3 carbon bonds. This type of

coating has many applications due to its surface properties such as low friction coefficient and roughness, high hardness and chemical inertness produced in manufactured parts. Various types of DLC coatings exist that are created by different methods and materials in order to achieve different tribological properties. These types include amorphous carbon (a-C), hydrogenated amorphous carbon (a-C:H), amorphous carbon nitride (a-C:N), fluorinated amorphous carbon (a-C:F), tetrahedral amorphous carbon (ta-C), hydrogenated tetrahedral amorphous carbon (ta-C:H) and some other more specialized varieties and alloys. These films are usually made by deposition of highly energetic ions onto the surface of a work piece. Some deposition methods are magnetron sputtering, chemical vapour deposition (CVD), physical vapour deposition (PVD), dielectric barrier discharge (DBD), and pulsed cathodic arc discharge (PCAD). Figure 1-2 shows the phase diagram of C-H systems which describes the sp3, sp2 and H content on some coatings. The mechanical Young's modulus and hardness of DLC coatings mostly depend on the C-C sp3 bonds as the C-C sp2 bonds have very minimal effect and C-H bonds are not a strong part of the network as they weaker bonds compared to C-C bonds.

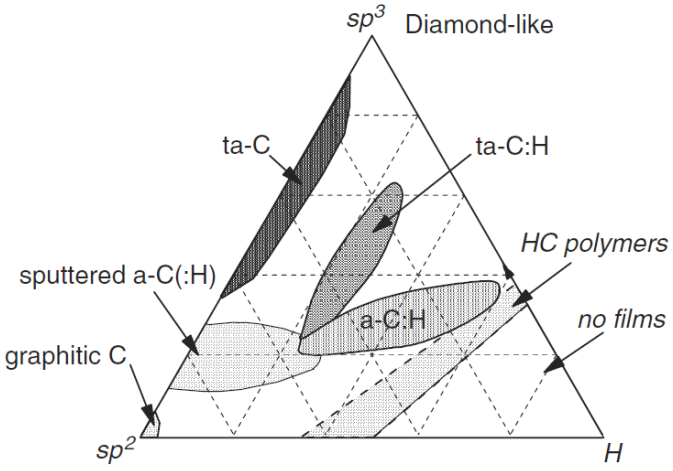

Figure 1-2: Ternary phase diagram of C-H system (Robertson, 2008)

DLC coating has many properties that can be used for different applications; however, this research focuses more on surface roughness and friction coefficient aspects. There is a big industrial demand for improving surface roughness and friction coefficient on a wide variety of parts and components.

For cutting, milling and punching tools that are used for cutting aluminium alloys, graphite, printed circuit boards (PCB), and plastics or punching through steel sheets DLC coating increases hardness and wear resistance which increases tool life. Longer tool life result is desired for the manufacturing processes due to saving in tool cost and the required tool set up times. Also, DLC decreases friction coefficient and roughness of the coated surface on the cutting tools, requiring less lubricant fluid and lower operation temperatures. Due to this property the quality of the machined surface is also increased.

For cold rolling tools, many common problems such as galling on mating surfaces, rolled-in scale, mill-sharing, scrubs and slivers are eliminated, resulting in better quality of end product. The maintenance interval is also increased, reducing costs.

DLC is also highly suitable for the flow control devices, check and stop valves used in oil and gas industries. By reduced roughness and friction coefficient, mating parts have trouble-free operations, without the problem of adhesion of mating parts. Also DLC creates corrosion and chemical resistance due to inert surfaces.

For dies, molds and extruders that are coated with DLC, due to low friction and roughness, molds operate smoothly with no jamming and also parts get released from

molds and dies more easily. DLC coating also increases the life of the molds, dies and extruders.

For the automotive industry, use of DLC makes it possible to have higher efficiency, reduced maintenance and therefore, reduced energy and power demand. Camshafts, crankshafts, pistons, valves, differential and gear box components can all be coated. DLC is also applicable to any mechanical part such as shafts, bearings, bushings where it can raise efficiency, allow simplified designs and improve wear resistance. Figure 1-3 shows some typical mechanical parts coated by DLC process.

Figure 1-3: Some DLC coated parts and tools

Companies that coat their products with DLC often have strict surface roughness and friction coefficient goals. This research investigates the surface roughness and friction coefficient properties of uncoated and DLC coated specimens in an effort to satisfy two particular requirements of the industry.

The first requirement is to know what uncoated surface roughness is needed to obtain a certain DLC coated surface roughness. Therefore, a mathematical relationship between uncoated and DLC coated surface roughness is needed. If this relationship can be approximated, the cost of surface finishing can be minimized by avoiding any unnecessary processes.

The second requirement is to know what uncoated surface roughness is needed to reach a specific friction coefficient after the DLC coating process. Therefore, a mathematical relationship between uncoated surface roughness and DLC coated friction coefficient is needed. This will also help minimize surface finishing costs.

This research focuses on DLC coating of steel as it is one of the most important engineering materials which is used in a wide range of applications. All the coating processes were conducted based on the optimized procedures available at Intellectual Alliance Inc. and were completed at their facility in Concord, Ontario. Using an experimental approach that includes surface roughness measurements along with dynamic friction measurements, various data is gathered to investigate and quantify the relationship of surface roughness and friction coefficient on DLC coated surfaces.

Chapter 2: Literature Review

The literature review of this research covers a wide spectrum of topics to create a better understanding of the dynamics of DLC coating, along with friction and roughness. The literature survey is divided into 4 sections; details about friction and its causes; relationship of coating parameters and sublayers with surface roughness and fiction coefficient; relationship between surface roughness and friction coefficient in general and modelling of friction coefficient and surface roughness.

2.1 Friction

Understanding the dynamics of friction is very important for the scope of this research. In general, DLC coatings have friction coefficients that vary from 0.001 to 0.6 which highly depends on hydrogen content of the coating and also the amount of sp3 and sp2 bonds (Borodich, Korach & Keer, 2007). Based on Fontaine, Donnet and Erdemir (2008), there are three main contributions to tangential friction force which are abrasion, shearing and adhesion. They are demonstrated in Equation 2-1 and are described visually in Figure 2-1.

$$F_{tangential} = F_{abrasion} + F_{shearing} + F_{adhesion} \quad (2\text{-}1)$$

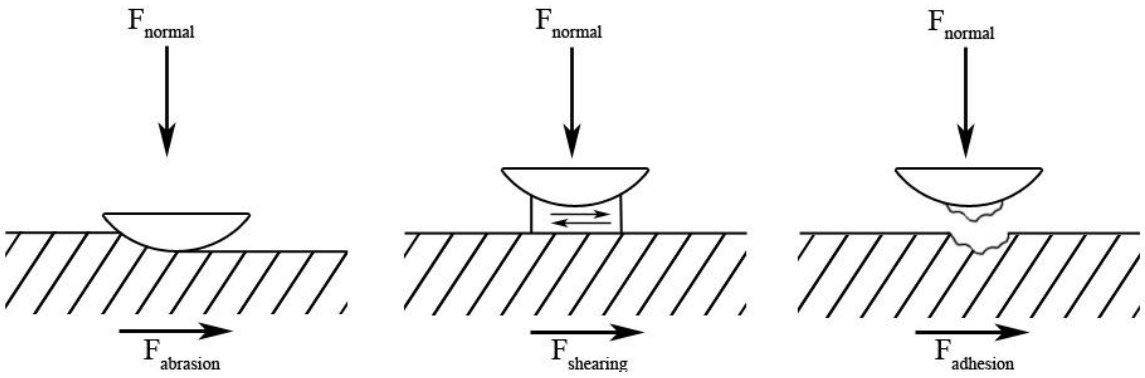

Figure 2-1: Details of tangential friction force

During abrasion, one surface is scratching the other. This mostly depends on the hardness of the materials and also the geometry of the contact patch. Roughness of the surface also seems to affect the abrasion. This phenomenon is not likely to happen on DLC coated surfaces because of the high hardness and strain tolerance properties of DLC. As a result of this, DLC is used to significantly decrease or eliminate the effects of abrasion. Small abrasive effects are seen when DLC is in contact with other materials that are not as hard and smooth. In this case, the abrasive effect is mostly dependant on the roughness and hardness of the counterpart, considering that DLC has low roughness and high hardness.

In shearing, the debris in between, also referred to as the third body, is sheared due to sliding. The third body is usually a transfer layer, or in other words, a tribofilm. There can be two types of sliding; intrafilm and interfilm. Intrafilm is defined as the shearing within the tribofilm itself whereas interfilm is the shearing at the surface of the tribofilm. Which one of these sliding conditions is existent depends on the rheological properties of the tribofilm such as composition, structure and mechanical properties. The t/l ratio also plays a role in type of sliding that is happening, where “t” is the thickness of the tribofilm and

“l” is the shearing length. However, the rheological properties of the tribofilm are relatively unknown. It is known that the tribofilms have higher levels of sp2 bonds compared to DLC coatings (Fontaine, Donnet, Erdemir, 2008). As the tribofilms are usually very thin (less than 100nm), shearing happens at the surface rather than internally, which means interfilm sliding is dominant. The thickness of the tribofilm mainly depends on the adhesion character of the contact patch. As the thickness of the tribofilm increases, the sliding characteristic is not only interfilm, but also intrafilm. Due to high hardness of DLC coatings, effects of shearing are minimized.

In adhesion, the two materials stick to each other and break off small portions, so it is more about the interaction of the two surfaces. This depends on electrostatic, capillary, polarization and bonding forces of the materials. The energy required to break this adhesion affects friction. This means that the main parameter that controls adhesive friction is the chemical reactivity of the two surfaces. The roughness of the surface also affects adhesion force significantly as it defines the size of the break off. The main part of friction of DLC films is adhesion, given that both contact surfaces have relatively low surface roughness. Furthermore, all the parameters that effect friction can vary during the sliding process based on tribochemical reactions, environmental effects and breakings

Hardness and elastic modulus also have effects on friction coefficient. It is very hard to examine the hardness of DLC coatings accurately as the hardness of some DLC’s are shown to be dependent on time. For example, a-C:H films seem to have excellent relaxation capabilities due to the free areas in the structure, which causes variation in hardness with time (Fontaine, Donnet, Erdemir, 2008). This variation in hardness can result in minor changes in friction coefficient.

Environment also has effects on friction. For example, the humidity of air seems to increase the friction of hydrogenated amorphous carbon (a-C:H) (Scharf, Singer, 2008). The opposite effect happens in amorphous carbon films (a-C and ta-C). Hydrogen bonds that are formed between hydrogen molecules on the DLC and water molecules on the air can be an explanation for this. Capillary forces can also have an effect on change in friction. As the surface coverage of water molecules increase, the adhesion and friction forces also increase. These capillary forces depend mostly on surface roughness and real contact area. Scharf and Singer (2008) concluded that the friction coefficient of DLC in moist air conditions is higher than dry air conditions and they also conclude that this is due to capillary forces.

The applied load has also shown to have effect on friction. Zhang et al. (2004) studied the effect of applied load on friction coefficient and found that at lower normal force, the friction coefficient is related to normal force (N) with $N^{-1/3}$. This means friction coefficient decreases with increasing normal force. However, after a certain load, the friction coefficient shows an increase. This was justified by the effects of plastic deformation and possible cracks on DLC coatings.

Scharf and Singer (2008) showed that the low friction coefficient of DLC coatings can be attributed to the transfer film that forms during dry sliding. They use an in situ Raman tribometer to study the transfer film that forms between the DLC coated piece and the sliding hemisphere. They observe that both sapphire and steel hemispheres show similar frictional behaviour even though they have very different mechanical properties. This again is attributed to the third body formation between the two materials that are in contact.

Wasche and Klaffe (2008) showed that DLC coatings are only effective in reducing friction coefficient up to about 100 °C. After this, as the temperature is increased further, the structure of the DLC becomes increasingly graphitic. This causes increased wear and friction coefficient. Life of the DLC coating is significantly decreased as well at these high temperatures.

2.2 Relationship of Coating Parameters and Sublayers with Surface Roughness and Friction Coefficient

There are many coating parameters that can be varied to get different surface roughness and friction coefficient properties. Some of these parameters are coating time, type of gas used, gas flow rate, bias voltage, ion energy and etc.

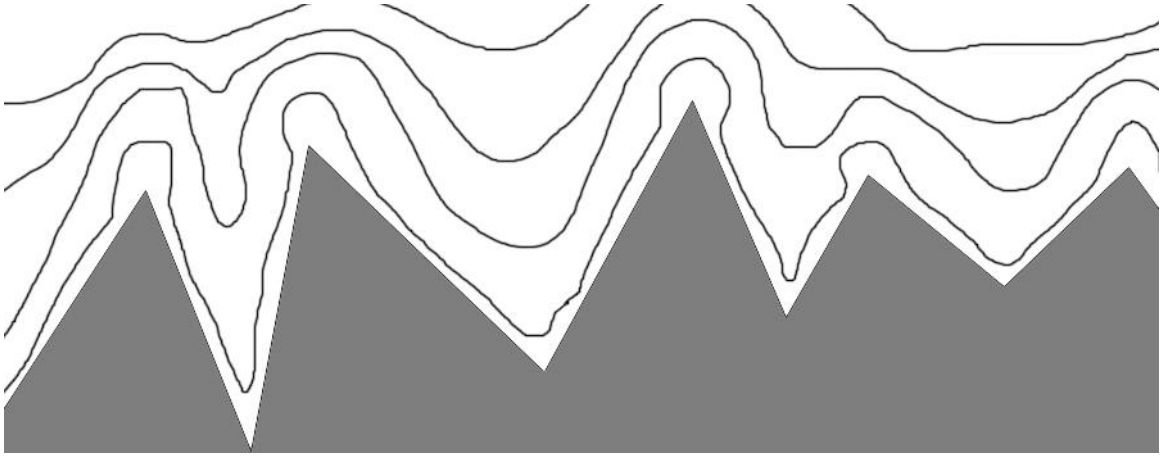

Figure 2-2: Reduction in surface roughness as the coating gets thicker

In terms of coating time which has direct influence on coating thickness, Salvadori et al. (2006) showed that increasing DLC thickness first creates a slight increase in roughness and then starts to decrease it as the coating gets thicker. This is explained in

their paper by the fact that DLC coating first starts to build up around the sharp edges due to the intensity of their magnetic fields and as the coating gets thicker, the gaps also start to fill up and that is when the roughness starts to decrease. Huang et al. (2004) also showed the same concept of decreasing surface roughness with increased coating thickness.

The issue of having very thick coatings is the delamination. As the DLC coating gets thicker, the stress level also increases, which in turn causes delamination. This problem can be avoided by using pulsed ion beams of high and normal ion energy, which helps to reduce internal stress by stress relaxation. Another method of reducing internal stress is alloying DLC with other elements such as aluminium or silicon.

In terms of type of gas used, the hydrogen content in the gas makes differences in the tribological properties of the coating. Use of acetylene for creating DLC is very common. This is because acetylene has the lowest hydrogen content out of all the gasses that can be used such as methane. Acetylene also has high deposition rate. However, it has about 1% impurity which is a drawback for using this gas as any type of impurity might cause defects on the coating surface. Another drawback of using acetylene is the necessity to use high ion energy in order to reduce stress. Methane is another gas that can be used for coating and it can be found at much lower impurity compared to acetylene. It can also be used at lower ion energy. If methane is used with very high ion energy (600-1200eV), super low friction films can be created (Robertson, 2008). This is because at high ion energy, the amount of hydrogen in the coating increases, which acts as a lubricant. Simply, more hydrogen in the DLC coating results in lower friction coefficient, however as the hydrogen bonds are weak, there is also more wear. If the hydrogen content of the

DLC coating is lower, very hard coatings can be made with very minimal wear. However, these types of coatings might have higher friction coefficient. Therefore, there is a trade-off between having less friction or more hardness.

In terms of bias voltage, Liu et al. (2006) showed that increasing the bias voltage results in decreasing of surface roughness.

In terms of nitrogen flowrate, Saha et al. (2011) showed that nitrogen flow-rate increases roughness on Si:DLC:N parts. Liu et al. (2003) also demonstrated the same concept.

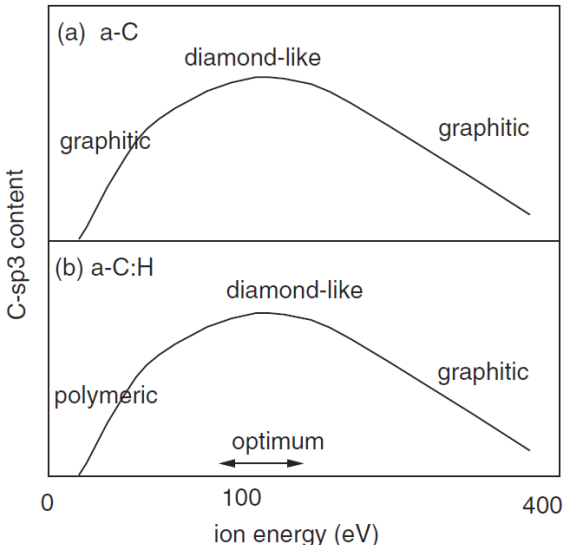

Figure 2-3: Structure of the coating as a function of ion energy (Robertson, 2008)

In terms of ion energy, it has been shown by Robertson (2008) that optimum ion energy is 100eV for best results. This can be seen in Figure 2-3. At the optimum ion energy level, the carbon atoms penetrate into the thin film which results in denser sp3 bonds. This is called subplanting. This also decreases the C to H bonds as they are turned into C to C bonds. Subplanting effect is described in Figure 2-4. At lower ion energy

levels, there are more C to H bonds and the result is polymeric. This is due to the fact that carbon atoms fail to penetrate into the surface and create bonds at the surface. At higher than optimum ion energy levels, there are more sp2 C to C bonds which makes the structure more graphitic. Subplanting still happens at high ion energy levels but the sp3 content decreases. The exact reason of this decrease in sp3 bonds is still debated.

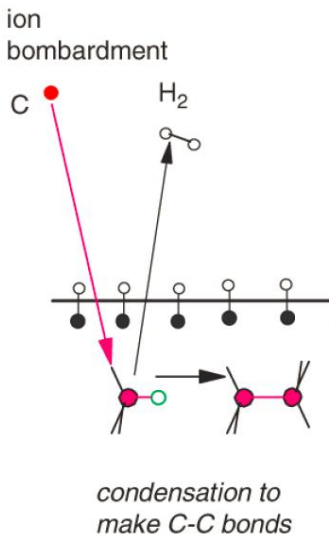

Figure 2-4: Subplanting (Robertson, 2008)

2.3 Relationship between Surface Roughness and Friction Coefficient

Many things such as ambient temperature, humidity, wear, linear or rotational speed and test duration can affect friction coefficient of a material and surface roughness is also one of them. Due to complexity of friction, it is very hard to find a direct correlation between surface roughness and friction. However, there are many experimental and theoretical studies that try to explain this relationship.

Stoudt et al. (2006) studied the relationship between surface roughness and friction behaviour to minimize the defects in the metal forming process. They used a specially designed test apparatus that can apply and measure a normal load on a rectangular piece and drag it with a certain speed while also measuring the friction force. This allowed them to measure friction coefficient of the material. They also use a scanning laser confocal microscope to measure the surface roughness of the test specimen before and after the friction test. They conducted multiple tests; first set of tests was done on a new test specimen whereas the second set of tests was done on the same specimens from the first test, after they are scratched due to friction, to see the effect of surface roughness. They also repeat the test under lubricated conditions and with two different normal force values. They see that the friction coefficient increased with increase in surface roughness in both dry and lubricated conditions. Also, increasing normal force caused increase in friction coefficient for fresh surfaces; however, the rougher surfaces did not show an increase in friction coefficient. This result can be seen in Table 2-1 where average normal force is changed between 250 N and 625 N while also playing with roughness and lubrication.

Table 2-1: Friction data comparison of specimens with as-received and scratched surfaces (Stoudt et al., 2006)

As-received				Pre-stained			
Average Normal Force	Lubricity	Average Friction Coefficient	Uncertainty (2σ)	Average Normal Force	Lubricity	Average Friction Coefficient	Uncertainty (2σ)
250	None	0.0619	0.013	250	None	0.1135	0.012
625	None	0.0939	0.005	625	None	0.1110	0.010
250	Paraffin oil	0.0335	0.006	250	Paraffin oil	0.0614	0.002
625	Paraffin oil	0.0454	0.011	625	Paraffin oil	0.0698	0.007

The obtained 2D surface roughness profile was compared to the friction coefficient profile along the length of the wear scar to relate the two properties. Probability density functions are created for both set of data and are shown in Figure 2-5.

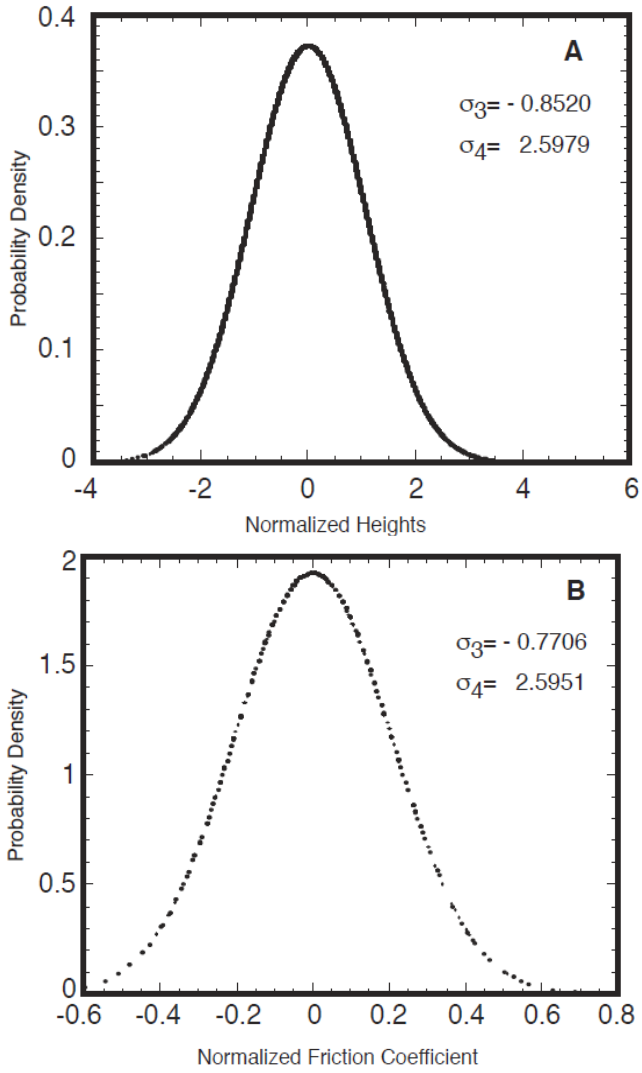

Figure 2-5: PDF of surface roughness and friction coefficient (Stoudt et al., 2006)

Based on the results, they see a very close relation between the two set of values in terms of skew (σ_3) and kurtosis (σ_4). Here, skew is the measure of asymmetry in the overall data and kurtosis is dependent on the shape of the tails of the distribution which

indicate the extremes of the data. As both values are within 10% of each other, the general shape of both distributions is considered very similar.

Another study on relationship between friction coefficient and surface roughness was done by Achanta et al. (2010). They study friction in nano, micro and macro scale due to the fact that friction is affected by atomic, chemical and mechanical interactions; all creating different frictional behaviour in different scales. They show that surface roughness, and therefore the true contact area, has an important effect on friction, especially for cases where adhesive friction is dominant, such as hard/hard interfaces. Surfaces that have higher roughness also have smaller contact area, which results in lower friction coefficient values.

Schultz (2002) also conducted a study for understanding the relationship between surface roughness and friction. He conducted a hydrodynamic test in which a plate is pulled inside water in nun-turbulent conditions. He prepared a total of 7 specimens which all had different surface roughness due to polishing or sanding. The first specimen was unsanded (Ra = 2.7 μm), specimens 2 to 6 were sanded with 60 (Ra = 0.96 μm), 120 (Ra = 0.58 μm), 220 (Ra = 0.47 μm), 400 (Ra = 0.43 μm), and 600 grit (Ra = 0.4 μm) to get progressively smoother surfaces. The 7^{th} specimen was polished and had the smoothest surface (Ra = 0.18 μm). His results showed that as the surface roughness is decreased from original untouched surface to a polished surface, the friction coefficient increased. However, after a certain point, the increase in friction coefficient was minimal along with the decrease in surface roughness. Their results can be seen in Table 2-2.

Table 2-2: Decrease in friction coefficient with respect to a polished surface (Schultz, 2002)

Specimen	Average % Increase in Friction Coefficient	Range of % Increase in Friction Coefficient
Unsanded	5.0	3.0-7.3
60-Grit	2.6	2.0-4.1
120-Grit	1.9	1.0-3.4
220-Grit	1.2	0.8-1.7
400-Grit	1.2	0.7-1.7
600-Grit	1.0	0.6-1.4

2.4 Modelling of Friction Coefficient and Surface Roughness

In order to model friction or surface roughness of DLC coatings, the first step is to model the coating process in order to obtain the DLC surface. Zhang et al. (2004) studied the effect of hydrogen concentration, applied load and relative humidity on the friction coefficient of DLC films and compared their results with molecular dynamics simulations. In order to model friction of DLC coated surfaces, they first modelled the coating process using Tersoff-Brenner form for interatomic potential. Brenner potential is best described in his paper (Brenner, 1990). He defines the hydrocarbon potential as

$$E_b = \sum_i \sum_{j(>i)} [V_R(r_{ij}) - \bar{B}_{ij} V_A(r_{ij}) \qquad 2\text{-}2$$

Here, i and j refer to atom numbers i and j. V_R and V_A are repulsive and attractive interactions respectively and they are defined as

$$V_R(r_{ij}) = f_{ij}(r_{ij}) {D_{ij}}^{(e)}/(S_{ij}-1)e^{-\sqrt{2S_{ij}}\beta_{ij}(r-{R_{ij}}^{(e)})} \quad 2\text{-}3$$

$$V_A(r_{ij}) = f_{ij}(r_{ij}) {D_{ij}}^{(e)}/(S_{ij}-1)e^{-\sqrt{2/S_{ij}}\beta_{ij}(r-{R_{ij}}^{(e)})} \quad 2\text{-}4$$

where r, r_{ij}, S_{ij}, β_{ij} and well depth D_{ij} are constant parameters.

$f_{ij}(r)$ is a function that restricts the pair potential to nearest neighbours and is defined by

$$f_{ij}(r) = \begin{cases} 1 & r < {R_{ij}}^{(1)} \\ \dfrac{\left[1 + cos\left[\dfrac{\pi\left(r - {R_{ij}}^{(1)}\right)}{({R_{ij}}^{(2)} - {R_{ij}}^{(1)})}\right]\right]}{2} & {R_{ij}}^{(1)} < r < {R_{ij}}^{(2)} \\ 0 & r > {R_{ij}}^{(2)} \end{cases} \quad 2\text{-}5$$

where R_{ij} is a constant parameter.

B_{ij} and B_{ji} are defined as many-body coupling and $\bar{B}_{ij}$ is the empirical bond order function. They can be calculated as follows:

$$\bar{B}_{ij} = \frac{B_{ij} + B_{ji}}{2} + F_{ij}({N_i}^{(t)}, {N_j}^{(t)}, {N_i}^{(t)}, {N_{ij}}^{(conj)}) \quad 2\text{-}6$$

$$B_{ij} = \left[1 + \sum_{k(\neq i,j)} G_i(\theta_{ijk}) f_{ik}(r_{ik})\, e^{a_{ijk}[(r_{ij} - {R_{ij}}^{(e)}) - (r_{ik} - {R_{ik}}^{(e)})]} + H_{ij}({N_i}^{(H)}, {N_i}^{(C)})\right]^{-\delta_1} \quad 2\text{-}7$$

$N_i^{(C)}$ and $N_i^{(H)}$ are the number of carbon or hydrogen atoms that are bonded to atom i and are defined as

$$N_i^{(H)} = \sum_{j(=hydrogen)} f_{ij}(r_{ij}) \quad 2\text{-}8$$

$$N_i^{(C)} = \sum_{j(=carbon)} f_{ij}(r_{ij}) \quad 2\text{-}9$$

$N_i^{(t)}$ and $N_j^{(t)}$ are total number of neighbours of atom i or j respectively and are defined as

$$N_i^{(t)} = N_i^{(H)} + N_i^{(C)} \quad 2\text{-}10$$

$G(\theta_{ikj})$ is a function that describes angles between bonds i-j and i-k and is defined as

$$G_c(\theta) = a_0 \left\{ 1 + \frac{c_0^2}{d_0^2} - c_0^2 / [d_0^2 + (1 + cos\theta)^2] \right\} \quad 2\text{-}11$$

where a_0, c_0, d_0 are constant parameters.

A simpler way of simulating the surfaces that will be in contact is to use finite element models as described by Muser (2006). The advantage of using a finite element model is to fact that the mesh size can be changed based on the importance of the region being analysed, which significantly reduces the computational time. Figure 2-6 shows an example of a finite element model used to simulate two surfaces that are in contact. The top surface has a certain roughness, which requires finer mesh along the contact patch, and the bottom surface is perfectly flat.

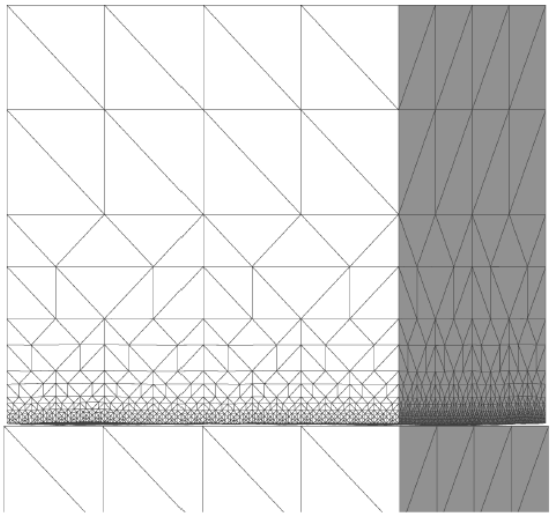

Figure 2-6: FEM model for simulating friction (Muser, 2006)

The next step in modelling is the simulation of sliding friction. Modelling of friction is a very hard task due to the fact that friction is a very complicated and multi variable problem. In order to have a good simulation for friction, it is necessary to have formulas that can approximate the friction force. The simplest form of friction coefficient, which considers only the pressure, was defined by G. Amontons as the Amontons law of friction and it is as follows:

$$\mu = \frac{F_f}{N} \qquad 2\text{-}12$$

where μ is the friction coefficient, F_f is the tangential friction force and P is the normal force.

This equation was updated by C. A. Coulomb (1821) later on, to include not only pressure, but also the sticking of the surfaces that are in contact and it is as follows:

$$F_f = A + \mu N \quad \text{2-13}$$

where A is a constant force that depends on the sticking of the two surfaces. G.A. Tomlinson (1929) showed that, given there is no wear and scratching happening at the friction interface, the constant force A can be calculated as the molecular interaction between the two materials. Simply, the atoms on one surface interact with atoms on the other and cause vibrations, which in turn results in energy loss. B. Derjaguin (1934) combined this information with Coulomb's equation and found the following relation:

$$F_f = \mu(N + Sp_0) \quad \text{2-14}$$

where S is the contact area of the two surfaces and p_0 is the specific attractive force. However, this model is only applicable to solids with crystal structure and cannot be generalized. The common method of representing friction currently is to have two friction forces; one for the mechanical interaction, and one for the molecular interaction between the two surfaces (Borodich, Korach & Keer, 2007). The concept is represented as follows:

$$F_f = F_{f,mech} + F_{f,mol} \quad \text{2-15}$$

Borodich, Korach and Keer (2007) divided the molecular interactions into two sections, one for the interatomic interactions and one for the remaining molecular effects between the two surfaces that are in contact. Their representation is as follows:

$$\mu = \mu_{mech} + \mu_{mol,1} + \mu_{mol,2} \quad (2\text{-}16)$$

where $\mu_{mol,1}$ is the friction caused by the interatomic interactions and $\mu_{mol,2}$ is the rest of the molecular effects. As it is extremely hard to model all of the three variables, Borodich, Korach and Keer (2007) focused only on the friction caused by the interatomic interactions which is the $\mu_{mol,1}$ term. They based their equations on a ball on disk friction tester and compared theory with experimental results. Their final version of the above equation is as follows:

$$\theta = \frac{N_c}{N} \quad (2\text{-}17)$$

$$\theta(k,i)|_{t+\Delta t(k,i)+0+} = \ln\{\exp[\alpha\theta(k,i)(1-p)] + \alpha B\Delta t(k,i)\}/\alpha \quad (2\text{-}18)$$

$$\mu(i) = \mu_{mech} + \frac{c}{n_m}\sum_{k=1}^{n_m}[\theta(k,i)]^{\mp} + \mu_{mol,2} \quad (2\text{-}19)$$

where θ is the fractional coverage of absorbate (assumed to be oxygen), N_c is the number of sites on the surface that have bonded with an absorbate, N is the total number of free sites on the surface that have the possibility of bonding with a substrate atom, c is a first-order constant, α and B are constants based on the experiment, t is time, p is a constant that depends on the specimen used, k is the point that the reading is taken, i is the cycle number. By making assumptions for some of the variables due to lack of

experimental data, Borodich et al (2007) were able to match the experimental and theoretical friction test results.

It is important to obtain a simulation for friction that can accurately reflect the reality, in other words, assumptions need to be minimized. M. H. Muser (2006) has conducted many studies in order to optimize the simulation of friction. He gave a lecture on the simulation of friction and the theory behind it. The lecture starts out by pointing out some important aspects to keep in mind while creating a simulation for friction. Firstly, all the boundary conditions must be set properly as they can make big differences in the final result, even if the simulation is working very accurately. For instance, conducting a test with fixed normal force and fixed speed can give very different results if the same test is repeated with fixed distance between the specimens. Second aspect is the simplification of the contact patch. Many studies on modelling of friction assume that both bodies that are in contact are perfectly flat and aligned, also called commensurate. However in many applications, the two bodies that are in contact have different shapes and can be misaligned, also called incommensurate. This difference can create huge variations on the final result of a simulation. For instance, the experimental setup that is used in this study to measure friction has an incommensurate contact patch. Therefore the surface curvature must be taken into account. The effects of temperature change at the contact patch must also be taken into account.

In a computer simulation, usually the bottom part is called substrate and it is held fixed while the top part which is called the slider is moved to test friction. The slider can have three types of movements according to Muser (2006). First method is to use a fixed trajectory, basically having a fixed distance between the two parts. Second method is to

use a fixed normal force. And the third method is to pull the slider with a spring. In our test mechanism, we use fixed normal force.

Once the type of movement is set, the next step is to define the top layers of both substrate and slider that will be in contact. There are three ways to simulate the surface, firstly, the atoms on the top layer can be considered to be rigidly connected to inner layer atoms. Second method is to have the top layer atoms connected to the inner layer atoms with springs of a certain stiffness to better simulate the elastic properties of a surface. Third and last method is to use a certain potential to simulate the surface as discussed earlier in this section. Using a certain potential like Brenner Potential also significantly reduces CPU time. Based on this, if the potential method is chosen, the friction force on the top layers can be calculated with the following formula:

$$F_f = F_{ext} + \sum_{n \in em} -\nabla_n V_s(r_n) \qquad 2\text{-}20$$

where n is the atom number, F_{ext} is the external force and $\nabla_n V_s$ is the gradient of the surface potential.

Another research that studies friction in atomic scale is done by Zhang et al (2004). They start by simulating the DLC coating process in order to get the surfaces, as discussed earlier in this section. For intralayer interactions within DLC coated surfaces, they use Brenner potential, and for the interlayer interactions between the two DLC coated surfaces they use Lennard-Jones potential. Lennard-Jones potential is defined as follows:

$$\phi_{LJ} = 4\varepsilon \left\{ \left(\frac{\sigma}{r}\right)^{12} - \left(\frac{\sigma}{r}\right)^{6} \right\} \qquad 2\text{-}21$$

Where r is a constant parameter and the parameters ε and σ change depending on the type of atoms that are in contact and are defined as follows:

$$\begin{aligned} \varepsilon_{CC} &= 1.663\ meV, \qquad \sigma_{CC} = 3.191\ A \\ \varepsilon_{CH} &= 2.762\ meV, \qquad \sigma_{CH} = 3.179\ A \\ \varepsilon_{HH} &= 3.180\ meV, \qquad \sigma_{HH} = 2.918\ A \end{aligned} \qquad 2\text{-}22$$

In their simulation, Zheng et al. (2004) consider the two outside layers of the parts that are in contact to be fully rigid, and the coating part can deform and act based on Newton's law of motion. They bring the two parts to a fixed distance and drag one part in one direction in steps. The fixed distance between the two parts defines the normal force that is applied, in other words, normal force is considered to be directly related to distance between the two parts that are in contact. At each step during sliding, they sum up all the Lennard-Jones potentials in order to obtain friction.

Chapter 3: Experimental Method

In the process of obtaining the necessary data, first, the specimens were coated with DLC, followed with surface roughness and friction coefficient tests. The process is explained in Figure 3-1.

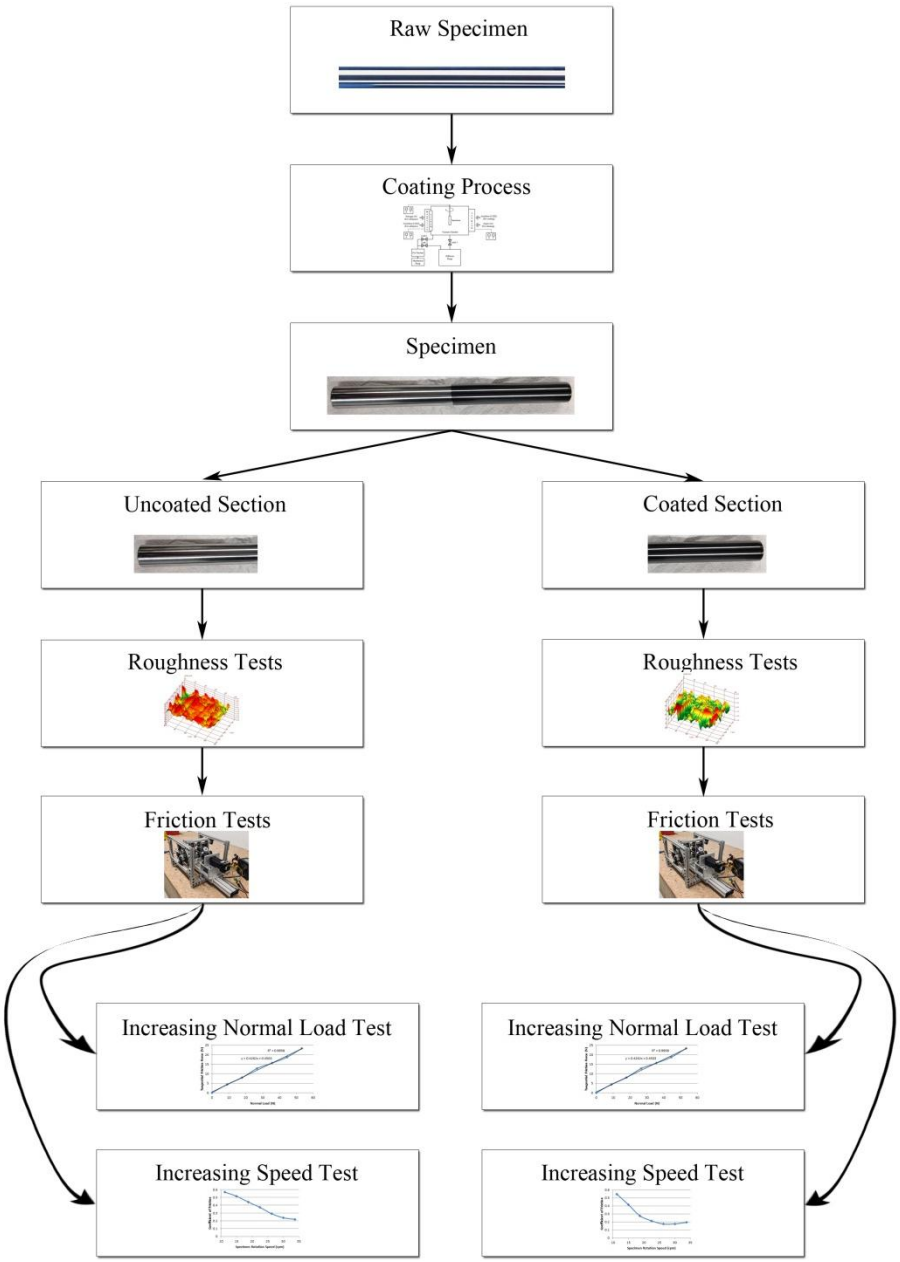

Figure 3-1: Flowchart of experimental procedure

3.1 Coating Method

The specimens used in this research were prepared by physical vapour deposition using ion beam technology. Depending on the properties of the material being coated, some sublayers might be needed, followed by DLC coating, or the DLC coating process is started right away with no sublayers. For coating with sublayers, Ti, TiN and TiCN sub-layers were created using magnetron sputtering and then the specimens were coated with DLC by using an ion beam and acetylene gas. Creation of sub-layers is also possible by using chromium (Cr) or titanium aluminum alloy (TiAl). All the coating processes were conducted based on the optimized procedures available at Intellectual Alliance Inc. and were completed at their facility in Concord, Ontario. Optimized coating parameters were used in the coating process which were determined after years of testing and improvements by the coating company. A schematic of the process and some controls can be seen in Figure 3-2.

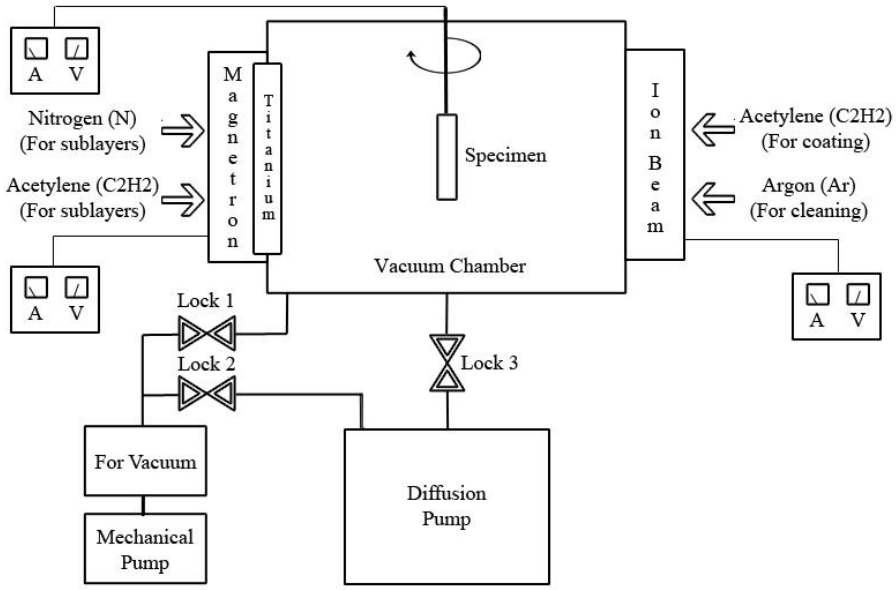

Figure 3-2: Schematic of the coating apparatus

Firstly, a vacuum is created in the chamber by opening lock 1 only with the use of for vacuum and mechanical pump. In the meantime, diffusion pump is also activated. In order to speed this process, lock 2 can be opened and closed. Once the pressures equalize, lock 1 is closed and lock 2 and 3 open to use all three pumps to create a good vacuum. After this, argon cleaning is done on the specimens by supplying argon gas through the ion beam to clean any unwanted particles. Next, a thin titanium coating is done by magnetron sputtering, followed by TiN coating with inclusion of nitrogen gas and TiCN with inclusion of acetylene. Once the sub layers are done, acetylene gas is supplied from the ion beam for DLC coating. Simply, carbon atoms in acetylene gas are ionized by the ion beam and then they are accelerated towards the specimen in a vacuum by a magnetic field. When these ionized carbon atoms hit the surface of the specimen, they form sp3 and sp2 bonds on the surface. Due to the hydrogen content in acetylene gas, some hydrogen atoms also hit the surface and create bonds. In order to minimize the amount of weak hydrogen to carbon bonds, acetylene gas is used as it has lowest possible carbon to hydrogen ratio. Gavrilov et al. (2010) also stated that acetylene is most suitable choice for DLC deposition.

3.2 Surface Roughness Measurement

There are many commercially available methods for measuring surface roughness. They can generally be divided into two categories of contact and non-contact methods. An example for contact method is the mechanical stylus method which has a resolution typically between 2 to 5 μm (Xu & Hu, 2009). Due to some disadvantages of the Contact

methods the non-contact methods have been developed and significantly improved in recent years. Some examples include atomic force microscopy (AFM), interference microscopy, vertical scanning interferometry, confocal microscopy, and scattering modelling (Xu & Hu, 2009).

3.2.1 Surface Roughness Measurement Setup

In this research, a non-contact method is used by implementing a microscope with camera and sensor provided by PhaseView™. The setup can be seen in Figure 3-3. GetPhase software was used for taking stacked images from the surface and for combining them to create 3D images and data of the surface. The resolution of the system was 0.091 μm/pixel and each surface roughness reading consisted of about 2,000,000 data points.

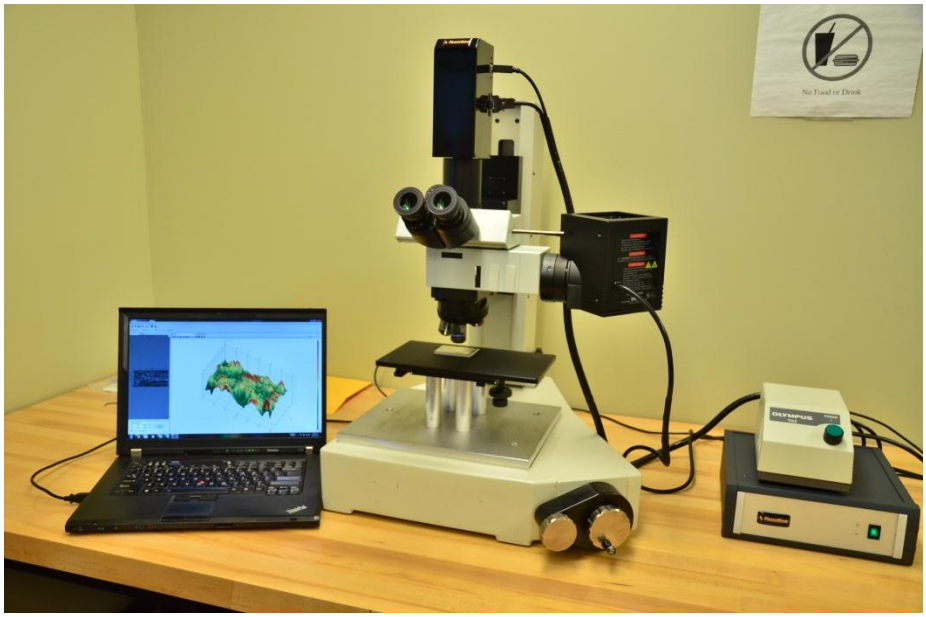

Figure 3-3: Roughness measurement setup

3.2.2 Surface Roughness Measurement Analysis

Using the obtained 3D cloud data, it was easy to calculate the required 3D roughness surface parameters based on the geometrical product specifications (GPS) provided in ISO 25178-2:2012 standard.

The average roughness, S_a, which is the average distance to the mean, can be calculated as follows:

$$S_a = \frac{1}{MN}\sum_{m=1}^{M}\sum_{n=1}^{N}|z_{mn} - \bar{z}| \quad 3\text{-}1$$

where M and N are the number of data points along the length (x) and width (y) respectively. z is the height (z) of the data point at index m and n. $\bar{z}$ is the mean of the heights of all data points. Average roughness is the main parameter that is used in this research to compare surface roughness of the specimens.

Root mean square roughness, S_q, which is the standard deviation of the surface, can be calculated as follows:

$$S_q = \sqrt{\frac{1}{MN}\sum_{m=1}^{M}\sum_{n=1}^{N}(z_{mn} - \bar{z})^2} \quad 3\text{-}2$$

Skewness, S_{sk}, which is the asymmetry of the height distribution, can be calculated as follows:

$$S_{sk} = \frac{1}{MNS_q}\sum_{m=1}^{M}\sum_{n=1}^{N}(z_{mn} - \bar{z})^3 \quad 3\text{-}3$$

When the skewness is a negative number, surface is mostly covered with holes and when the skewness is a positive number, surface is mostly covered with peaks. Kurtosis, S_{ku}, which is the width of the height distribution, can be calculated as follows:

$$S_{ku} = \frac{1}{MNS_q^4} \sum_{m=1}^{M} \sum_{n=1}^{N} (z_{mn} - \bar{z})^4 \quad 3\text{-}4$$

A kurtosis of 3 corresponds to Gaussian distribution. Valley depth, S_v, which is the depth of the deepest valley, can be calculated as follows:

$$S_v = |min(z_{mn})| \quad 3\text{-}5$$

Peak height, S_p, which is the height of the highest peak, can be calculated as follows:

$$S_p = |max(z_{mn})| \quad 3\text{-}6$$

Total roughness, S_t, which is the distance from the deepest valley to the highest peak, evaluated over the entire surface, can be calculated as follows:

$$S_t = S_v + S_P \quad 3\text{-}7$$

Averaged total roughness, S_z, which is the distance from the deepest valley to the highest peak evaluated over the base surface and averaged, can be calculated as follows:

$$S_z = \langle S_v + S_p \rangle_{eval.surf} \quad 3\text{-}8$$

3.2.3 Surface Roughness Measurement Procedure

A total of 40 measurements were done on each specimen of which 20 were taken from uncoated and 20 were taken from coated surface of the parts. This resulted in a total of 280 surface roughness readings from 7 specimens. The specimen on the microscope can be seen in Figure 3-4.

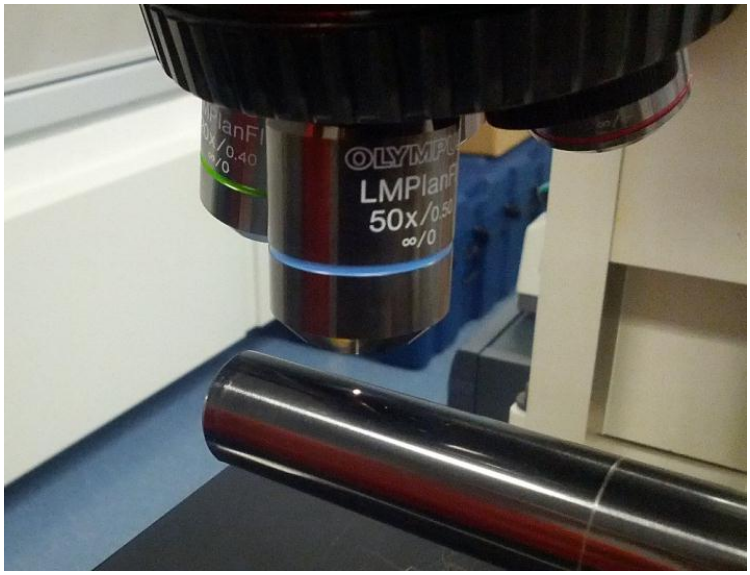

Figure 3-4: Surface roughness measurement

A stratified-random sampling approach was used for sampling (Barari, Elmaraghy & Knopf, 2007). The measurement points were selected randomly from the stratified regions of the surface. All surface roughness parameters including the average 3D surface roughness values (*Sa*) are calculated. Three 3D images of surfaces with relatively low, average and high surface roughness can be seen in Figures 3-5 through 3-7.

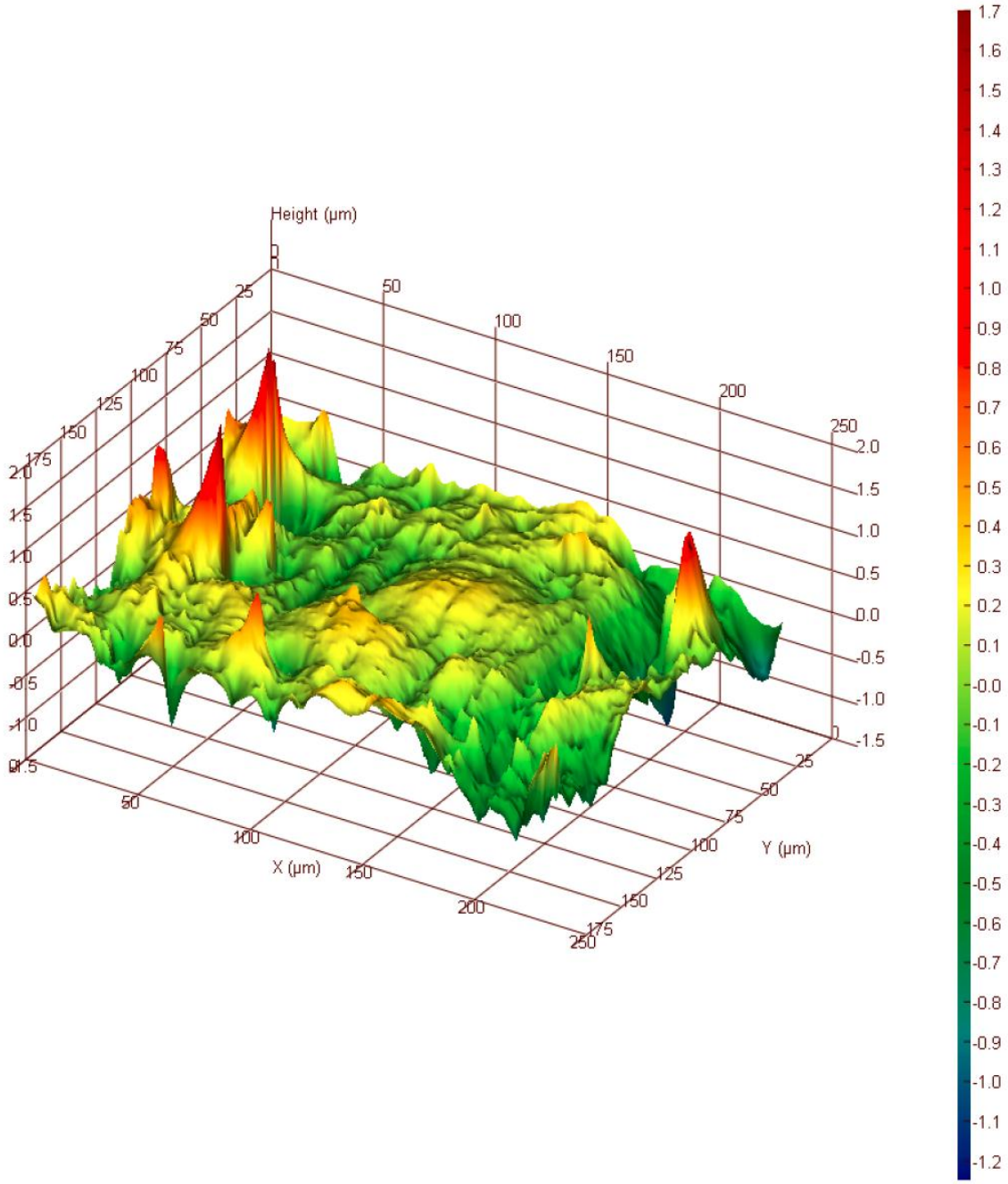

Figure 3-5: Example of a surface with relatively low surface roughness. (S_a = 0.186 µm)

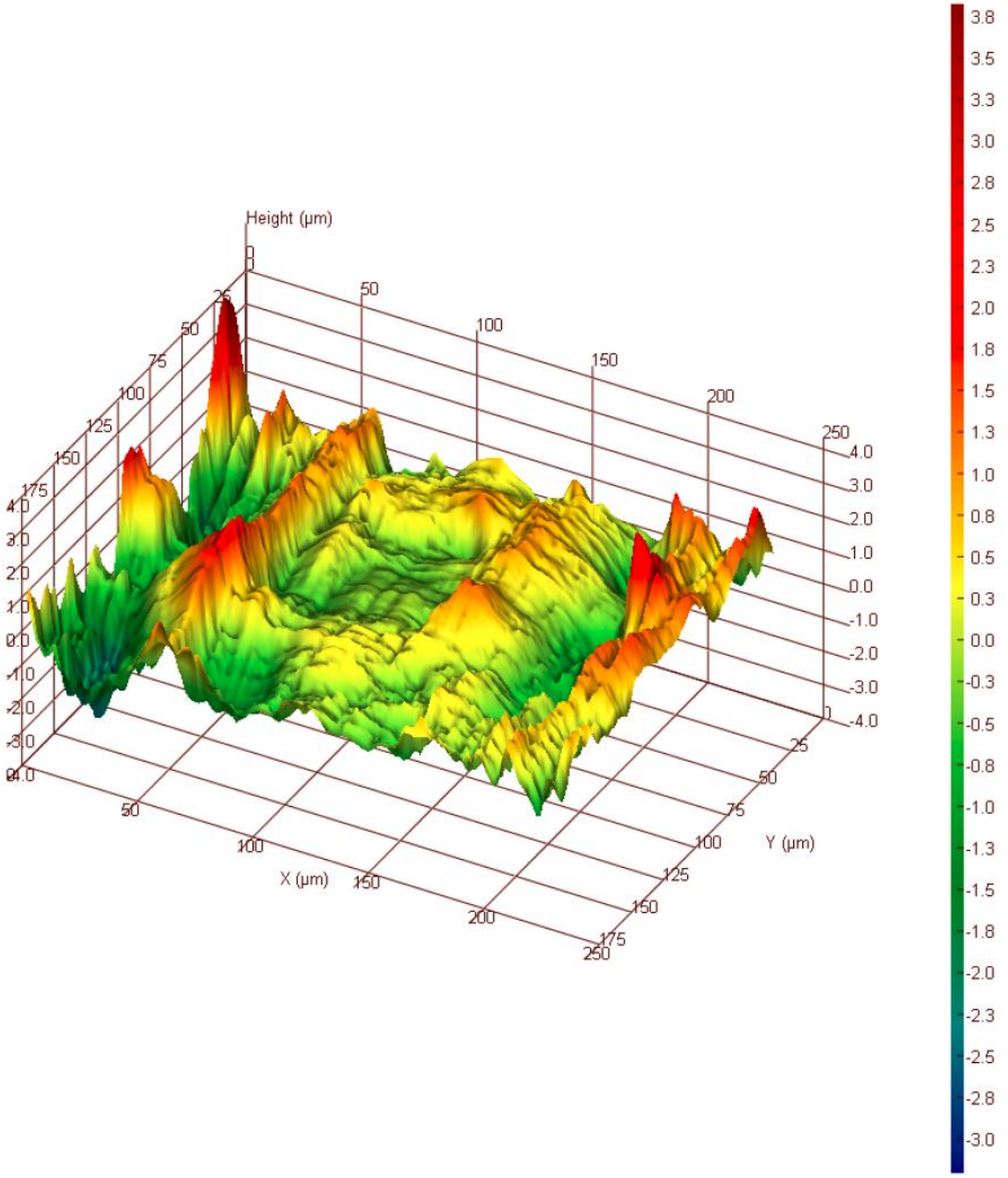

Figure 3-6: Example of a surface with relatively average surface roughness. (S_a = 0.549 µm)

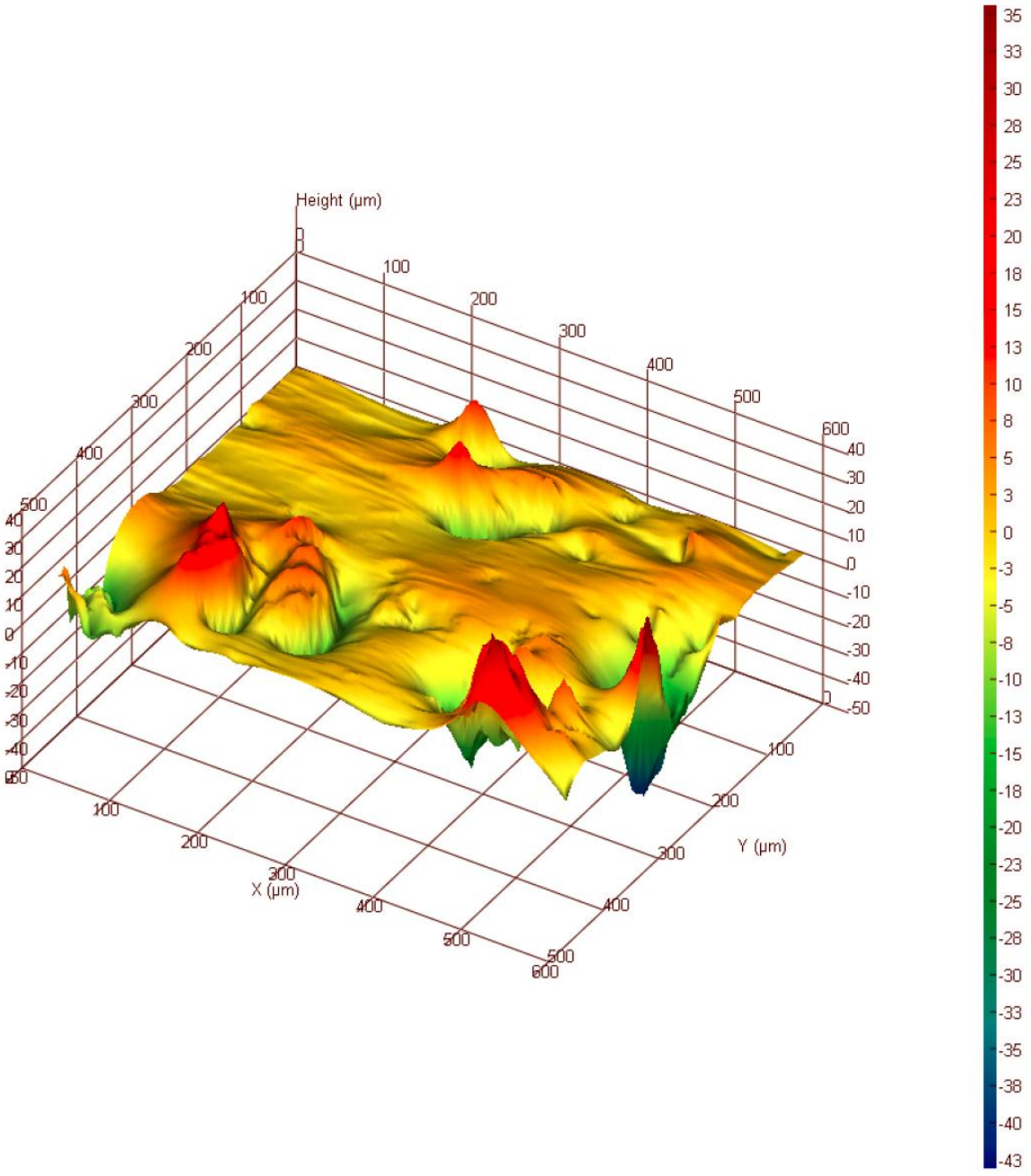

Figure 3-7: Example of a surface with relatively high surface roughness. (S_a = 3.59 µm)

3.2.4 Uncertainty of Roughness Measurement

Before starting the tests on the specimens, the accuracy of the roughness measurement method needed to be tested. A calibration plate with a known surface roughness value of 0.5 μm was tested with the roughness measurement microscope. The plate can be seen in Figure 3-8.

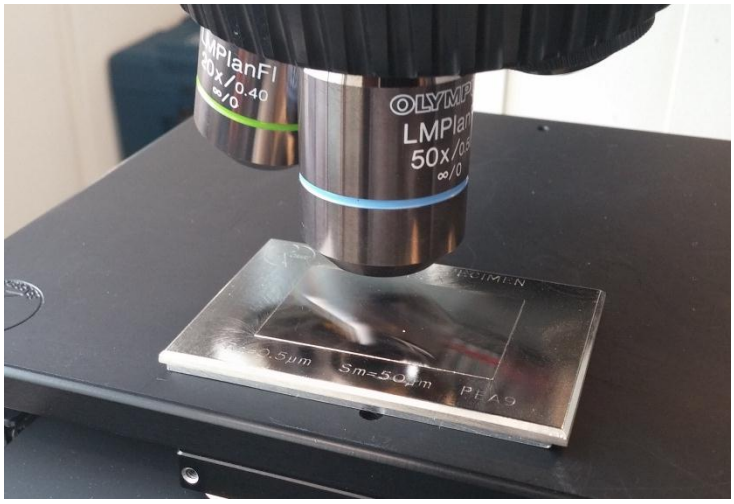

Figure 3-8: Calibration plate on the microscope

A total of 10 readings were taken at the exact same location of the specimen. The experimental average surface roughness was found to be 0.5282 μm with standard deviation of 0.0204 μm resulting in an error of the roughness measurement about 0.028 μm with 0.02 μm uncertainty. It must be kept in mind that a portion of this error was due to imperfections on the calibration plate. The calibration plate might not have exactly 0.5μm average surface roughness due to some microscopic wear and any kind of residues that might be on the surface after couple years of usage.

The next step was to test the repeatability of the roughness tests. Using the same 10 readings, the standard deviation was calculated to be 0.0204 μm. The data can be seen in Figure 3-9.

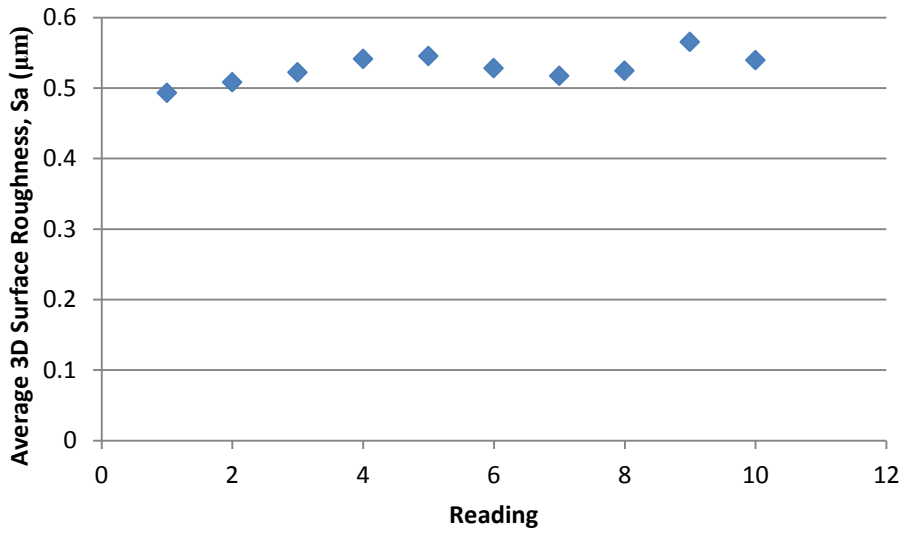

Figure 3-9: Repeatability test for roughness measurement

3.3 Friction Measurement

There are many commercially available machines that are designed to measure the friction coefficient on a surface. Some use a ball on a disc system to measure friction on any rotating disc, some can only measure friction on two flat surfaces and some measure friction by scratching. There are also specific test machines such as the one developed by Hughes and James (2002). However in this research, all the specimens used are shafts and a machine that can measure friction on a shaft that is rotating at a certain speed was not commercially available. Modifications of readily available machines would be very costly so a new machine is designed and built for testing of shafts.

3.3.1 Friction Measurement Setup

3.3.1.1 Concept Generation

The concept generation process started with the design of a system that can apply equal amounts of normal force from both sides of a rotating shaft, without the use of two separate force application points to reduce cost and simplify design. The main influence on the design was the working principle of brake callipers on cars, which use only one cylinder to apply the brake force on the brake disc while applying equal force on both sides of a brake disc. A preliminary sketch for such a system can be seen in Figure 3-10.

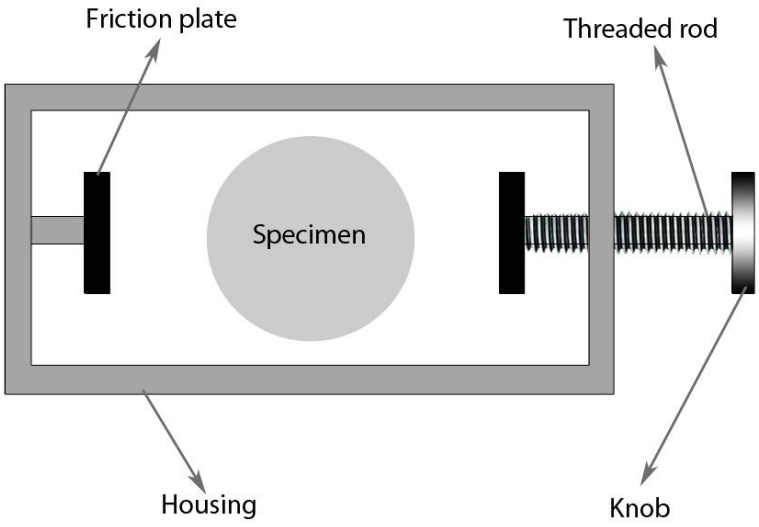

Figure 3-10: Initial system for applying equal normal force on both sides of shaft

In order to apply equal force from both sides of the shaft, the cylinder pushes one pad onto the brake disk. Upon contact, as the cylinder continues to apply force; the pad on the other side of brake disk is pushed towards it. A similar system is used in the design of the friction measurement device. A threaded rod inside the housing is rotated, pushing a friction plate towards the specimen, in this case a shaft. Once the friction plate makes

contact with the specimen, further tightening of the threaded rod causes the housing to move. This movement allows the other friction plate to get closer and eventually touch the shaft. This way, equal amount of normal force is applied on both sides of the specimen.

In order to further reduce cost, a threaded rod with a knob was utilized to apply the normal force from just one side, instead of using an actuator. The whole system is placed inside a rectangular housing which can slide on linear bearings attached onto two parallel precision shafts. The right side of the housing has a threaded hole for the rod with the knob that is used for pushing the friction plates onto the specimen shaft. As the threaded rod with knob is screwed in, first the right side friction plate is pushed towards the test specimen. Once the right side friction plate makes contact with the test specimen, further tightening of the threaded rod moves the whole housing to the right on the precision shafts, pushing the left friction plate towards the test specimen. This simple design allows equal amount of normal force to be applied from both sides of the test specimen while keeping the production and design costs to a minimum. An analogue force gauge is placed between the left friction plate and the left side of the housing. This allows the user to read the amount of normal force that is being applied on the test specimen from both sides and set it to a specific force for the test. The final design can be seen in Figure 3-11.

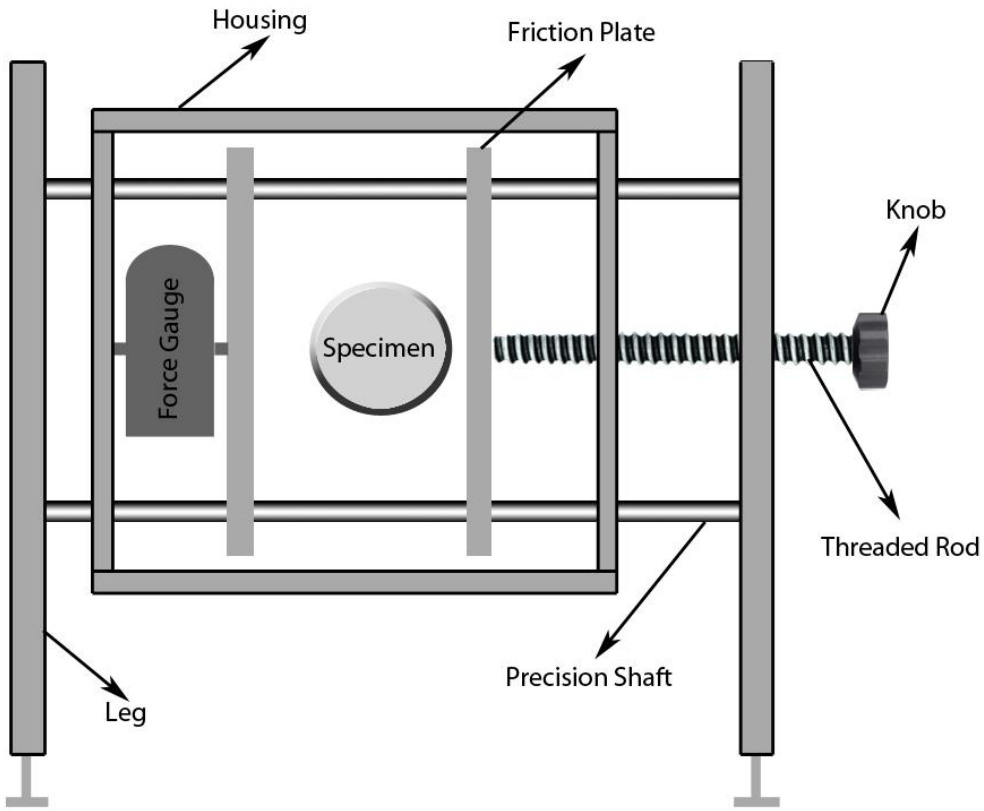

Figure 3-11: Final design sketch of the friction measurement device

Once the method of applying normal force was finalized, the next step was to focus on the measurement of the tangential friction force in order to obtain the friction coefficient. The initial idea was to use a torque sensor in order to record the peak torque that initiates a rotation, which would be used to obtain the static friction force. However, this would limit the system to only static case without the possibility of examining dynamic friction. Therefore, the final decision was to use a stepper motor to rotate the shaft at a fixed speed and to use a data logging ampere meter in order to see the difference in current usage once the normal force is applied. This current change can be related to power, which can be related to torque and eventually to tangential friction force. Once the friction force and

the normal force are known, the friction coefficient can easily be obtained. The detailed calculations can be found in the theoretical background section.

3.3.1.2 Computer Aided Design

After finalizing the concept, the next step was to have a full CAD model of the friction measurement device. This model made it possible to simulate the working principles of the device and set the proper dimensions for all components. The main focus was to minimize all the components in order to reduce material costs, while making sure that the device can function safely and sufficiently. Once the CAD model is finalized, 2D drawings of each component were created to custom fabricate them. These 2D drawings can be found in the appendix section. Figure 3-12 shows the final CAD model that was made in Siemens PLM Software NX 7.5.

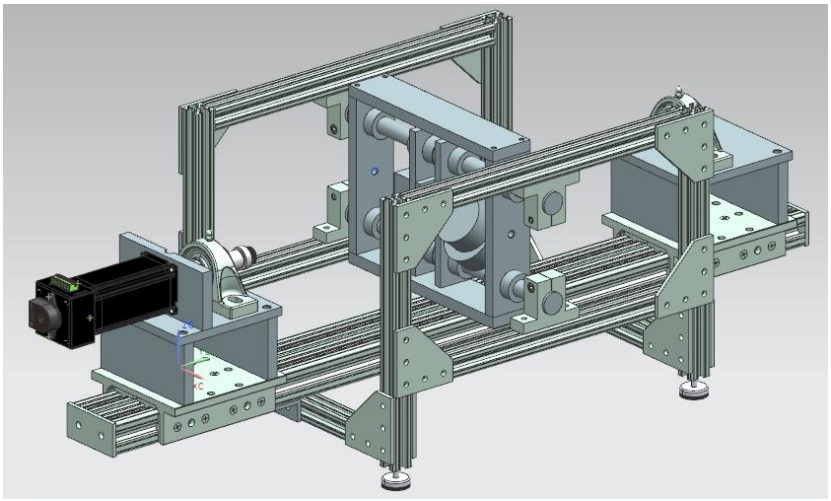

Figure 3-12: CAD model of the friction measurement device

3.3.1.3 Final Working Prototype

An initial prototype machine was first created based on the CAD models which was functional but needed minor improvements and adjustments due to misalignment and vibration issues. The simple set screw locking journal bearings were replaced with concentric locking bearings, along with an addition of a coupler between the motor and the spindles to solve misalignment and vibration issues. Also, the custom made spindles did not have tight enough tolerances and resulted in chuck run out while rotation. This problem was solved by ordering the original spindles designed for the particular lathe chucks that are being used. Minor modification of these spindles allowed them to easily replace the old custom made spindles. The friction measurement device can be seen in Figure 3-13.

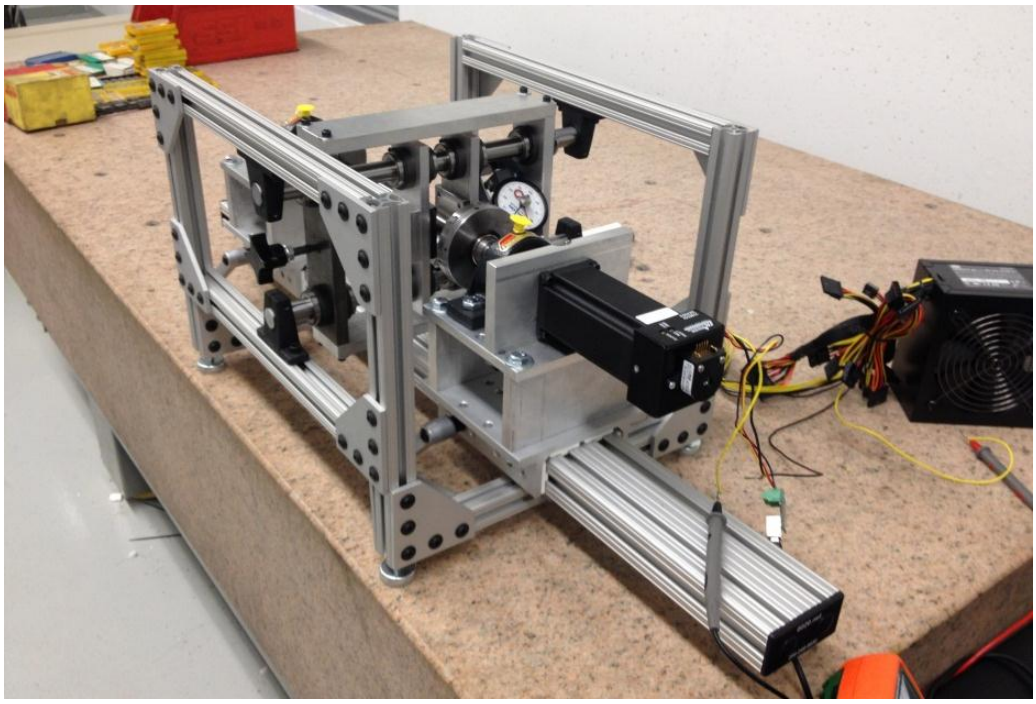

Figure 3-13: Friction measurement device

Friction measurement device is capable of testing shafts with diameters ranging from 0.25” to 3” and lengths ranging from 3” to 23”. Specimen that is going to be tested is held in place with two small lathe chucks which are attached to spindles. These chucks are self-centering 3 jaw type for making it easy to attach or remove the shaft specimens. The chuck spindles are free to rotate inside concentric locking precision journal bearings, one on each side of the test specimen. There is a stepper motor on one side that is connected to the spindle with a coupler to prevent misalignment and vibration issues. The chuck, spindle, journal bearing and the coupler can be seen in Figure 3-14.

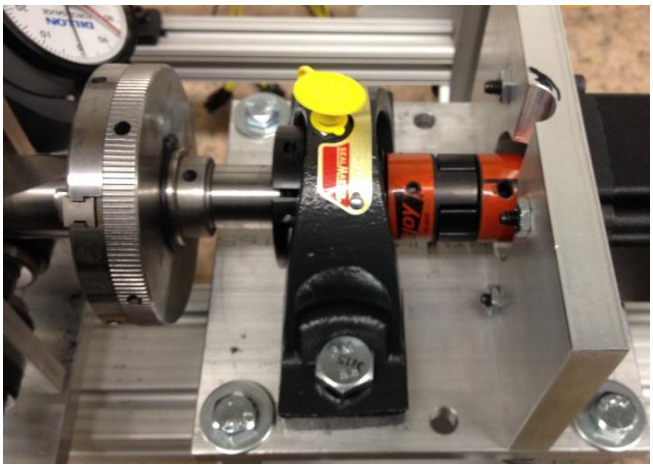

Figure 3-14: Chuck, spindle, journal bearing and coupling

A stepper motor is used to rotate the test specimens. It is controlled by computer software and it is possible to rotate it at various speeds. It is also possible to start the motor at a certain speed and accelerate at a given rate to another speed. Basically, having a stepper motor makes it very simple to control the movement of the motor while keeping constant rotational speed and voltage. The stepper motor and its power supply can be seen in Figure 3-15.

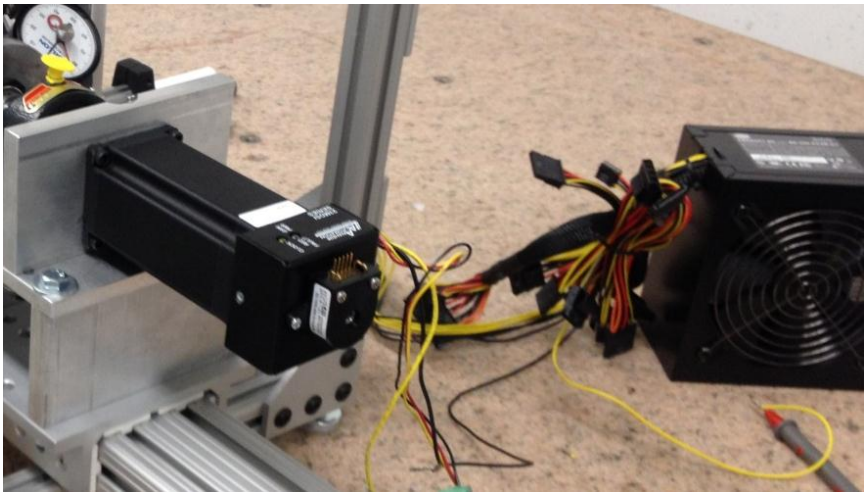

Figure 3-15: Stepper motor and its power supply

A high accuracy digital multimeter with data logging function is used to transmit current readings from the stepper motor to the computer. The data can be recorded every one second. The multimeter can be seen in Figure 3-16.

Figure 3-16: Digital multimeter with data logging function

Two stainless steel plates of grade 304 are used for the friction contact which is the counterbody in all the experiments. An analogue force gauge is used to apply a fixed normal force to the specimen being tested. This force gauge can be seen in Figure 3-17, along with the mechanism for applying equal amount of normal force from both sides of the shaft through the stainless steel friction plates.

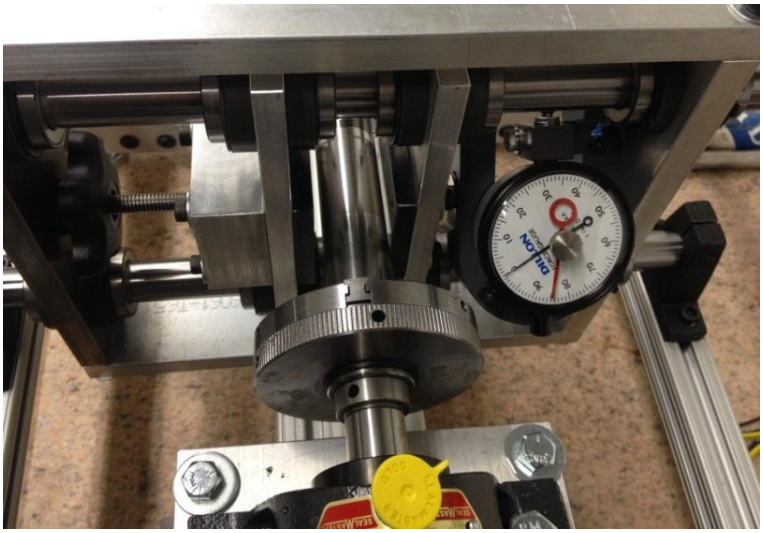

Figure 3-17: Force gauge and mechanism for applying normal load

The load is increased or decreased manually by rotating a knob that pushes the friction plates closer to the shaft specimen. A second knob is added to counter tighten the threaded knob in order to prevent loosening of the threaded rod which would result in change of normal force during a test. Figure 3-18 shows these knobs.

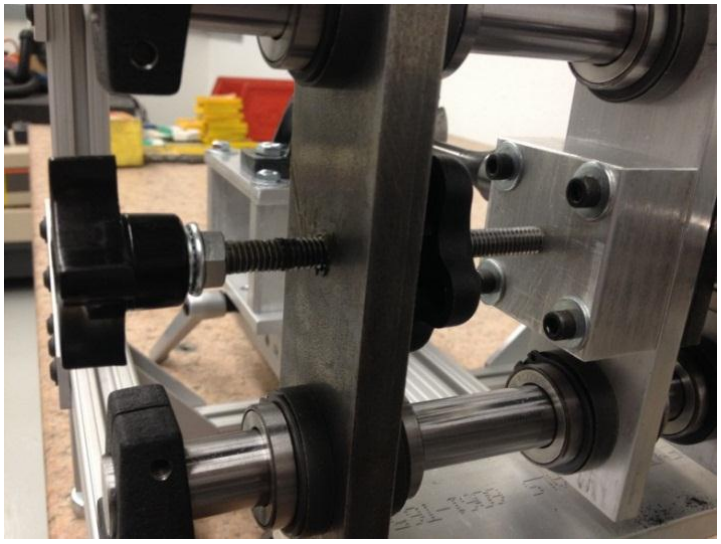

Figure 3-18: Knobs and threaded rod for applying the normal force

The chucks on both sides of the shaft specimen are able to move, allowing for shafts with various lengths to be tested on the same machine. This also makes it easier to test different areas of the same shaft without removing it from the machine. The mechanism that allows this movement can be seen in Figure 3-19.

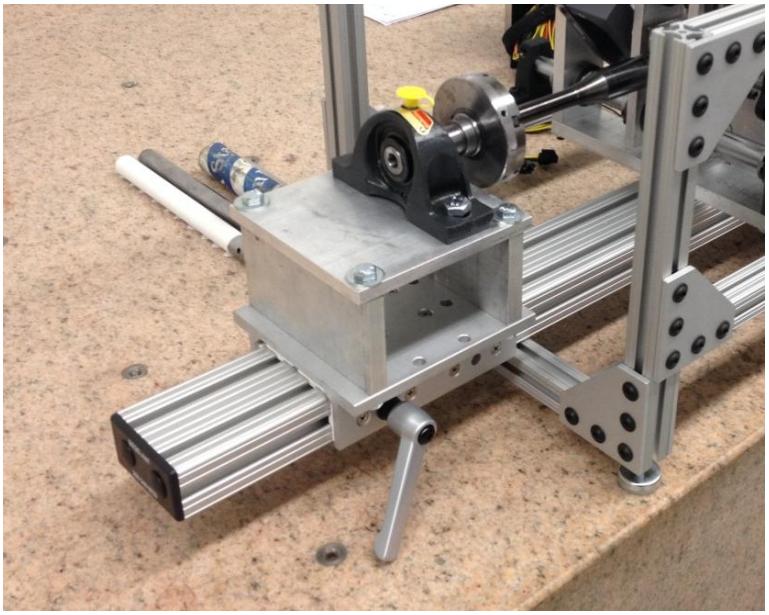

Figure 3-19: Mechanism that allows the two shaft attachment points to move

3.3.2 Friction Measurement Analysis

In order to obtain the friction coefficient value from current usage of the motor and normal force readings, the tangential friction force must be calculated. Firstly, the power usage of stepper motor with the shaft specimen attached is calculated. Based on Jewett (2004), power consumption during free rotation is calculated as follows:

$$P_0 = I_0 V \tag{3-9}$$

where I_0 is the current usage during free rotation and V is the voltage. Also based on Jewett (2004), power lost to friction from the normal force being applied is calculated as follows:

$$P_f = T_f \omega \tag{3-10}$$

where T_f is the friction torque due to normal force being applied and ω is the angular speed. Based on Jewett (2004), friction torque due to normal force being applied can be defined as

$$T_f = F_f d \tag{3-11}$$

where d is the diameter of the specimen and F_f is the tangential friction force. Plugging in equation 3-11 into 3-10 gives the power lost to friction due to the normal force being applied:

$$P_f = F_f d\omega \tag{3-12}$$

The total power usage is equal to the current usage when the normal load is applied multiplied by the voltage around the stepper motor:

$$P_{tot} = I_{load} V \tag{3-13}$$

Total power usage is also equal to the summation of power usage during free rotation and power lost to friction due to normal force being applied:

$$P_{tot} = I_0 V + F_f d\omega \tag{3-14}$$

Equating equations 3-13 and 3-14 and solving for the tangential friction force gives:

$$F_f = \frac{V(I_{load} - I_0)}{d\omega} \tag{3-15}$$

Once the tangential friction force is found, the friction coefficient can be easily calculated as the normal force is also known:

$$F_f = \mu \mathrm{N} \tag{3-16}$$

Equation 3-16 can only be used if a linear relationship between tangential friction force and normal force exists. If this linear relationship does not hold, some other mathematical models would need to be tested for fit into the data of this research.

Therefore, next step before obtaining the data was to prove that a linear relationship exists. In order to show the relationship between the tangential friction force and the normal force, tests were done on three random specimens with various surface finishes and same material. Normal force is varied from 0 to 45N while rotation speed is kept fixed at 18.75 rpm. The results can be seen in Figure 3-20.

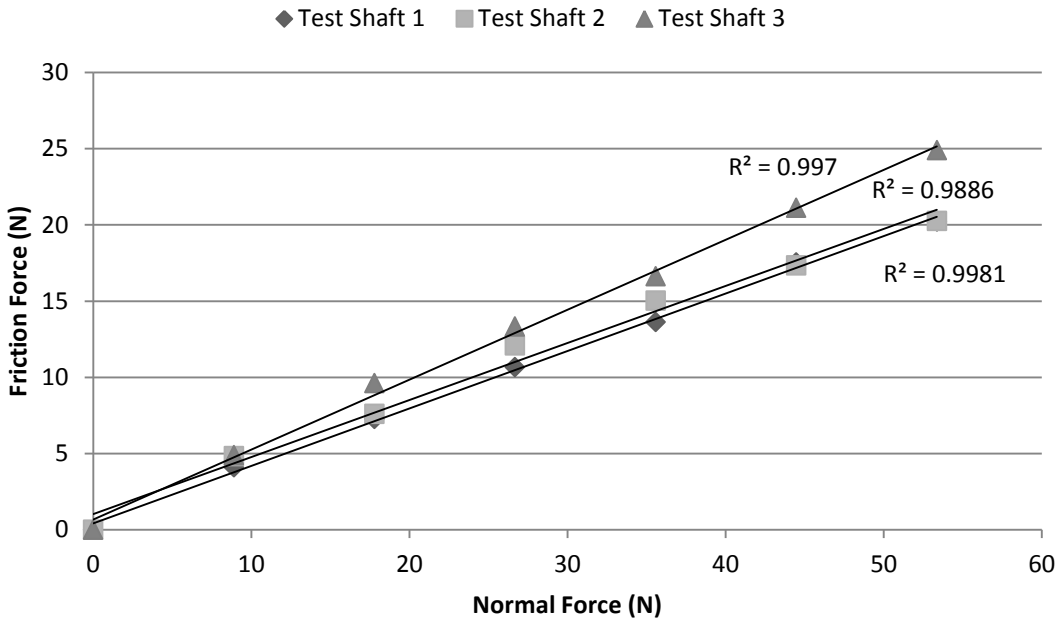

Figure 3-20: Experimental relationship between tangential friction force and normal force

It can be seen from Figure 3-20 that the relationship is mostly linear. This finding eliminated the need for implementing other complicated theoretical relationships between the tangential friction force and normal force that were discussed in the literature review section. Achanta et al. (2010) also found a linear relationship between normal force and tangential force for hard/hard interfaces in macro scale. Based on this, the next step was to show that the same linear relationship exists on coated and uncoated surfaces. Tests were done with normal force varying from 0 to 90N, and rotation speed was kept constant

at 18.75 rpm. It was observed that some data sets had variations and oscillations after about 55N normal force, whereas some were perfectly linear all the way up to 90N normal force. Therefore, the rest of the tests were done at normal forces up to 45N, in order to make sure all the data sets will have a linear relationship. The reason behind this behaviour is thought to be excessive wear on the specimen along with possible machine errors. It is known that wear can create abrasive particles which are very dynamic and can result in increased friction coefficient and some variations (Achanta et al., 2006). While the friction coefficient starts to increase for uncoated specimens in very high normal forces, it decreases for coated specimens tested with high normal forces. The low friction coefficient of DLC coatings in relatively higher normal loads is mostly related to formation of small graphite particles at the contact patch (Achanta & Celis, 2010). An example of an uncoated specimen with nonlinear properties after 55N can be seen in Figure 3-21.

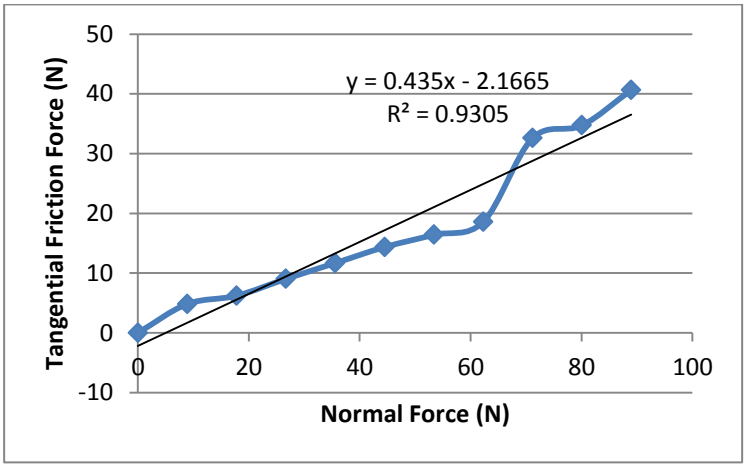

Figure 3-21: Data with nonlinear relationship after about 55N normal force

Two results from different specimens, one that is coated with DLC, and one that is not coated, are shown in Figure 3-22 which also includes linear trendline fitting along with the equation for the linear trendline. The slope of the trendline shows the friction coefficient. In order to quantify the linearity of the data, the R-squared values are shown on the graphs, which is a measure of goodness of fit. A value of 1 would mean a perfect fit to the linear trendline. Both coated and uncoated surfaces have very high R-squared values of 0.9948 and 0.9958 respectively.

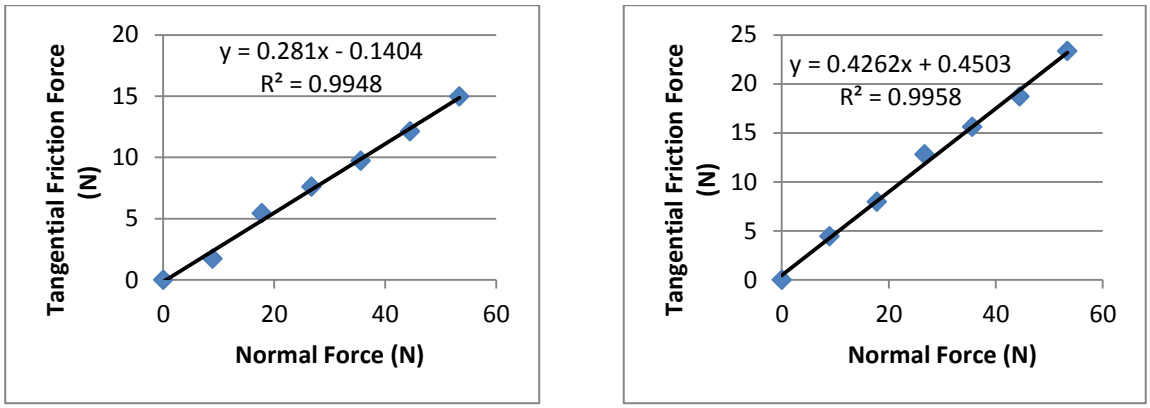

(a) (b)

Figure 3-22: Relation between tangential friction force and normal force on; (a) coated surface, (b) uncoated surface

3.3.3 Friction Measurement Procedure

Two types of tests were done on the specimens. The first test was an increasing normal load test in which the specimen is first rotated with no normal load being applied, and then the test is repeated with normal loads of 8.896, 17.792, 26.688, 35.584 and 44.48 N. During all these tests, the rotation speed was always constant at 18.75 rpm. At each load, 30 current readings were taken, each 1 second apart, to find the average current usage

with that specific normal force. The data from this test was used to calculate the friction coefficient values for comparison of before and after DLC coating. The stainless steel plates that push onto the specimen were sanded and cleaned with alcohol between each test to minimize the effects of wear.

Second test was an increasing speed test. This test was done on the first two specimens in order to observe the effect of increasing rotation speed on friction coefficient. The normal force was kept fixed at 22.241 N and the tests were done at rotation speeds of 11.25, 15, 18.75, 22.5, 26.25, 30 and 30.75 rpm. Similar to the increasing normal load test, 30 current readings were taken at each rotation speed level, in order to find the average current usage at a specific speed. This was then converted into friction coefficient for different speeds.

3.3.4 Uncertainty of Friction Measurement

Before starting the tests on the specimens, the accuracy of the friction measurement method needed to be tested. There were many factors that played a role on the accuracy of the friction coefficient measurement. First factor was the force gauge used on the machine which had an accuracy of ±1 %. Considering that the normal force readings during the tests were changed from 8.896N to 44.48N, the accuracy of the normal force was between ±0.089 N to ±0.445 N. The second factor that played a role on the accuracy of the friction measurement was the step motor rotation speed which had an accuracy of ±5 %. Considering that the rotation speed was kept constant at 18.75 rpm for the increasing normal load test, the accuracy of the rotation speed reading was ±0.9375 rpm.

On the other hand, the rotation speed was changed from 11.25 rpm to 30.75 rpm on the increasing speed test which meant that the accuracy of the speed reading changed from ±0.5620 rpm to ±1.5375 rpm. The third and last factor that played role in the accuracy of the friction coefficient reading was the multimeter that was used to read current data. The multimeter had an accuracy of ±0.06% for the current readings. As the current readings were usually between 1 A to 1.5 A, the accuracy was changing between ±0.0006 A and ±0.0009 A.

The next step was to test the repeatability of the friction measurements. To test this, the 30 current readings at the same normal load level were compared to see the fluctuation in the data. Each current reading was taken 1 second apart and the standard deviation of the readings was found to be 0.003819 A. In all tests, a slight increase in current is observed which is a major part of the standard deviation. The data and this effect can be seen in Figure 3-23. This increase is attributed to polishing effect on the surface during the test. As the surface is polished, roughness is decreased, resulting in an increase in current usage in small scale.

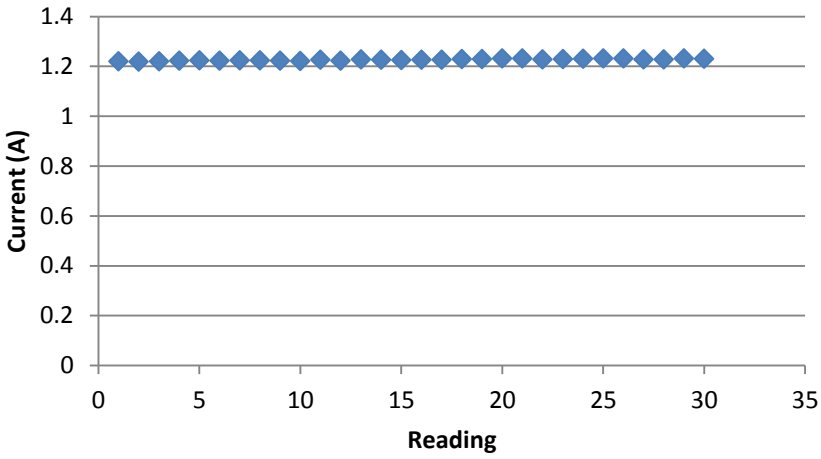

Figure 3-23: Repeatability test for friction measurement

3.4 Specimens

A total of 7 specimens were used to test both roughness and friction coefficient properties and all were 1045 steel. The specimens were coated with DLC half way, and left uncoated on the other half in order to obtain friction and roughness data from both before and after the DLC coating process. All specimens had different surface finishes in order to observe the change in surface roughness after the coating process. Having specimens with different surface roughness properties also helped to observe the possible relation between surface roughness and friction coefficient on DLC coated surfaces. An 8^{th} specimen was also used for calibrating the friction measurement machine and to obtain general data such as the test of linear relationship between tangential friction force and normal force. One of the samples can be seen in Figure 3-24.

Figure 3-24: One of the specimens used for testing

Chapter 4: Results and Discussion

4.1 Roughness Tests

All 7 specimens were tested before the friction tests to find the surface roughness parameters. The 3D average surface roughness value (Sa) was used as it gives a very good representation of the surface. The results of the roughness tests can be seen in Table 4-1.

Table 4-1: Surface roughness data for the specimens that were tested

	Coated (µm)	**Uncoated (µm)**	**Percent Change**
Specimen 1	0.674	1.2236	44.91663942
Specimen 2	0.4178	0.6145	32.00976404
Specimen 3	0.51205	0.8063	36.49386085
Specimen 4	2.1575	4.7780	54.84512348
Specimen 5	0.3085	0.34025	9.33137399
Specimen 6	0.27515	0.29975	8.206839033
Specimen 7	0.3291	0.36555	9.971276159

When the specimens were put in order with respect to the uncoated surface roughness, an interesting result was found. The specimens with rougher surfaces had higher percentage of roughness decrease after the coating process. The change in surface roughness for before and after coating can be seen in Figure 4-1.

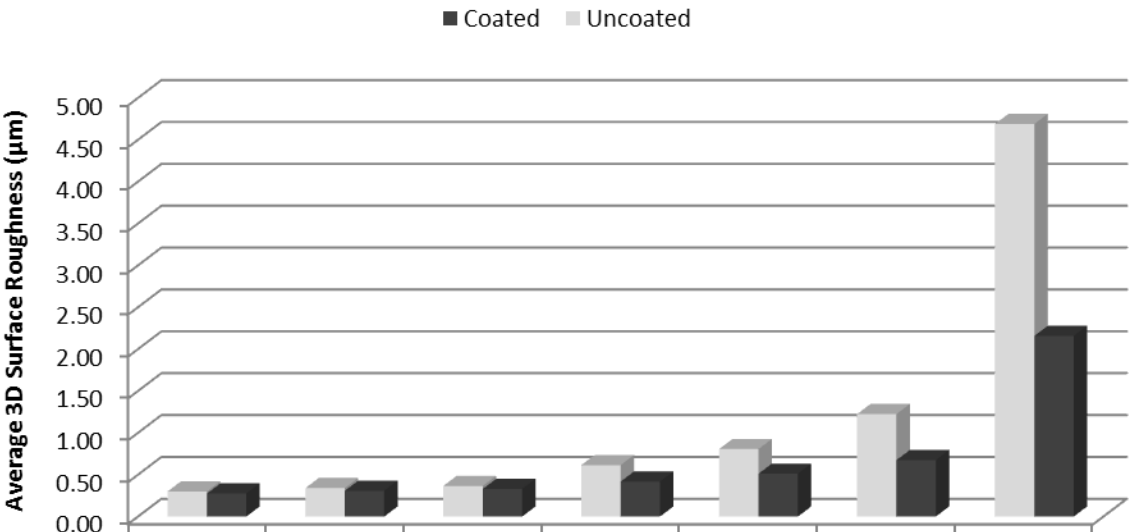

	Specimen 6	Specimen 5	Specimen 7	Specimen 2	Specimen 3	Specimen 1	Specimen 4
Coated	0.27515	0.3085	0.3291	0.4178	0.51205	0.674	2.1575
Uncoated	0.29975	0.34025	0.36555	0.6145	0.8063	1.2236	4.6880

Figure 4-1: Surface roughness change in all 7 specimens in order of increasing uncoated surface roughness

In order to reach the goal of determining the necessary uncoated surface roughness for achieving a certain coated surface roughness, a mathematical relationship must be found between uncoated and coated roughness. Plotting the coated surface roughness with respect to uncoated surface roughness shows that a linear relationship exists between the two values. The slope of the linear graph is higher for specimens with uncoated surface roughness of about 0.3 µm to 0.35 µm compared to specimens with uncoated surface roughness of 0.35 µm to 5 µm. These linear relationships can be used to know what type of surface finish is needed in order to reach a certain surface finish after the coating process which would help minimize the time and money spent on surface finishing. Plots can be seen in Figure 4-2. Both the equation of the linear trendline and the R-squared value for quantifying goodness of fit are shown on the graphs.

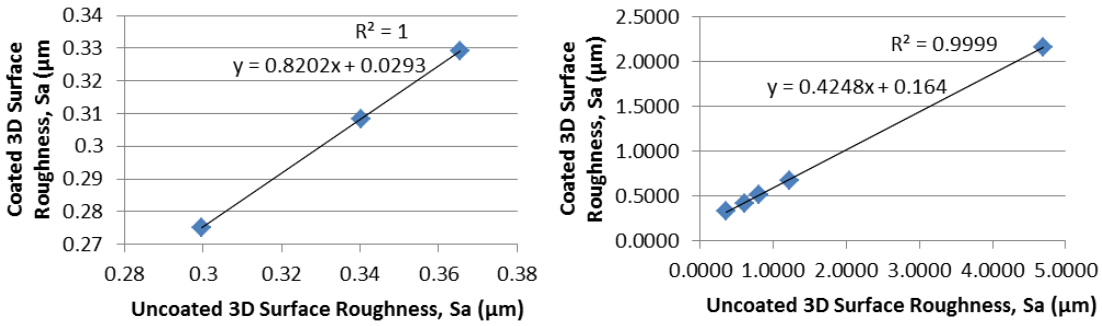

(a) (b)

Figure 4-2: Relationship between and coated surface roughness; (a) 0.3 µm to 0.35 µm, (b) 0.35 µm to 5 µm

Another way of quantifying the decrease in surface roughness is to check the percent change in surface roughness before and after the DLC coating process. The percent change in roughness can also be defined as roughness reduction efficiency (RRE) of DLC coating. RRE can be calculated as follows:

$$RRE = \frac{Uncoated\ Roughness - Coated\ Roughness}{Uncoated\ Roughness}\ x\ 100 \qquad 4\text{-}1$$

Plotting RRE with respect to the uncoated surface roughness shows that rougher surfaces have higher RRE compared to smoother surfaces. The relationship is shown in Figure 4-3.

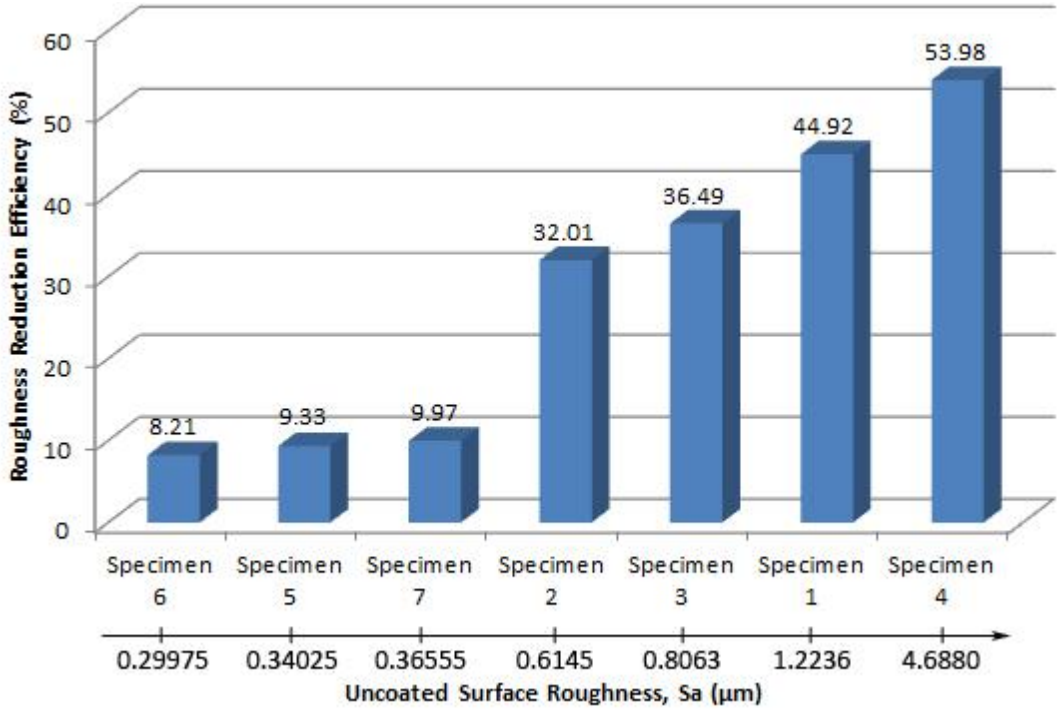

Figure 4-3: Roughness reduction efficiency of all specimens in order of increasing uncoated surface roughness for all specimens.

The closer inspection of the roughness test results show that the relationship between uncoated surface roughness and percent change in surface roughness after DLC coating can be divided into three sections. These three sections can be seen in Figure 4-4.

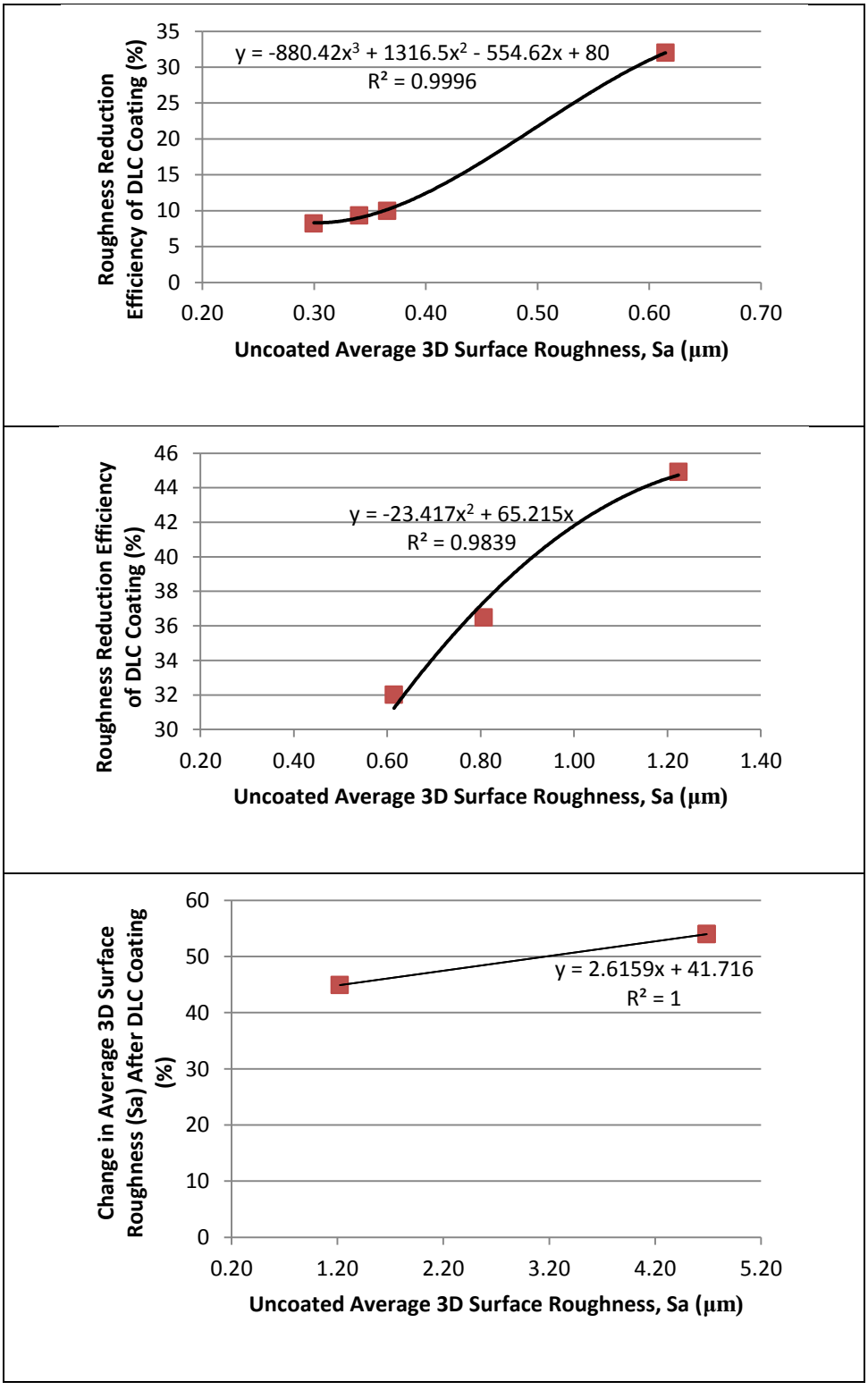

Figure 4-4: Three stages of RRE of DLC coating as a function of uncoated surface roughness

Combining the three sections gives a good idea of the relation between uncoated surface roughness and the RRE of DLC coating. Figure 4-5 covers uncoated surface roughness from 0.3 μm to about 5 μm.

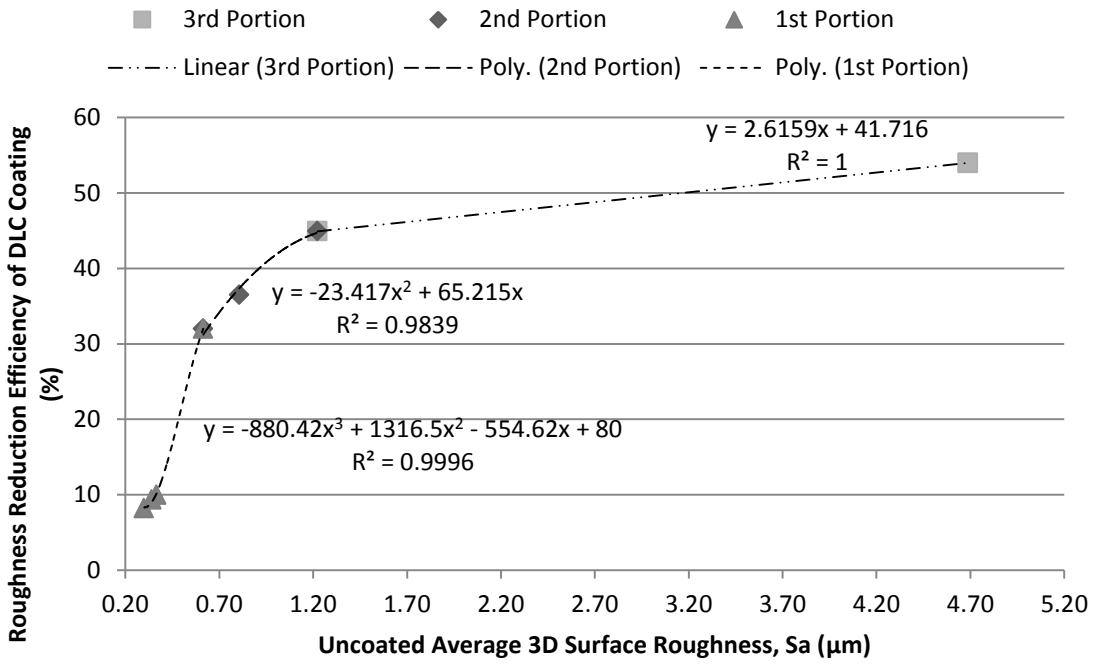

Figure 4-5: Roughness reduction efficiency of DLC coating as a function of uncoated surface roughness

A pattern can be seen in the first and second portions of Figure 4-5. The change in surface roughness is very minimal for specimens with uncoated surface roughness between 0.3 μm and 0.35 μm. However, after about 0.35 μm uncoated surface roughness, the RRE starts to increase significantly until about 1.2 μm uncoated surface roughness where RRE starts to cap off in the second portion of the graph. The first two portions of the graph cover a wide variety of engineering surfaces that are commonly used such as crank shafts on car engines that usually have 0.38 μm surface roughness (Havel, 2009).

Therefore, most of the specimens were taken within this region. The relation between RRE and uncoated surface roughness is a combination of second and third degree polynomial equations. In order to obtain the best fit, the least square of errors fitting criteria was used. The equations for the 2^{nd} and 3^{rd} degree polynomial fitting along with the R-squared value for goodness of fit are shown on the graphs. These equations can be used to estimate what the surface roughness will be like after the DLC coating, given the uncoated surface roughness is known. This is particularly useful for companies that need to coat their products with DLC but need a specific surface finish. By knowing approximately what kind of surface finish they need to provide for a DLC coating process, in order to obtain a set goal of surface roughness, they can avoid spending extra time and money on surface finishing. The last point on the graph which has the highest uncoated surface roughness of about 4.7 μm is an extreme case that was added to the experiments to observe the effect of extreme roughness and is not a roughness amount that would be used on shafts or bearings. As the roughness range in the third portion of Figure 4-5 is beyond the scope of this research, no specimens were prepared in that range to study the relationship of RRE and uncoated surface roughness closely. Therefore, the linear relationship of the third portion just demonstrates the shift in data along the direction of the linear fit as roughness is increased further.

It must be noted that all mathematical relationships are specific to the coating process used for preparing the specimens, including the coating parameters such as bias voltage, ion beam voltage, chamber pressure, gas flow rates etc. This means that if a DLC supplier needs to find such a relationship to tell their customers what kind of surface finish is needed to reach a certain surface roughness goal, they will have to repeat the

experimental methodology described in this research to get the process specific relationship between uncoated surface roughness and percent change in roughness after DLC coating. The relationship can also be modified to accommodate average 2D surface roughness (Ra), which is a commonly used term for surface roughness.

4.2 Friction Tests

4.2.1 Increasing Normal Load Test

In order to obtain the friction coefficient of a specimen, increasing normal load tests were done to plot the tangential friction force with respect to normal force. The slope of these graphs is the friction coefficient. The results can be seen in Table 4-2.

Table 4-2: Friction coefficient data for the specimens that were tested

	Coated	**Uncoated**	**Percent Change**
Specimen 1	0.3202	0.3669	12.72826
Specimen 2	0.281	0.4262	34.06851
Specimen 3	0.2667	0.379	29.63061
Specimen 4	0.4237	0.5628	24.71571
Specimen 5	0.468	0.5545	14.24645
Specimen 6	0.6016	0.6389	5.838159
Specimen 7	0.4547	0.5397	15.74949

When the specimens were put in order with respect to the uncoated surface roughness, an interesting result was found. The friction coefficient seems to be decreasing for both coated and uncoated specimens as the roughness of the surface is increased and it seems to level off around an uncoated surface roughness of about 0.8 μm to 1.2 μm where we observe the lowest friction coefficient. After this point, further increase in uncoated surface roughness results in increase of friction coefficient. The change in friction coefficient for before and after coating can be seen in Figure 4-6.

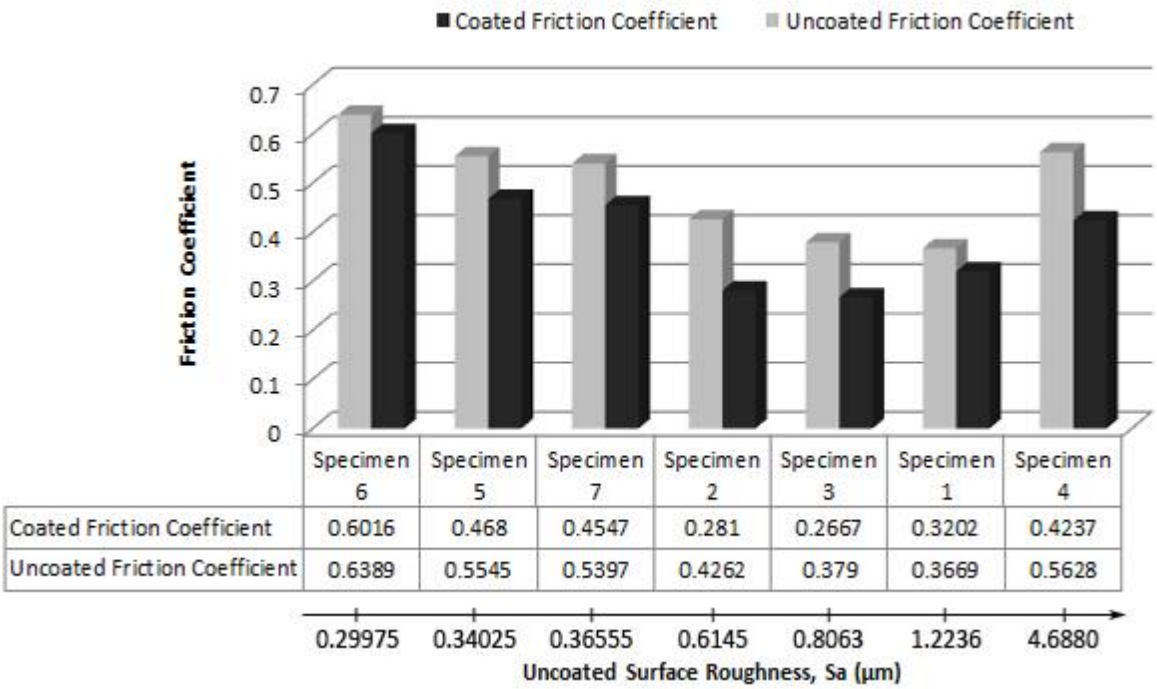

Figure 4-6: Friction coefficient change in all 7 specimens in order of increasing uncoated surface roughness

The decrease in friction coefficient as the surface roughness is increased can be explained by the fact that the contact area between the two surfaces is also decreasing as the roughness increases, resulting in lower friction. The same concept seems to apply for DLC coated surfaces as well. Rough DLC has lower friction coefficient than smooth

DLC. Achanta et al. (2010) also found similar results where rough DLC coating has lower friction coefficient compared to smooth DLC. They believe that the lower friction force in rough DLC is caused by the decrease in contact area. They conclude that decrease in contact area results in less capillary bridges between the two surfaces, which significantly decreases the friction caused by adhesion. According to Achanta et al. (2010), decrease of friction coefficient with increasing surface roughness is only seen on hard-hard interfaces where adhesive friction forces have dominant effect. Schultz (2002) found similar results where increase in surface roughness caused decrease in friction coefficient.

After some point, as the surface roughness is further increased, we observe an increase in friction coefficient. The increase in abrasion friction mechanism between the extremely rough surfaces can be an explanation for the increase in friction coefficient.

Based on finding of this research along with supporting findings from other studies, it can be concluded that adhesion friction mechanism is dominant in hard-hard contacts, especially DLC. However, if the roughness is significantly increased, the abrasion friction mechanism becomes dominant, resulting in increase of friction coefficient.

The percent change in friction coefficient between coated and uncoated surfaces is not linear, similar to the case with roughness change. The change in friction coefficient seems to be largest for specimens with uncoated surface roughness between 0.6 μm and it decreases below 0.6 μm and above 0.8 μm. However, after some point, the percent change starts to increase again as the roughness is increased further. An average friction coefficient reduction of 20% was observed throughout all 7 specimens. The results can be seen in Figure 4-7.

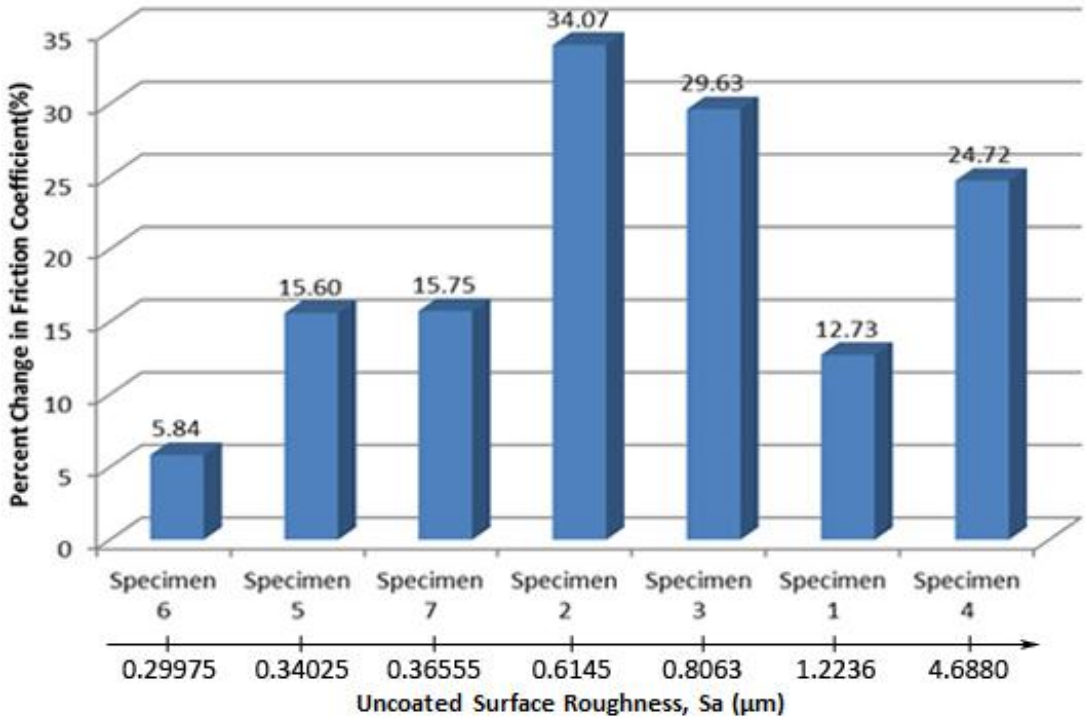

Figure 4-7: Percent change in friction coefficient before and after DLC coating in order of increasing surface roughness.

4.2.2 Combined Results of Roughness Test and Friction Test

In order to determine the uncoated surface roughness that is necessary to reach a certain friction coefficient after DLC coating process, a relationship must be found between the uncoated surface roughness and coated friction coefficient. Plotting the data for coated friction coefficient with respect to uncoated surface roughness gives Figure 4-8 which is named CF-UR graph for easy reference. Similar to previous cases, least square of errors fitting criteria was used to estimate the polynomials that mathematically show the relationship between coated friction coefficient and uncoated surface roughness.

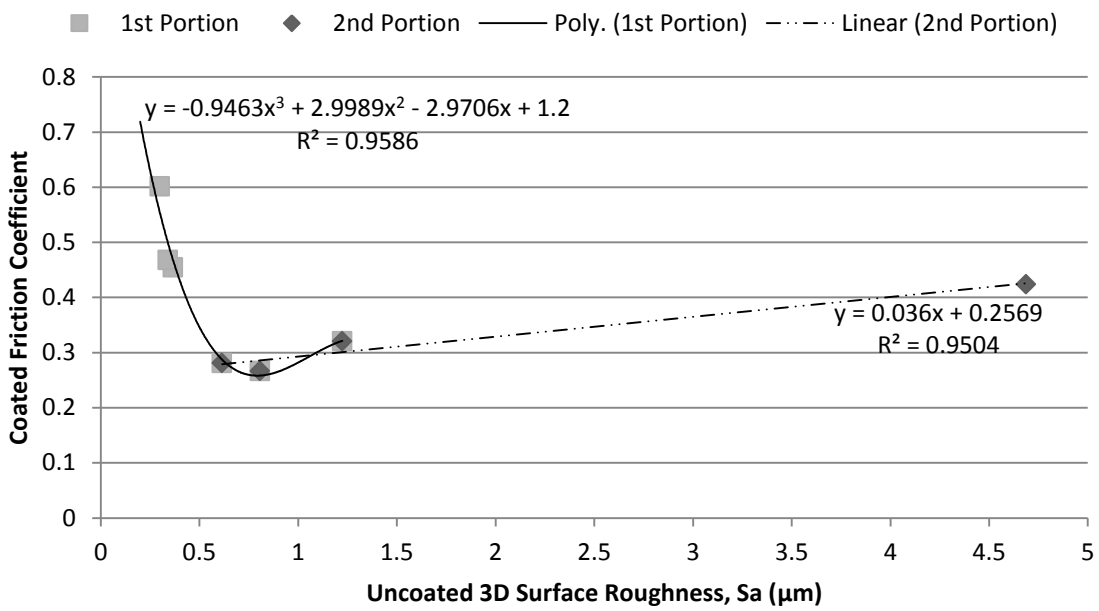

Figure 4-8: Relation between coated friction coefficient and uncoated surface roughness (CF-UR graph)

The data is divided into two sections. The first section, similar to the roughness tests, covers the region of uncoated surface roughness generally used in engineering surfaces on shafts and it shows a pattern that was discussed previously in the chapter where the friction coefficient first decreases with increase in surface roughness; and starts to slowly increase as the surface roughness gets very high. A 2nd order polynomial was used to estimate the relationship between coated friction coefficient and uncoated surface roughness. The last point with significantly high surface roughness was used to show the extreme case, as discussed before. Similar to the case with roughness tests, the second portion of Figure 4-8 shows a shift in data along the direction of the linear fit as the roughness is increased further. Finding the exact behaviour of the relationship in the second region of the graph was outside the scope of this research as shafts used in

industry that are in rotational contact with other parts do not have surface roughness properties that are as high as the second region of the graph.

It must be noted that the relationship between coated friction coefficient and uncoated surface roughness is specific to the DLC coating process that was used to prepare the specimens and changing a single coating parameter might give different polynomials. However, the general shape of the relationship would be the same as can be seen in Figure 4-9 where the relationship between uncoated friction coefficient and uncoated surface roughness, along with coated friction coefficient and coated surface roughness is shown.

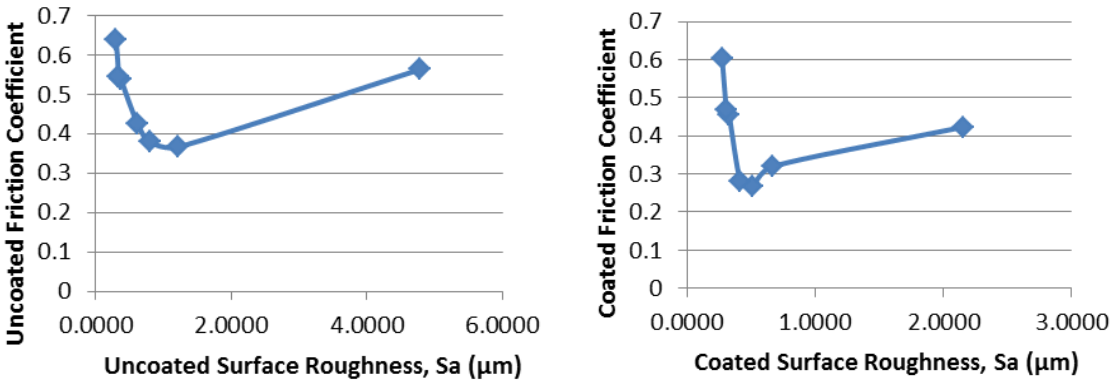

(a) (b)

Figure 4-9: Relationship between friction coefficient and surface roughness; (a) uncoated friction coefficient with respect to uncoated surface roughness, (b) friction coefficient with respect to coated surface roughness

4.2.3 Validation of CF-UR Graph

The experimental CF-UR graph that was introduced in Figure 4-8 can be mathematically estimated by combining the experimental data from relationship between coated roughness and uncoated roughness (CR-UR) and coated friction and coated roughness (CF-CR). This mathematical estimation process is shown in Equation 4-2 and also visualized in Figure 4-10.

$$\begin{matrix} CR = f(UR) \\ CF = g(CR) \end{matrix} \rightarrow CF = g\big(f(UR)\big) \qquad 4\text{-}2$$

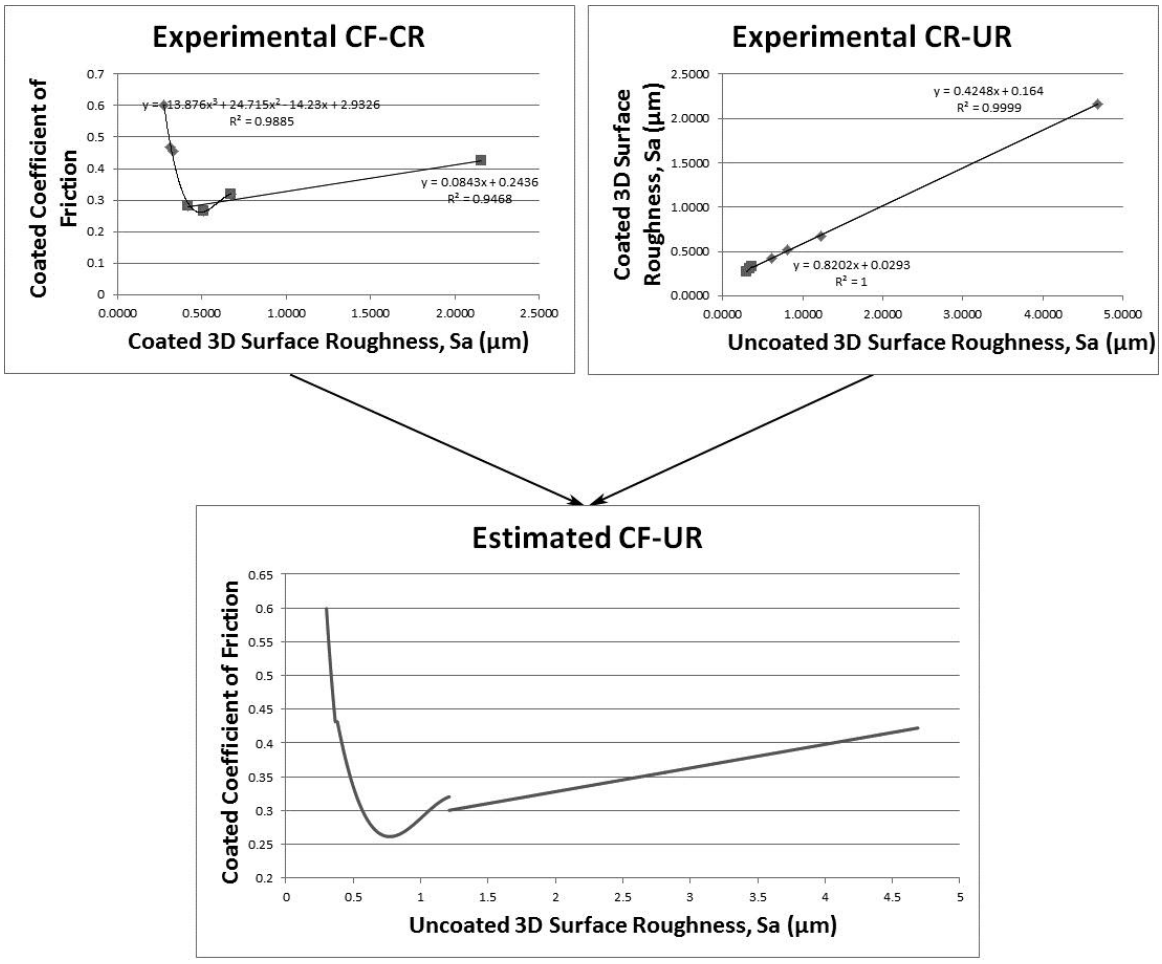

Figure 4-10: Validation of CF-UR Graph

In order to see the effectiveness of the mathematical approximation of the relationship between coated friction coefficient and uncoated surface roughness, the mathematically estimated results and the experimental results can be combined on the same plot which shows the similarity of estimated and experimental relationship of coated friction and uncoated surface roughness. The combined results can be seen in Figure 4-11.

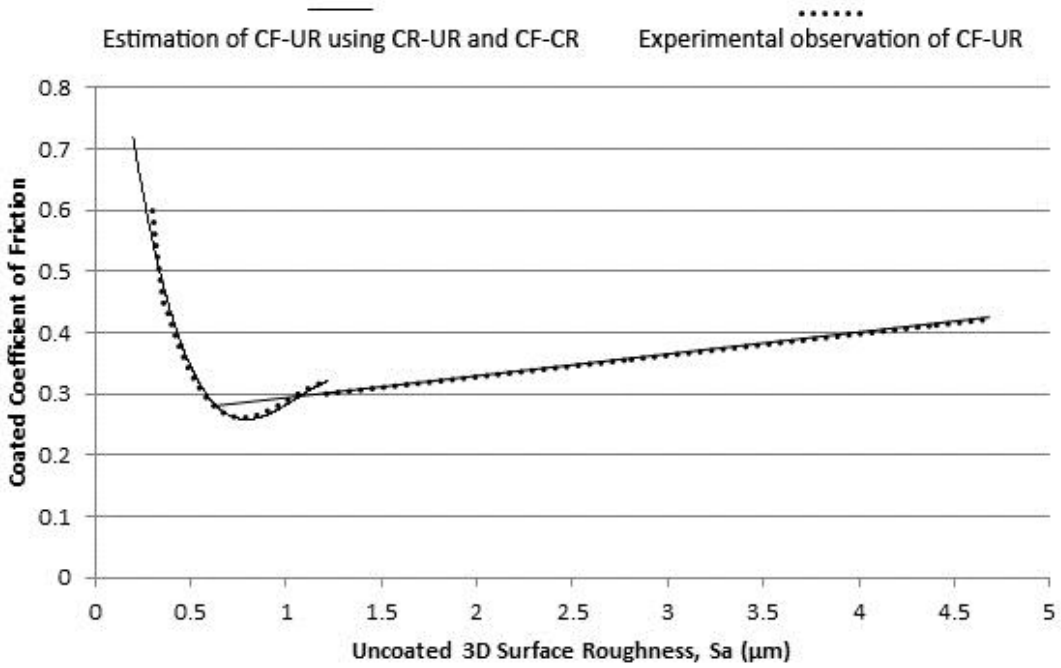

Figure 4-11: Mathematical estimation and experimental observation of CF-UR relationship plotted together

It can be seen from Figure 4-11 that the mathematically estimated relationship between coated friction and coated roughness is almost identical to the experimental observation of the same relationship. This validates the accuracy of the experimental process.

4.2.4 Increasing Speed Test

In order to understand the effect of rotation speed on dry friction, tests were done on both coated and uncoated specimens which showed approximately the same results.

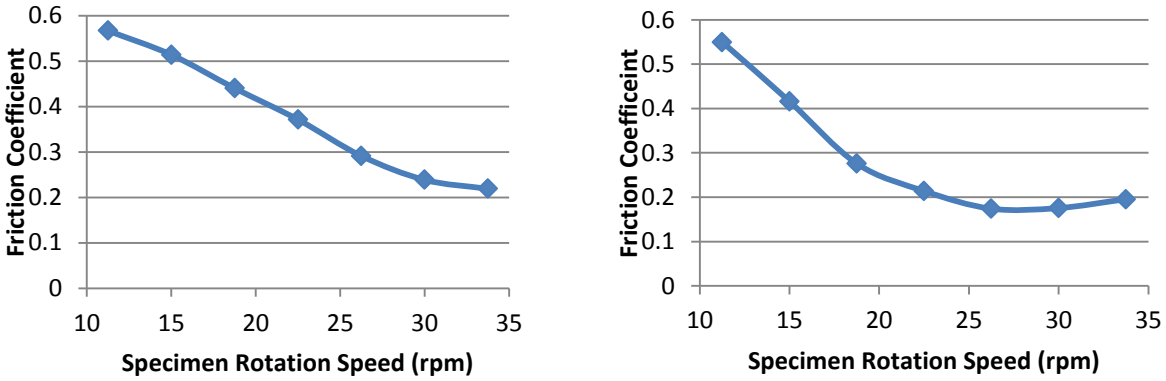

(a) (b)

Figure 4-12: Dependence of friction coefficient on rotation speed, (a) Uncoated specimen, (b) Coated specimen

In one example, the uncoated friction coefficient was decreased from 0.566 to 0.218 while the coated friction coefficient was decreased from 0.549 to 0.195 as the rotation speed was increased from 11.25 rpm to 33.75 rpm. The results can be seen in Figure 4-12.

Chang (2009) also found decrease in friction coefficient as the test speed was increased. The decrease was very minimal in his tests compared to the results we have but it must be kept in mind that the materials, speeds and the experimental method was completely different.

Awrejcewicz and Pyryev (2002) also concluded that as the relative speed is increased, the friction coefficient decreases. However, they showed that the friction coefficient starts to increase after a relative speed of about 0.04 m/s. The maximum rpm of 33.75 that was

used in our tests can be converted to 0.0449 m/s. This is roughly the same relative speed that Awrejcewicz and Pyryev (2002) found friction coefficient to be minimum. Their findings can be seen in figure 4-13.

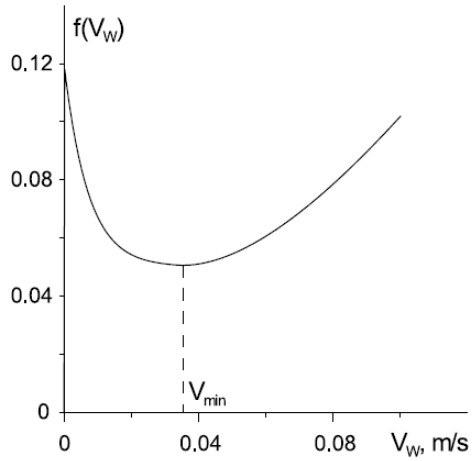

Figure 4-13: Dependence of kinetic friction versus relative velocity (Awrejcewicz & Pyryev, 2002)

Chapter 5: Conclusions and Recommendations

5.1 Conclusions

A model relating roughness of DLC coated surface to its uncoated roughness is developed. Also, relationships between dynamic friction coefficient and surface roughness of uncoated and coated rotating shafts are modelled. Results showed that it is possible to get 2^{nd} and 3^{rd} degree polynomial curves that model the relationship between uncoated surface roughness and coated surface roughness. Furthermore, similar polynomial relationships were found between coated friction coefficient and uncoated roughness. These curves can be used to estimate the required uncoated surface roughness to reach a certain DLC coated surface roughness. Similarly, they can also be used to estimate uncoated surface roughness needed to achieve a desired friction coefficient for the final product after the DLC coating process. Employing the developed models can minimize the amount of time and money spent on surface finishing by companies that need to coat their products with DLC and have a certain target for the final product's surface roughness and/or friction coefficient.

The other development in this research was a systematic approach to develop experimental models based on planed experiments. The experimental methodology described in this thesis can be applied to other DLC coating companies with different DLC coating setups and different coating parameters and using various materials.

The experimental relationship between coated friction coefficient and uncoated surface roughness was in a very good agreement with the mathematical estimation of the same

relationship. This is a reliable validation of suitability in experimental setup and the conducted modelling process. It must be kept in mind that both findings are specific to the coating process. Coating process covers all the variables including the coating methods such as PVD,CVD etc. and coating parameters such as coating time, gas pressures, bias voltage, ion beam voltage, types of sub-layers, chamber vacuum level etc.

The other novel approach described in this thesis is the design and development of the test machine capable of measuring dynamic friction coefficient of rotating shafts. The machine is designed specifically for the purpose of dynamic friction coefficient measurement and it is well employed in completing this research project.

Understanding the surface finish requirement as well as estimating the final surface roughness and the dynamic friction coefficient of the rotating shafts provides valuable sources of information to manufacturers in variety of industrial sectors, particularly in automotive industry.

5.2 Recommendations

Future work can be done to firstly improve the accuracy of the friction measurement device. Even though tests and improvements of the machine were conducted continuously over months, there is always room for improvement.

The developed systematic approach and the experimental modelling procedure can be employed by other DLC coating providers with different DLC coating methods and

setups with variation of process parameters. The same methodology can also be used for understanding and modelling the behaviour of different materials under DLC coating.

In addition to that, the number of specimens might be increased to cover the range of surface roughness values that were not covered within this research. This can also prove the accuracy of the findings of this research.

Another aspect of friction that can be tested in the future is the effect of lubrication on dynamic friction coefficient of DLC coated surfaces. The developed friction testing machine can be used to test rotating shafts under lubricated conditions and to compare the results of dry friction and lubricated friction.

References

Achanta, S., Drees, D. et al. (2006) A new tool for industrial tribology filling the gap between macro and nano tribology. *Tribotest*, 11 (2), 137-149.

Achanta, S., Celis, J.-P. (2010). On the scale dependence of coefficient of friction in unlubricated sliding contacts. *Wear*, 269, 435-442.

Ai-hia, L. (2009). Frictional contact analysis of turbocharger compressor-shaft sleeve-shaft. *International Conference on Measuring Technology and Mechatronics Automation*, 817-820

Amontons, G. (1699). De la résistance causée dans les machines. *Mém. De l'Académie Royale*, A, 275–282.

Athey, R. D. (2010). An overview of coatings technology. *Metal Finishing*, 108(11-12), 74-77

Awrejcewicz, J., Pyryev, Y. (2002). Thermoelastic contact of a rotating shaft with a rigid bush in conditions of bush wear and stick-slip movements. *International Journal of Engineering Science*, 40, 1113-1130.

Barari, A., ElMaraghy, H. A. and Knopf, G. K. (2007). Search-guided sampling to reduce uncertainty of minimum zone estimation. *Journal of Computing and Information Science in Engineering*, 7(4), 360-371.

Bengisu, M. T., Akay, A. (1997). Relation of dry-friction to surface roughness. *Journal of Tribology*, 119, 18-25.

Borodich, F. M., Korach, C. S., Keer, L. M. (2007). Modeling the tribochemical aspects of friction and gradual wear of diamond-like-carbon films. *Journal of Applied Mechanics.* ASME, 74, 23-30.

Brenner, D. W. (1990). Empirical potential for hydrocarbons for use in simulating the chemical vapor deposition of diamond films. *Physical Review B.* 42(15), 9458-9471.

Chang, W. (1998). The effect of surface roughness on dynamic friction between neolite and quarry tile. *Safety Science,* 29, 89-105.

Coulomb, C. A. (1821). Theorie des Machines Simples, en Ayant égard au Frottement de Leurs Parties et à la Roideur des Cordages. Bachelier, Paris.

Derjaguin, B. (1934). Molekulartheorie der äußeren Reibung. *Z. Phys,* 88, 661–164.

Donnet, C., Erdemir, A. (2008). Diamond like carbon films: a historical overview. *Tribology of diamond like carbon films: fundamentals and applications, Springer,* 1-10.

Erdemir, A., Bindal, G.R., et al. (1995) Friction and wear properties of smooth diamond films grown in fullerene + argon plasmas. *Diamond and Related Materials,* 5, 923-931

Fontaine, J., Donnet, C., Erdemir, A. (2008). Funtamentals of the tribology of DLC coatings. *Tribology of diamond like carbon films: fundamentals and applications,* Springer, 139-154.

Gavrilov, N.V., Mamaev, A.S., Plotnikov, S.A., et al. (2010). Comparison testing of diamond-like a-C:H coatings prepared in plasma cathode-based gas discharge and ta-C coatings deposited by vacuum arc. *Surface & Coatings Technology,* 204, 4018-4024.

Havel, J. (2009). Crankshaft surface finish. *Engine Professional, July-Sept 2009,* 52-54.

Heau, C. (2008). DLC films in mechanical and manufacturing industry. *Tribology of diamond like carbon films: fundamentals and applications,* Springer, 139-154.

Huang, L., Lu, J. and Xu, K. (2003). Investigation of the relation between structure and mechanical properties of hydrogenated diamond-like carbon coatings prepared by PECVD. *Materials science and engineering,* A (373), 45-53.

Hughes, R. C., James, D. I. (2002). The Hughes gauge: a new method for measuring coefficient of friction. *Polymer testing,* 21. 39-42

ISO 25178-2 (2012). Geometrical product specifications (GPS) - Surface texture: Areal -- Part 2: Terms, definitions and surface texture parameters

Jewett, S. (2004). Physics for Scientists and Engineers, *6th Edition*. Belmont: Thomson Learning. Print.

Lemoine, P., Quinn, J. P., et al. (2008). Mechanical characterisation and properties of DLC films. *Tribology of diamond like carbon films: fundamentals and applications,* Springer, 83-101.

Liu, D., Benstetter, G., Lodermeier, E. et al. (2003). SPM investigation of diamond-like carbon and carbon nitride films. *Surface and coating technology,* 172, 194-203.

Liu, D., Liu, Y. and Chen, B. (2006). Surface roughness of various diamond-like carbon films. *Plasma science and technology,* 8 (6), 701-707.

Mordo, S., Popravko, V., Barari, A. (2013). Study of the effect of coating parameters and substrate on 3D surface roughness in Diamond-Like-Carbon coating process. *Manufacturing, modelling, management and control,* 7(1), 1861-1866.

Müser, M. H., Campana, C. (2005). A theoretical study of superlubricity and the role of the roughness exponent. *World Tribology Congress III,* 2pp.

Müser, M. H. (2006). Theory of simulation of friction and lubrication. *Lecture Notes Physics.* Springer. 704, 65-104.

Müser, M. H. (2011). Velocity dependence of kinetic friction in the Prandtl-Tomlinson model. *Physical Review.* B (24), 13pp.

Paleu, V., Cretu, S., et al. (2004). Test rig for friction torque measurement in rolling bearings. *The annuals of university "Dunarea De Jos" of Galati Fascicle VIII, Tribology.* 85-91

Park, S.J., Lee, K.R. and Ko, D.H. (2005). Tribological behaviour of nano-undulated surface of diamond-like carbon films. *Diamond and related materials,* 14, 1291-1296.

Plath, S., Meyer, S. et al. (2005). Friction torque of a rotary shaft lip type seal – a comparison between test results and finite element simulation. *Mechanika,* 4 (54), 55-59.

Robertson, J. (2008). Classification of diamond like carbons. *Tribology of diamond like carbon films: fundamentals and applications.* Springer. 13-24.

Robbins, M. O., Müser, M. H. (2001). Computer simulations of friction, lubrication and wear. *Handbook of Modern Tribology.* CRC Press. 717-765

Saha, B., Liu, E., Tor, S.B. et al. (2009). Anti-sticking behaviour of DLC-coated silicon micro-molds. *Journal of Micromechanics and Microengineering.* 19(10),7pp.

Saha, B., Liu, E., Tor, S.B. et al. (2011). Modification of surface properties of silicon micro-molds by nitrogen and silicon doped diamond-like carbon deposited with magnetron co-sputtering. *Vacuum,* 85, 1105-1107.

Salvadori, M.C., Martins, D.R. and Cattani, M. (2006). DLC coating roughness as a function of film thickness. *Surface Coatings Technology*, 200, 5119-5122.

Scharf, T. W., Singer, I. L. (2008). Third bodies and tribochemistry of DLC coatings. *Tribology of diamond like carbon films: fundamentals and applications, Springer,* 201-236.

Schultz, M. P. (2002). The relationship between frictional resistance and roughness for surfaces smoothed by sanding. *Journal of Fluids Engineering*, 124, 18-25.

Silvestri, M., Prati, E., Tasora, A. (2006) Radial lip seal efficiency under dynamic operating conditions. *International Conference on Tribology.*

Sui, J. H., Cai, W., Liu, L.H., et al. (2006). Surface characteristics and electrochemical corrosion behaviour of NiTi coated with diamond-like carbon. *Materials Science and Engineering*, A (438), 639-642.

Stoudt, M. R., Hubbard, J.B. et al. (2006). Evaluating the relationships between surface roughness and friction behaviour during metal forming. *SAE international journal of materials and manufacturing. 114(5), 183-190.*

Tomlinson, G. A. (1929). A Molecular Theory of Friction. *Philos. Mag. Ser*. 7, 7, 905–939.

Van der Donck, T., Muchlado, M. et al. (2009). Effect of hydrogen content in a-C:H coatings on their tribological behaviour at room temperature up to 150 °C. *Surface Coating Technology*. 203, 3472-3479.

Wasche, R., Klaffe, D. (2008). Tribology of DLC films under fretting conditions. *Tribology of diamond like carbon films: fundamentals and applications, Springer,* 362-382.

Xu, X., Hu, H. (2009). Development of non-contact surface roughness measurement in last decades. *2009 International conference on measuring technology and mechatronics automation.* Zhangjiajie, Hunan, China 11-12. Piscataway, NJ, USA: IEEE.

Zhang, S., Wagner, G., et al.(2004). Experimental and molecular dynamics simulation studies of friction behavior of hydrogenated carbon films. *Surface & Coatings Technology*. 818-823.

Zhou, Z. F., Li, K. Y., et al. (2005) Study of tribological performance of ECR-CVD diamond like carbon coatings on steel substrates Part 1. The effect of processing parameters and operating conditions. *Wear.* 258, 1577-1588

Zhou, Z. F., Li, K. Y., et al. (2005) Study of tribological performance of ECR-CVD diamond like carbon coatings on steel substrates Part 2. The analysis of wear mechanism. *Wear.* 258, 1589-1599

Appendix 1: Sample Data for Surface Roughness Analysis

Table A.1.1: Sample data for surface roughness analysis

Reading	Uncoated Average Surface Roughness, Sa (µm)	Coated Average Surface Roughness, Sa (µm)
1	1.06	0.81
2	0.975	0.665
3	0.853	0.546
4	1.43	0.599
5	1.23	0.646
6	2.17	0.646
7	0.935	1.09
8	0.862	0.892
9	1.09	0.907
10	1.25	0.72
11	0.804	0.803
12	1.09	0.754
13	1.04	0.571
14	1.25	0.605
15	1.32	0.586
16	1.82	0.45
17	1.19	0.47
18	1.88	0.529
19	1.23	0.534
20	0.993	0.657
Average	**1.2236**	**0.674**

Appendix 2: Sample Data for Friction Coefficient Analysis

A.2.1 Increasing Normal Load Test

Table A.2.1: Sample data for friction coefficient analysis

	Current Readings at different normal force levels (A)					
Reading	**0N**	**8.896N**	**17.792N**	**26.688N**	**35.584N**	**44.48N**
1	1.228	1.244	1.252	1.225	1.274	1.273
2	1.232	1.243	1.255	1.26	1.272	1.28
3	1.234	1.243	1.251	1.266	1.272	1.281
4	1.234	1.244	1.255	1.266	1.274	1.278
5	1.233	1.247	1.257	1.265	1.274	1.28
6	1.235	1.242	1.255	1.263	1.271	1.28
7	1.233	1.244	1.255	1.267	1.275	1.28
8	1.234	1.249	1.259	1.266	1.277	1.278
9	1.238	1.246	1.255	1.266	1.274	1.284
10	1.235	1.248	1.256	1.268	1.274	1.28
11	1.236	1.248	1.257	1.27	1.277	1.285
12	1.237	1.247	1.259	1.267	1.275	1.286
13	1.236	1.247	1.261	1.271	1.274	1.284
14	1.238	1.248	1.26	1.267	1.279	1.284
15	1.243	1.247	1.263	1.267	1.279	1.287
16	1.24	1.249	1.263	1.27	1.278	1.284
17	1.236	1.252	1.261	1.273	1.279	1.288
18	1.24	1.249	1.258	1.272	1.278	1.289
19	1.242	1.25	1.262	1.271	1.279	1.285
20	1.242	1.251	1.263	1.272	1.278	1.286
21	1.24	1.249	1.265	1.27	1.28	1.287
22	1.242	1.247	1.263	1.271	1.28	1.285
23	1.242	1.252	1.264	1.276	1.28	1.284
24	1.244	1.253	1.264	1.275	1.281	1.287
25	1.241	1.251	1.262	1.274	1.281	1.288
26	1.242	1.252	1.266	1.275	1.28	1.286
27	1.24	1.253	1.265	1.276	1.281	1.288
28	1.244	1.251	1.266	1.273	1.279	1.289
29	1.24	1.251	1.267	1.277	1.281	1.286
30	1.24	1.256	1.266	1.278	1.283	1.286
Average	**1.238033**	**1.248433**	**1.260167**	**1.268567**	**1.2773**	**1.283933**

Table A.2.2: Sample data for friction coefficient analysis

	Tangential Friction Force at different normal force levels (N)					
Reading	**0N**	**8.896N**	**17.792N**	**26.688N**	**35.584N**	**44.48N**
1	0	6.159689	9.239534	-1.15494	17.70911	17.32413
2	0	4.234786	8.854553	10.77946	15.39922	18.47907
3	0	3.464825	6.54467	12.31938	14.62926	18.09409
4	0	3.849806	8.084592	12.31938	15.39922	16.93915
5	0	5.389728	9.239534	12.31938	15.7842	18.09409
6	0	2.694864	7.699612	10.77946	13.8593	17.32413
7	0	4.234786	8.469573	13.08934	16.16918	18.09409
8	0	5.774709	9.624514	12.31938	16.55416	16.93915
9	0	3.079845	6.54467	10.77946	13.8593	17.70911
10	0	5.004747	8.084592	12.70436	15.01424	17.32413
11	0	4.619767	8.084592	13.08934	15.7842	18.86405
12	0	3.849806	8.469573	11.54942	14.62926	18.86405
13	0	4.234786	9.624514	13.47432	14.62926	18.47907
14	0	3.849806	8.469573	11.16444	15.7842	17.70911
15	0	1.539922	7.699612	9.239534	13.8593	16.93915
16	0	3.464825	8.854553	11.54942	14.62926	16.93915
17	0	6.159689	9.624514	14.24428	16.55416	20.01899
18	0	3.464825	6.92965	12.31938	14.62926	18.86405
19	0	3.079845	7.699612	11.16444	14.24428	16.55416
20	0	3.464825	8.084592	11.54942	13.8593	16.93915
21	0	3.464825	9.624514	11.54942	15.39922	18.09409
22	0	1.924903	8.084592	11.16444	14.62926	16.55416
23	0	3.849806	8.469573	13.08934	14.62926	16.16918
24	0	3.464825	7.699612	11.9344	14.24428	16.55416
25	0	3.849806	8.084592	12.70436	15.39922	18.09409
26	0	3.849806	9.239534	12.70436	14.62926	16.93915
27	0	5.004747	9.624514	13.8593	15.7842	18.47907
28	0	2.694864	8.469573	11.16444	13.47432	17.32413
29	0	4.234786	10.39448	14.24428	15.7842	17.70911
30	0	6.159689	10.00949	14.62926	16.55416	17.70911
Average	**0**	**4.003798**	**8.520903**	**11.75474**	**15.1169**	**17.67061**

A.2.2 Increasing Speed Test

Table A.2.3: Sample data for current readings in increasing speed test

Speed	11.25 rpm		15 rpm		18.75 rpm	
Normal Load	0 N	5 N	0 N	5 N	0 N	5 N
1	1.212	1.238	1.225	1.263	1.237	1.264
2	1.212	1.242	1.225	1.263	1.238	1.27
3	1.213	1.243	1.23	1.268	1.236	1.275
4	1.215	1.243	1.23	1.272	1.243	1.272
5	1.213	1.247	1.228	1.267	1.241	1.277
6	1.216	1.243	1.231	1.267	1.239	1.283
7	1.221	1.244	1.23	1.275	1.243	1.28
8	1.219	1.248	1.233	1.263	1.243	1.281
9	1.215	1.247	1.231	1.269	1.239	1.28
10	1.218	1.247	1.231	1.276	1.246	1.29
11	1.219	1.252	1.233	1.275	1.245	1.286
12	1.221	1.248	1.235	1.27	1.243	1.283
13	1.22	1.248	1.234	1.27	1.248	1.29
14	1.22	1.251	1.234	1.266	1.244	1.287
15	1.221	1.25	1.234	1.267	1.244	1.287
16	1.22	1.252	1.235	1.278	1.246	1.293
17	1.225	1.251	1.236	1.274	1.246	1.287
18	1.222	1.254	1.236	1.267	1.246	1.288
19	1.221	1.255	1.238	1.278	1.246	1.292
20	1.222	1.254	1.236	1.277	1.249	1.282
21	1.225	1.262	1.236	1.277	1.246	1.284
22	1.227	1.258	1.239	1.271	1.249	1.292
23	1.222	1.255	1.238	1.277	1.25	1.287
24	1.222	1.259	1.238	1.274	1.248	1.29
25	1.225	1.259	1.238	1.276	1.246	1.299
26	1.226	1.26	1.239	1.282	1.25	1.292
27	1.222	1.262	1.239	1.279	1.251	1.289
28	1.227	1.257	1.238	1.276	1.248	1.295
29	1.228	1.265	1.24	1.276	1.25	1.299
30	1.228	1.266	1.238	1.275	1.251	1.298
Average	1.2206	1.252	1.2343	1.2723	1.245	1.2857

Table A.2.4: Sample data for current readings in increasing speed test

Speed	22.5 rpm		26.25 rpm		30 rpm		30.75 rpm	
Normal Load	0 N	5 N	0 N	5 N	0 N	5 N	0 N	5 N
1	1.25	1.283	1.234	1.285	1.134	1.171	0.998	1.039
2	1.25	1.272	1.237	1.286	1.137	1.172	0.997	1.05
3	1.245	1.292	1.239	1.288	1.134	1.171	1.009	1.037
4	1.251	1.294	1.238	1.301	1.138	1.171	1.003	1.039
5	1.252	1.288	1.239	1.301	1.136	1.174	1.006	1.034
6	1.256	1.302	1.237	1.293	1.138	1.172	1.007	1.05
7	1.252	1.291	1.242	1.287	1.136	1.173	1.006	1.045
8	1.249	1.303	1.241	1.29	1.139	1.172	1.012	1.032
9	1.255	1.288	1.236	1.284	1.139	1.171	1.003	1.048
10	1.257	1.296	1.237	1.278	1.136	1.174	1.007	1.044
11	1.257	1.291	1.242	1.28	1.136	1.171	1.007	1.034
12	1.25	1.29	1.239	1.275	1.139	1.173	1.005	1.05
13	1.255	1.291	1.242	1.278	1.137	1.173	1.002	1.042
14	1.254	1.298	1.238	1.277	1.139	1.173	1.002	1.041
15	1.257	1.288	1.242	1.275	1.138	1.17	1.001	1.032
16	1.252	1.293	1.245	1.275	1.14	1.174	1.003	1.042
17	1.256	1.304	1.244	1.275	1.138	1.173	1.001	1.046
18	1.259	1.297	1.239	1.273	1.139	1.173	1.003	1.036
19	1.255	1.308	1.241	1.27	1.138	1.175	1.001	1.037
20	1.258	1.301	1.243	1.274	1.139	1.174	1.001	1.047
21	1.26	1.297	1.243	1.269	1.137	1.171	1.002	1.031
22	1.256	1.313	1.243	1.273	1.14	1.173	1.001	1.038
23	1.26	1.303	1.245	1.27	1.138	1.176	0.997	1.047
24	1.257	1.298	1.242	1.27	1.138	1.176	1.005	1.034
25	1.261	1.304	1.246	1.275	1.139	1.176	1.008	1.045
26	1.258	1.293	1.244	1.273	1.14	1.175	1.005	1.033
27	1.262	1.314	1.244	1.273	1.139	1.174	1.012	1.042
28	1.258	1.298	1.245	1.273	1.141	1.175	1.007	1.05
29	1.259	1.296	1.245	1.271	1.138	1.175	1.006	1.033
30	1.259	1.31	1.241	1.272	1.138	1.176	1.014	1.046
Average	1.2553	1.2965	1.2411	1.2788	1.1379	1.1732	1.0044	1.0408

Table A.2.5: Sample data for friction force in increasing speed test

Friction Force						
11.25 rpm	15 rpm	18.75 rpm	22.5 rpm	26.25 rpm	30 rpm	30.75 rpm
10.4265	11.42905	6.496514	6.61682	8.765138	5.564144	5.480242
12.03058	11.42905	7.699572	4.411213	8.421407	5.26338	7.084215
12.03058	11.42905	9.383854	9.423956	8.421407	5.564144	3.742604
11.22854	12.63211	6.977737	8.621917	10.82752	4.962615	4.81192
13.63466	11.72982	8.662019	7.218349	10.65566	5.714526	3.742604
10.82752	10.82752	10.58691	9.223446	9.624465	5.112997	5.747571
9.223446	13.5344	8.90263	7.819878	7.733945	5.564144	5.212913
11.62956	9.022936	9.143242	10.82752	8.421407	4.962615	2.673289
12.83262	11.42905	9.865077	6.61682	8.249542	4.812233	6.014899
11.62956	13.5344	10.58691	7.819878	7.046484	5.714526	4.945584
13.23364	12.63211	9.865077	6.81733	6.530887	5.26338	3.60894
10.82752	10.52676	9.624465	8.020388	6.187156	5.112997	6.014899
11.22854	10.82752	10.10569	7.218349	6.187156	5.413762	5.346577
12.4316	9.624465	10.3463	8.822427	6.702753	5.112997	5.212913
11.62956	9.92523	10.3463	6.215801	5.67156	4.812233	4.143597
12.83262	12.93288	11.30875	8.220898	5.155964	5.112997	5.212913
10.4265	11.42905	9.865077	9.624465	5.327829	5.26338	6.014899
12.83262	9.323701	10.10569	7.619368	5.843425	5.112997	4.410926
13.63466	12.03058	11.06814	10.62701	4.984098	5.564144	4.81192
12.83262	12.33135	7.940184	8.621917	5.327829	5.26338	6.148564
14.83772	12.33135	9.143242	7.418859	4.468502	5.112997	3.876269
12.4316	9.624465	10.3463	11.42905	5.155964	4.962615	4.945584
13.23364	11.72982	8.90263	8.621917	4.296636	5.714526	6.683222
14.83772	10.82752	10.10569	8.220898	4.812233	5.714526	3.876269
13.63466	11.42905	12.75242	8.621917	4.984098	5.564144	4.945584
13.63466	12.93288	10.10569	7.017839	4.984098	5.26338	3.742604
16.04078	12.03058	9.143242	10.4265	4.984098	5.26338	4.009933
12.03058	11.42905	11.30875	8.020388	4.812233	5.112997	5.747571
14.83772	10.82752	11.78997	7.418859	4.468502	5.564144	3.60894
15.23874	11.12829	11.30875	10.22599	5.327829	5.714526	4.277262
12.60538	11.42905	9.792894	8.260999	6.479328	5.308494	4.869841

Table A.2.6: Sample data for friction coefficient in increasing speed test

Friction Coefficient						
11.25 rpm	15 rpm	18.75 rpm	22.5 rpm	26.25 rpm	30 rpm	30.75 rpm
0.468794	0.513871	0.292095	0.297504	0.394096	0.250174	0.246402
0.540917	0.513871	0.346187	0.198336	0.378642	0.236651	0.318519
0.540917	0.513871	0.421915	0.423718	0.378642	0.250174	0.168274
0.504856	0.567963	0.313732	0.387657	0.486825	0.223128	0.216353
0.613039	0.527394	0.38946	0.32455	0.479098	0.256935	0.168274
0.486825	0.486825	0.476007	0.414703	0.432733	0.22989	0.258421
0.414703	0.608531	0.400278	0.351596	0.347732	0.250174	0.234382
0.522886	0.405688	0.411097	0.486825	0.378642	0.223128	0.120196
0.576978	0.513871	0.443552	0.297504	0.370914	0.216367	0.270441
0.522886	0.608531	0.476007	0.351596	0.316823	0.256935	0.222362
0.595008	0.567963	0.443552	0.306519	0.29364	0.236651	0.162264
0.486825	0.473302	0.432733	0.360611	0.278186	0.22989	0.270441
0.504856	0.486825	0.45437	0.32455	0.278186	0.243413	0.240392
0.558947	0.432733	0.465188	0.396672	0.301368	0.22989	0.234382
0.522886	0.446256	0.465188	0.279474	0.255004	0.216367	0.186304
0.576978	0.581485	0.508462	0.369626	0.231821	0.22989	0.234382
0.468794	0.513871	0.443552	0.432733	0.239549	0.236651	0.270441
0.576978	0.41921	0.45437	0.342581	0.262731	0.22989	0.198323
0.613039	0.540917	0.497643	0.47781	0.224094	0.250174	0.216353
0.576978	0.55444	0.357005	0.387657	0.239549	0.236651	0.276451
0.667131	0.55444	0.411097	0.333565	0.200912	0.22989	0.174284
0.558947	0.432733	0.465188	0.513871	0.231821	0.223128	0.222362
0.595008	0.527394	0.400278	0.387657	0.193185	0.256935	0.30049
0.667131	0.486825	0.45437	0.369626	0.216367	0.256935	0.174284
0.613039	0.513871	0.573372	0.387657	0.224094	0.250174	0.222362
0.613039	0.581485	0.45437	0.315535	0.224094	0.236651	0.168274
0.721222	0.540917	0.411097	0.468794	0.224094	0.236651	0.180294
0.540917	0.513871	0.508462	0.360611	0.216367	0.22989	0.258421
0.667131	0.486825	0.530098	0.333565	0.200912	0.250174	0.162264
0.685161	0.500348	0.508462	0.459779	0.239549	0.256935	0.192313
0.56676	0.513871	0.440306	0.371429	0.291322	0.238679	0.218957

Appendix 3: Engineering Drawings of the Friction Coefficient Measurement Device

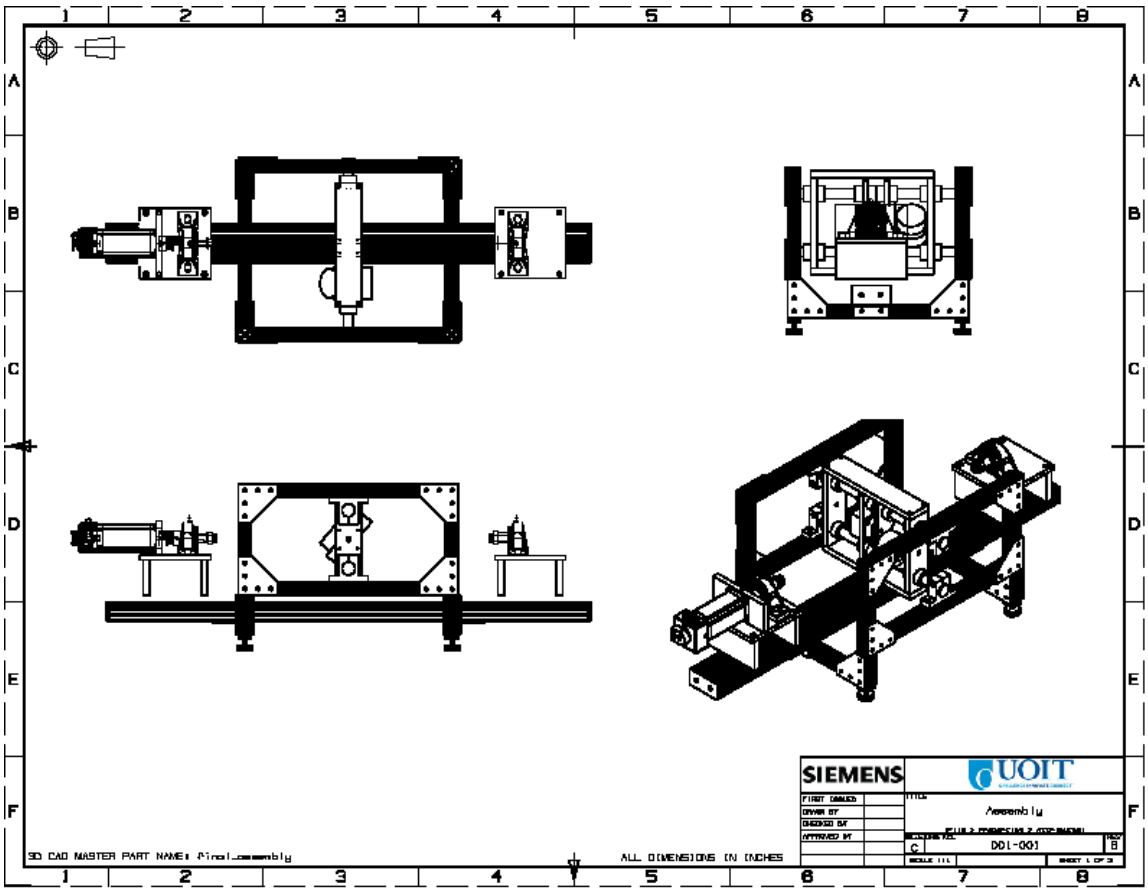

Figure A.3.1: Assembly drawing

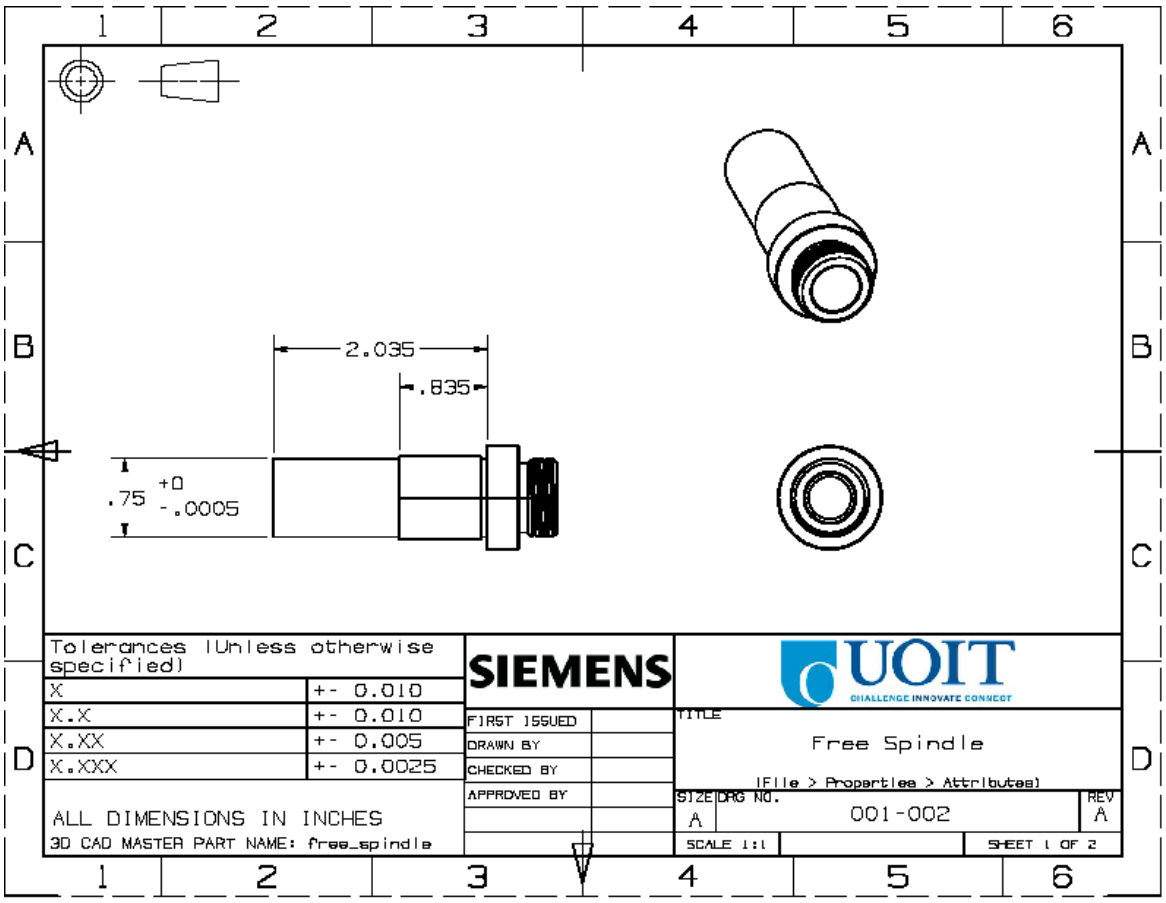

Figure A.3.2: Free Spindle drawing (Modified from Sherline Products part number 40230)

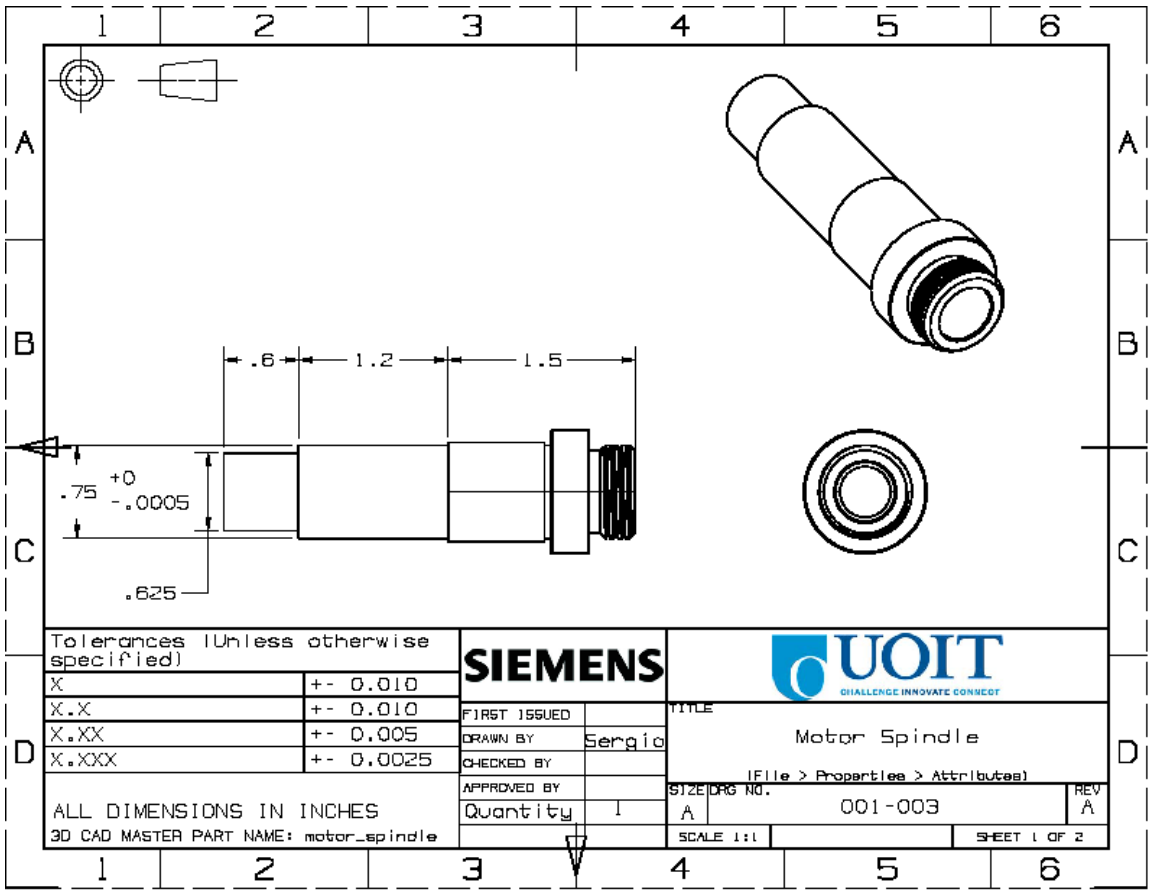

Figure A.3.3: Motor Spindle drawing (Modified from Sherline Products part number 40230)

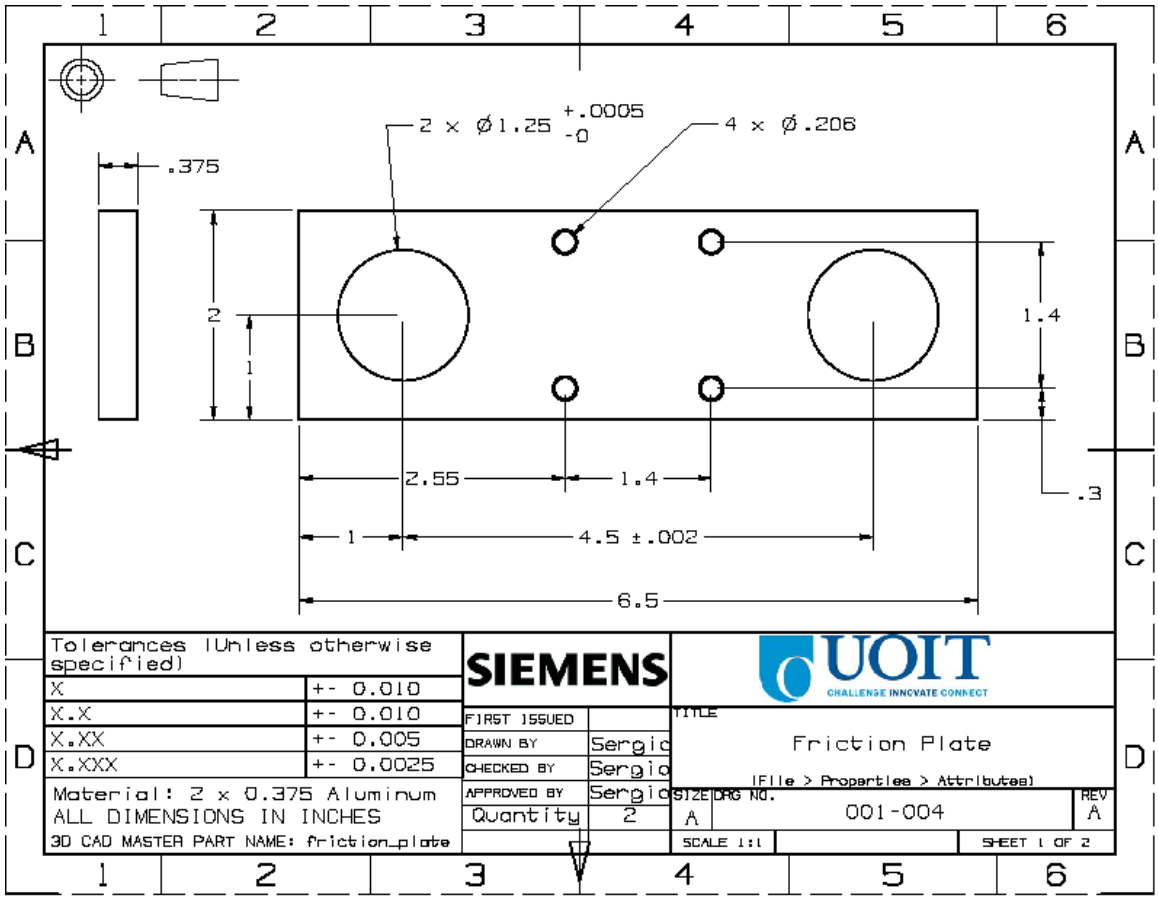

Figure A.3.4: Friction Plate drawing

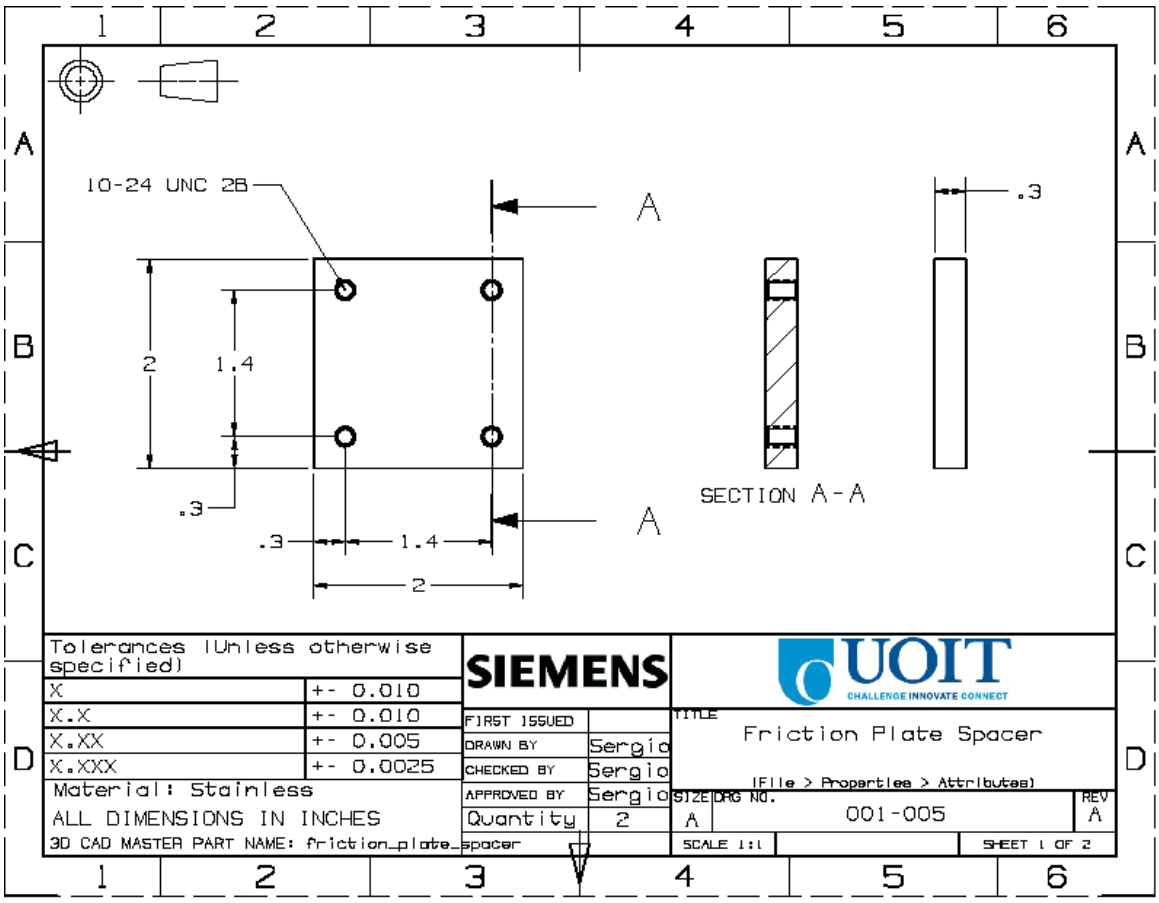

Figure A.3.5: Friction Plate Spacer drawing

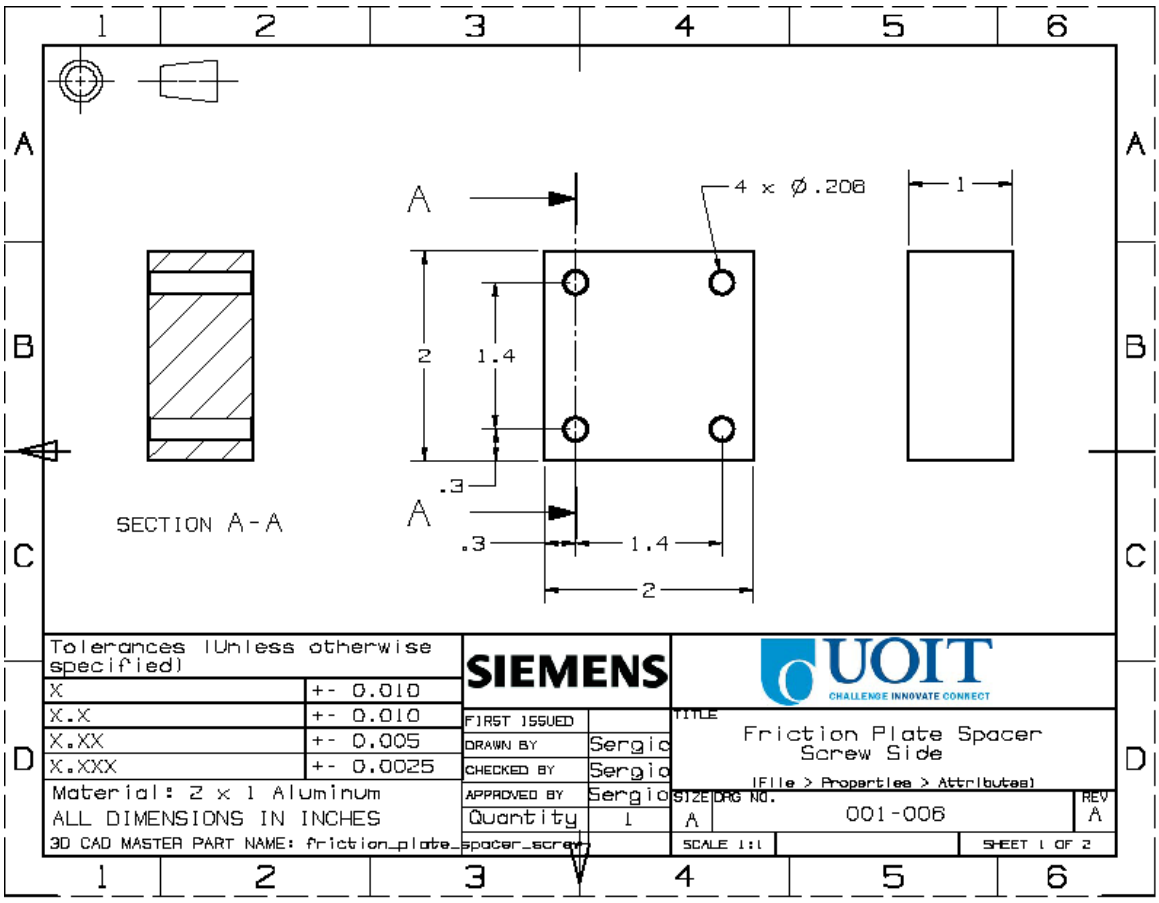

Figure A.3.6: Friction Plate Spacer Screw Side drawing

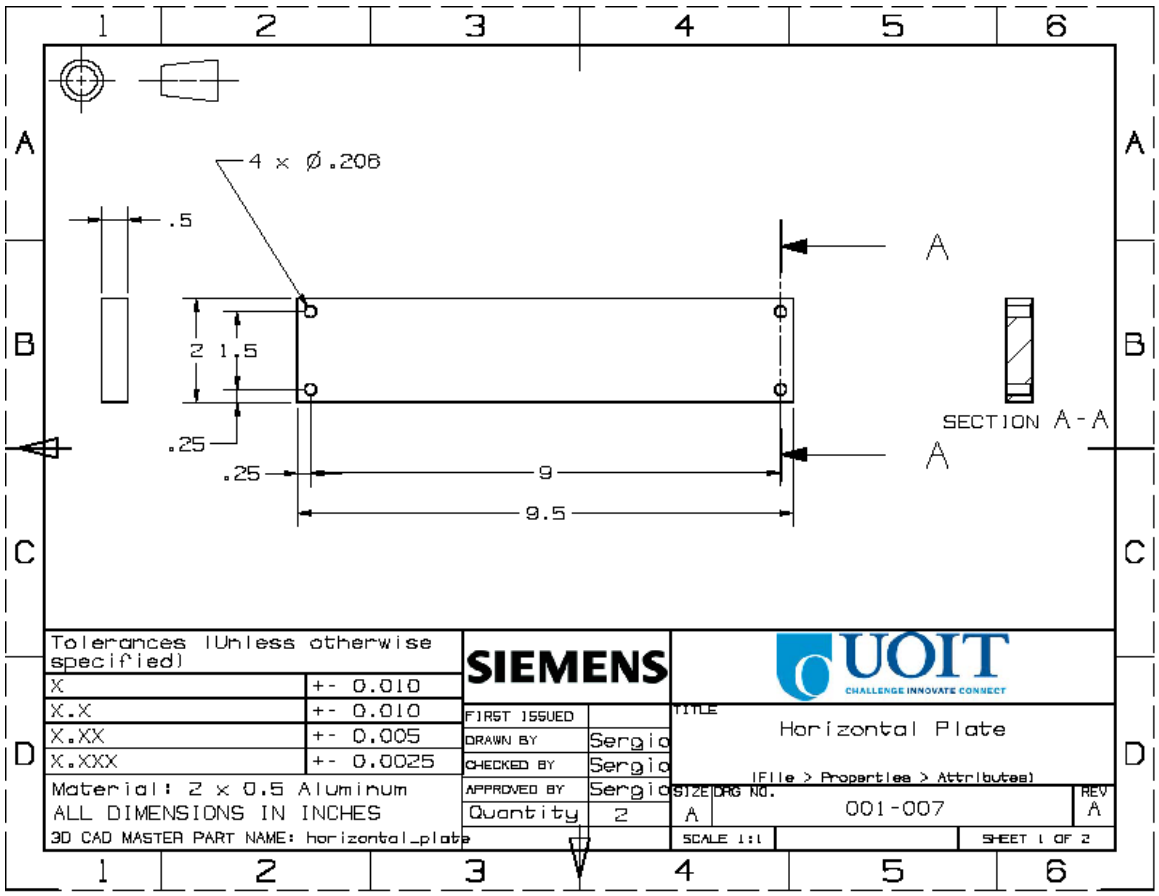

Figure A.3.7: Horizontal Plate drawing

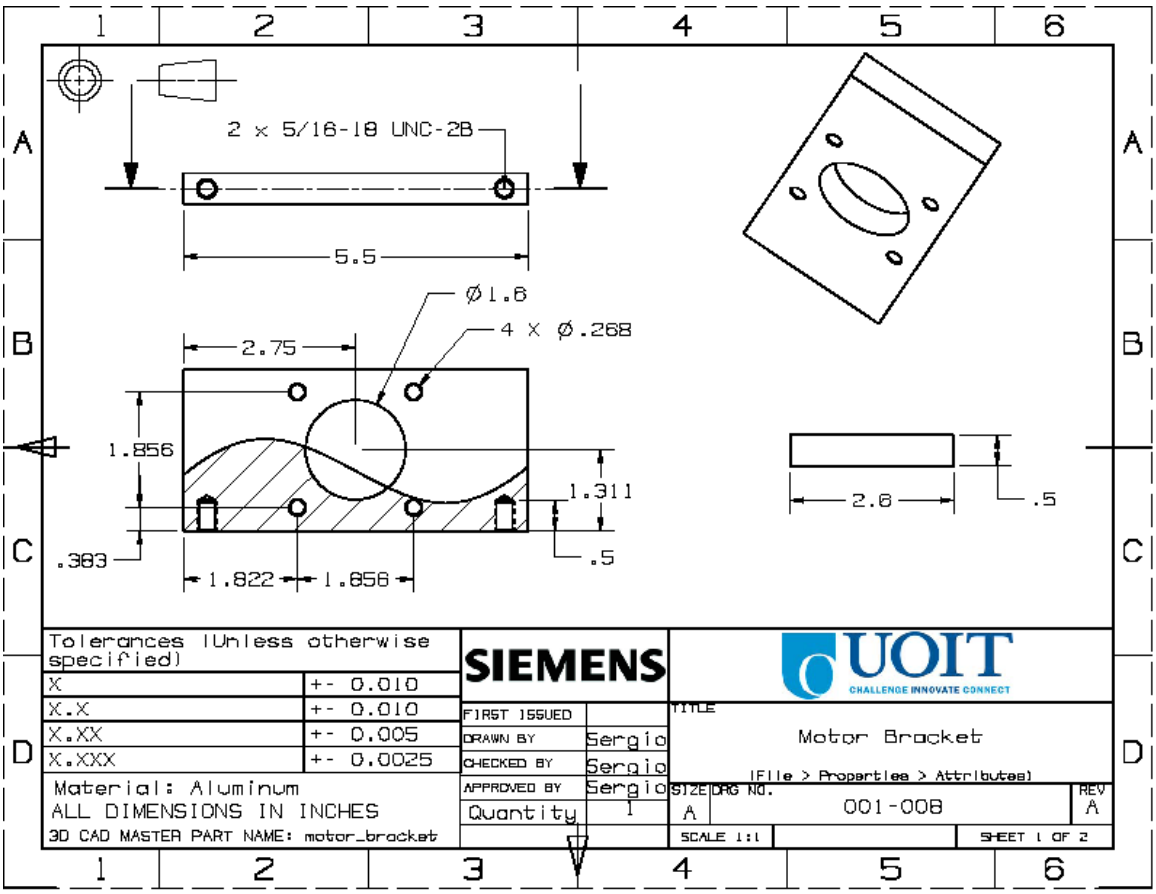

Figure A.3.8: Motor Bracket Drawing

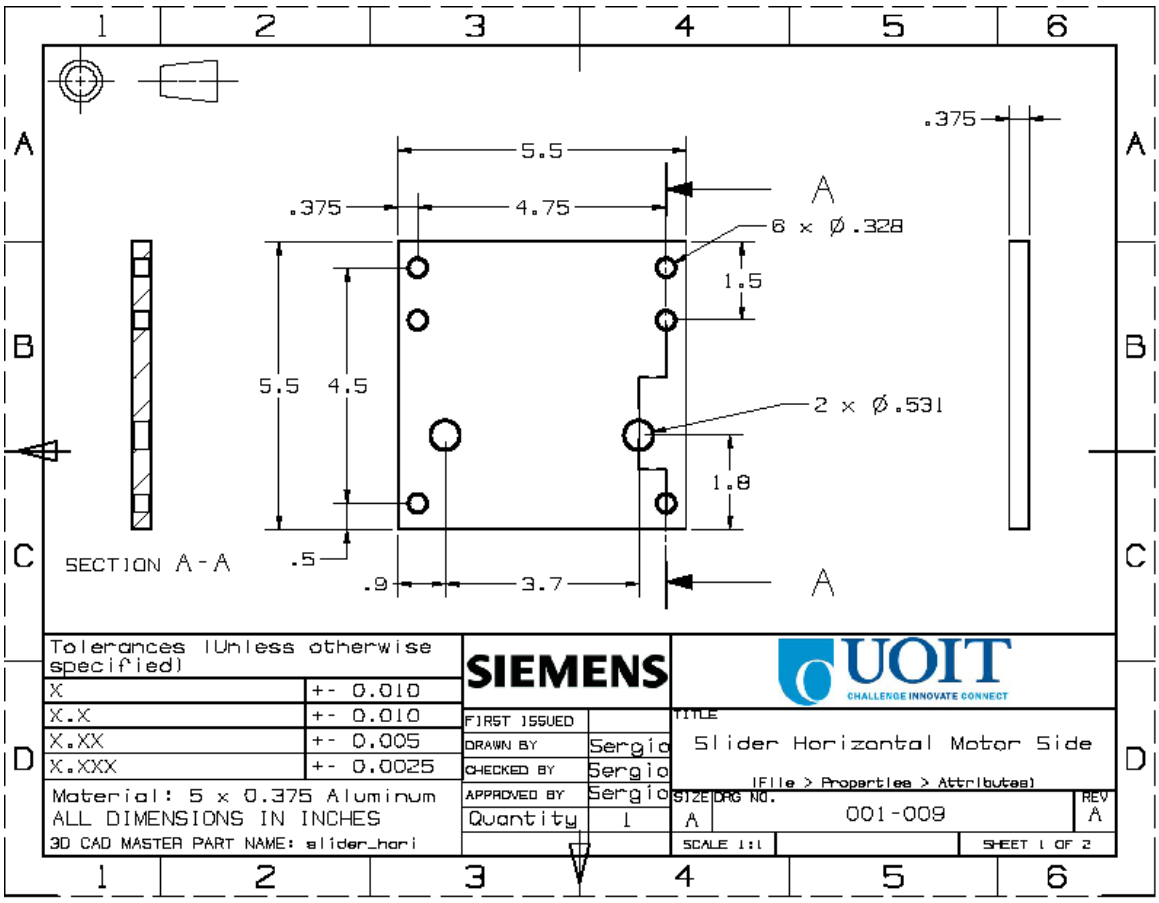

Figure A.3.9: Slider Horizontal Motor Side drawing

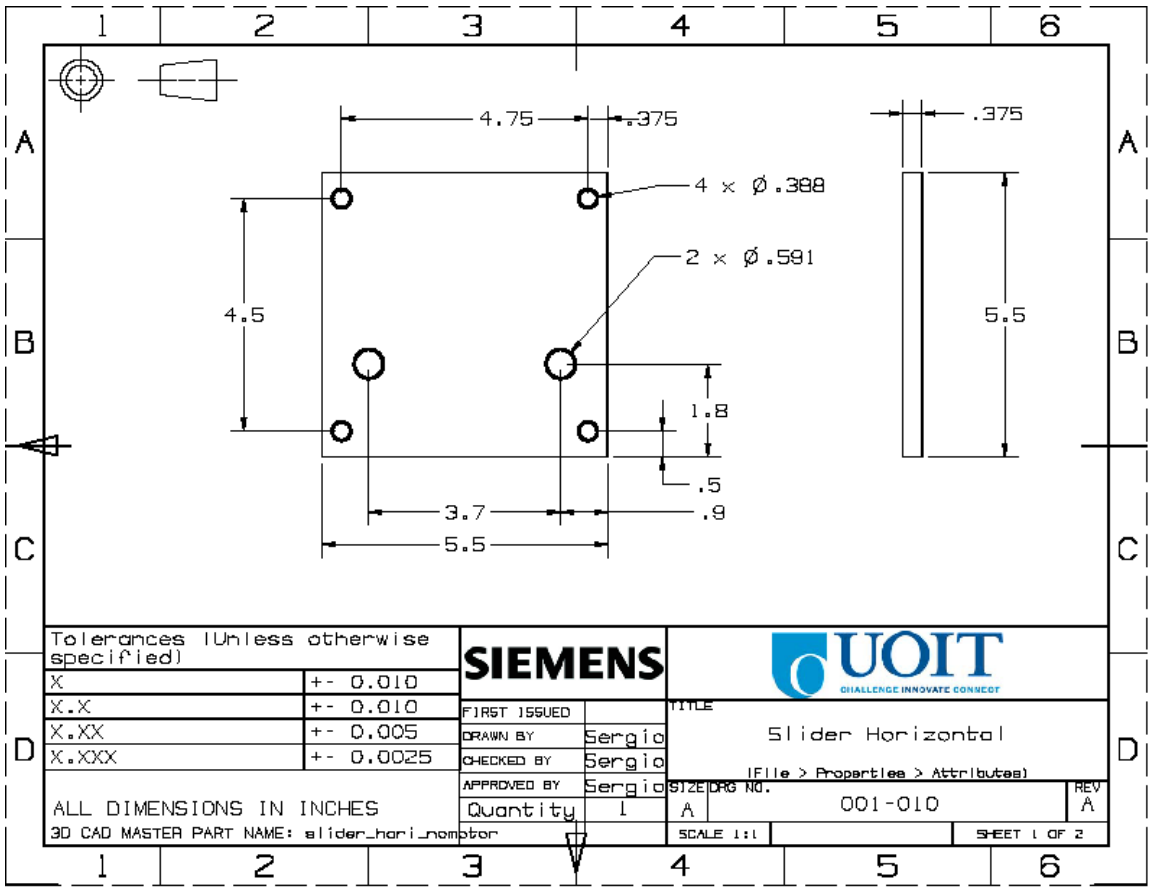

Figure A.3.10: Slider Horizontal drawing

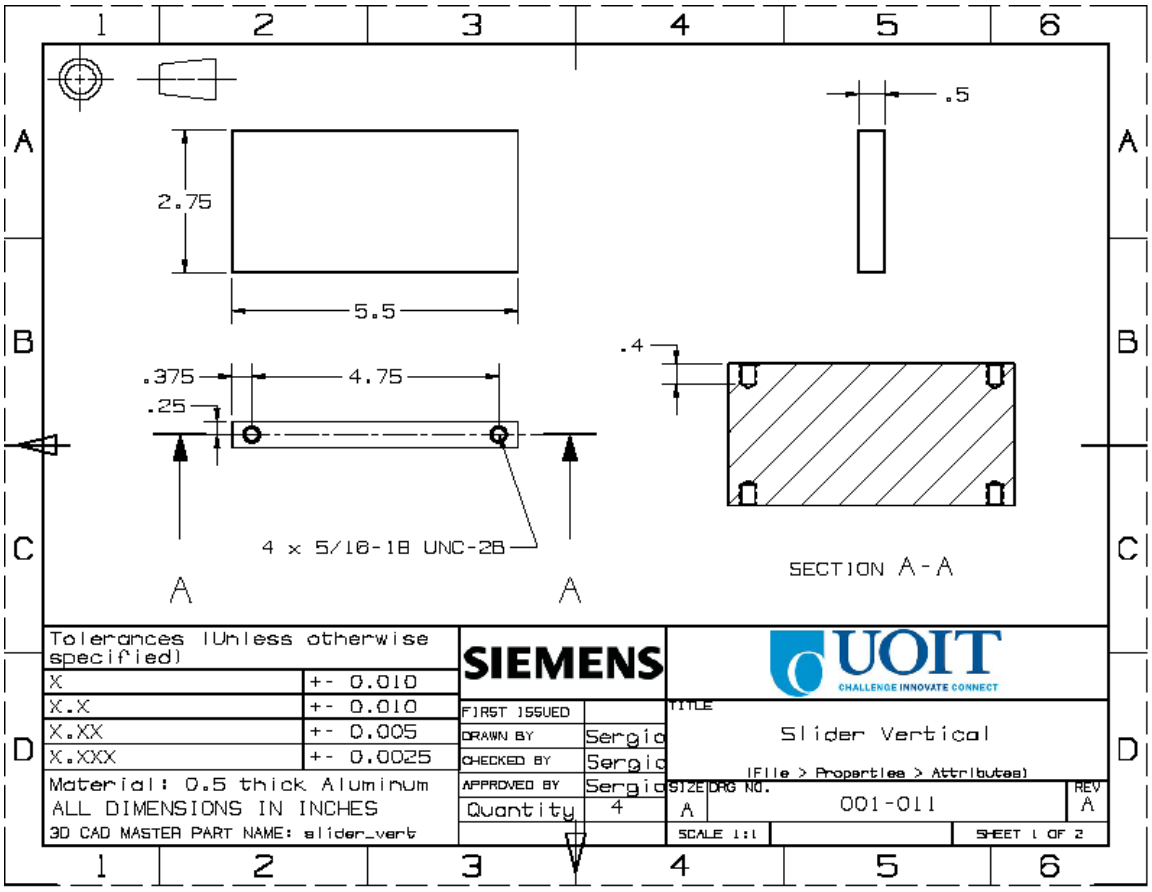

Figure A.3.11: Slider Vertical drawing

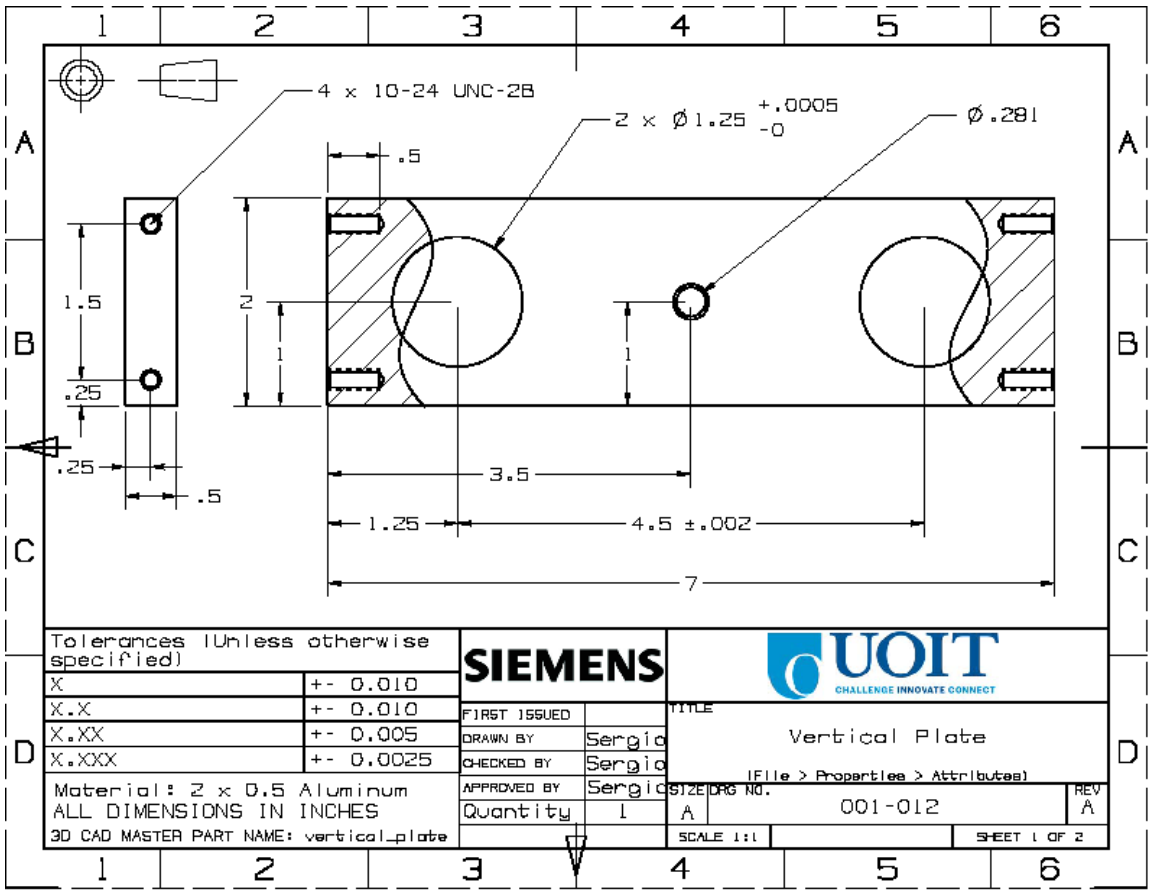

Figure A.3.12: Vertical Plate drawing

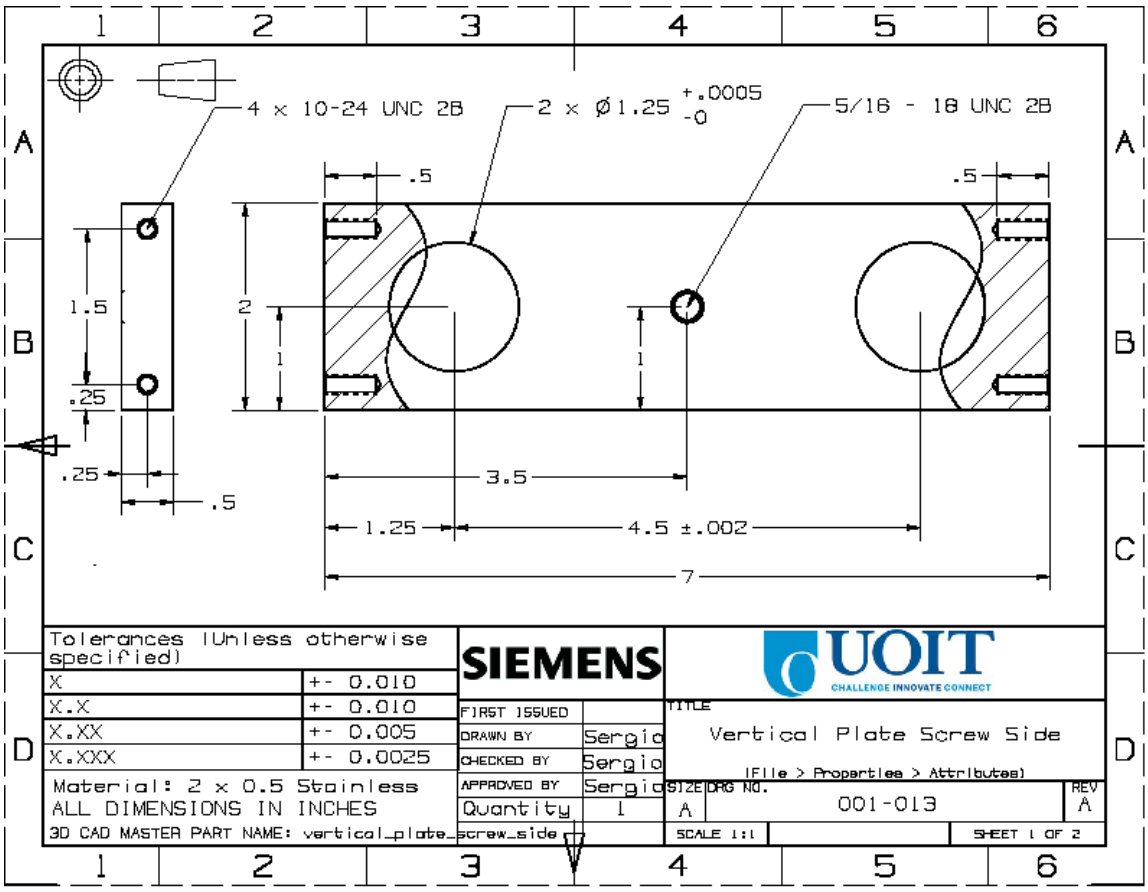

Figure A.3.13: Vertical Plate Screw Side drawing

Appendix 4: Study of the Effect of Substrate on 3D Surface Roughness in Diamond-Like-Carbon Coating Process

Sergio Mordo*, Valery Popravko**
Ahmad Barari***

*Faculty of Engineering and Applied Science, University of Ontario Institute of Technology, Oshawa, Canada (email: sergio.mordo@uoit.ca)
** Intellectual Alliance Inc., Toronto, Canada, (email: valery.popravko@intcan.com)
*** Faculty of Engineering and Applied Science, University of Ontario Institute of Technology, Oshawa, Canada (email: ahmad.barari@uoit.ca)

Abstract: This paper presents an experimental platform which is used to study the effect of Diamond-Like-Carbon (DLC) coating on surface roughness. Variety of experiments is conducted and the effect of variation of the coating process parameters and type and combination of sub-layers on the surface roughness of the coated part is discussed. It is shown how DLC coating can decrease the surface roughness and the amount of decrease has direct relationship with the coating thickness. It is shown that with a thick enough coating, approximately the same surface roughness results can be obtained from surfaces with different uncoated roughness. This observation can be used to minimize the manufacturing costs of the parts that are going to be DLC-coated.

Keywords: Surface texture, Diamond-Like-Carbon Coating, DLC, Surface Roughness, 3D Surface Metrology

1. INTRODUCTION

Diamond like carbon (DLC) is a thin film made from amorphous carbon with high concentration of sp3 carbon bonds. This type of coating has many applications due to its surface properties such as low coefficient of friction and roughness, high hardness and chemical inertness produced in manufactured parts. Various types of DLC coatings exist that are created by different methods and materials in order to achieve different tribological properties. These types include amorphous carbon (a-C), hydrogenated amorphous carbon (a-C:H), amorphous carbon nitride (a-C:N), fluorinated amorphous carbon (a-C:F), tetrahedral amorphous carbon (ta-C), hydrogenated tetrahedral amorphous carbon (ta-C:H) and some other more specialized varieties and alloys. These films are usually made by deposition of highly energetic ions onto the surface of a work piece. Some deposition methods are magnetron sputtering, chemical vapour deposition (CVD), physical vapour deposition (PVD), dielectric barrier discharge(DBD), and pulsed cathodic arc discharge (PCAD).

The specimens used in this research were prepared by physical vapour deposition using ion beam technology. Ti, TiN and TiCN sub-layers were created using magnetron sputtering and then the specimens were coated with DLC by using an ion beam and acetylene gas. Creation of sub-layers is also possible by using chromium (Cr) or titanium aluminum alloy (TiAl). A schematic of the process and some controls can be seen in figure 1. Firstly, a vacuum is created in the chamber by opening lock 1 only with the use of for vacuum and mechanical pump. In the meantime, diffusion pump is also activated. In order to speed this process, lock 2 can be opened and closed. Once the pressures equalize, lock 1 is closed and lock 2 and 3 open to use all three pumps to create a good vacuum. After this, argon cleaning is done on the specimens by supplying argon gas through the ion beam to clean any unwanted particles. Next, a thin titanium coating is done by magnetron sputtering, followed by TiN coating with inclusion of nitrogen gas and TiCN with inclusion of acetylene. Once the sub layers are done, acetylene gas is supplied from the ion beam for DLC coating. Simply, carbon atoms in acetylene gas are ionized by the ion beam and then they are accelerated towards the specimen in a vacuum by a magnetic field. When these ionized carbon atoms hit the surface of the specimen, they form sp3 and sp2 bonds on the surface. Due to the hydrogen content in acetylene gas, some hydrogen atoms also hit the surface and create bonds. In order to minimize the amount of weak hydrogen to carbon bonds, acetylene gas is used as it has lowest possible carbon to hydrogen ratio. Gavrilov et al. (2010) also stated that acetylene is most suitable choice for DLC deposition.

DLC coating has many properties that can be used for different applications; however, the main focus of this paper is the effect of DLC coating on the surface roughness of workpiece. There is a big industrial demand for improving surface roughness on a wide variety of parts and components. For cutting, milling and punching tools that are used for cutting aluminium alloys, graphite, printed circuit boards (PCB), and plastics or punching through steel sheets DLC coating increases hardness and wear resistance. This results

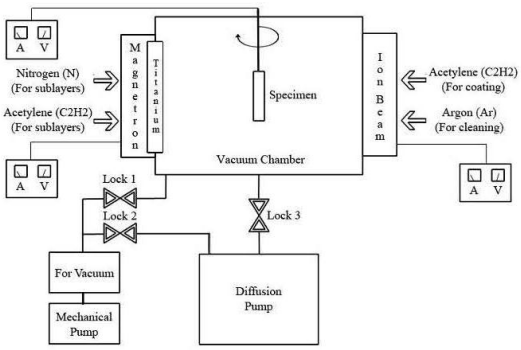

Fig. 1. Schematic of the coating apparatus.

in improving tools' life for up to 20 times longer. Longer tool life result is desired for the manufacturing processes due to saving in tool cost and the required tool set up times. Also, DLC decreases coefficient of friction of the coated surface by decreasing roughness on the cutting tools, requiring less lubricant fluid and lower operation temperatures. Due to this property the quality of the machined surface is also increased. For cold rolling tools, many common problems such as galling on mating surfaces, rolled-in scale, mill-sharing, scrabs and slivers are eliminated, resulting in better quality of end product. The maintenance interval is also increased 4 to 5 times, reducing costs. DLC is also highly suitable for the flow control devices, check and stop valves used in oil and gas industries. By reduced roughness and coefficient of friction, mating parts have trouble-free operations, without the problem of adhesion of mating parts. Also DLC creates corrosion and chemical resistance due to inert surfaces. For dies, molds and extruders that are coated with DLC, due to low friction and roughness, molds operate smoothly with no jamming and also parts get released from molds and dies more easily. DLC coating also increases the life of the molds, dies and extruders. For the automotive industry, use of DLC makes it possible to have higher efficiency, reduced maintenance and therefore, reduced energy and power demand. Camshafts, crankshafts, pistons, valves, differential and gear box components can all be coated. DLC is also applicable to any mechanical part such as shafts, bearings, bushings where it can raise efficiency, allow simplified designs and improve wear resistance. Figure 2 demonstrates some typical mechanical parts coated by DLC process.

The goal of this research is to understand how DLC coating can affect the 3D surface roughness of the coated surface. Using an experimental approach and actual measurement of the resulting surface effect of DLC coating parameters and the employed sub-layers on the three-dimensional surface roughness parameters is studied.

2. LITERATURE REVIEW

Significant research has been conducted to study the effect of DLC coating on the tribological properties of parts and tools. There are two types of studies regarding the roughness of DLC coated parts, one type focuses on the effect of DLC

Fig. 2. Some DLC coated parts and tools.

coating and sub-layers on roughness of the part's surfaces, and the other type focuses on the effect of roughness on the properties related to the use of the part.

In terms of effect of DLC on surface roughness, Sui et al. (2006) stated that DLC coating decreases roughness of NiTi alloy. Saha et al. (2011) showed that nitrogen flow-rate increases roughness on Si:DLC:N parts. Liu et al. (2003) also demonstrated the same concept. Salvadori et al. (2006) showed that increasing DLC thickness first creates a slight increase in roughness and then starts to decrease it as the coating gets thicker. This is explained in their paper by the fact that DLC coating first starts to build up around the sharp edges due to the intensity of their magnetic fields and as the coating gets thicker, the gaps also start to fill up and that is when the roughness starts to decrease. Huang et al. (2004) also showed the same concept of decreasing surface roughness with increased coating thickness. Liu et al. (2006) showed that increasing the bias voltage results in decreasing of surface roughness.

In terms of effect on roughness on the properties of the part, Park et al. (2005) stated that increasing roughness results in decreased environmental reaction. Huang et al. (2004) showed that decreased surface roughness resulted in increased scratch resistance.

3. EXPERIMENTAL PLATFORM

There are many commercially available methods for measuring surface roughness. They can generally be divided into two categories of contact and non-contact methods. An example for contact method is the mechanical stylus method which has a resolution typically between 2 to 5 μm. (Xu and Hu, 2009). Due to some disadvantages of the Contact methods the non-contact methods have been developed and significantly improved in recent years. Some examples include atomic force microscopy (AFM), interference microscopy, vertical scanning interferometry, Confocal microscopy, and scattering modelling (Xu and Hu, 2009). In this research, a non-contact method is used by implementing a microscope with camera and sensor provided by

PhaseView™. The developed software was used for taking stacked images from the surface and for combining them to create 3D images and data of the surface. By using this data, it will be easy to calculate the required 3D roughness surface parameters as described in Table 1 based on the Geometrical product specifications (GPS) provided in ISO 25178-2:2012 standard (ISO 25178-2, 2012). The resolution of the system was 0.091 µm which. A total of 20 measurements were done on each specimen of which 10 were taken before coating and 10 were taken after applying coating on the surface of the parts. A stratified-random sampling approach was used for sampling (Barari et al. 2007). The measurement points were selected randomly from the stratified regions of the surface. All surface roughness parameters including the average 3D surface roughness values (*Sa*) explained in Table 1 are calculated. Various specimens were used with different initial surface finishes to observe the effects of DLC. Three 3D images of surfaces with relatively low, average and high surface roughness can be seen in Figures 3 through 5 as examples of the observations.

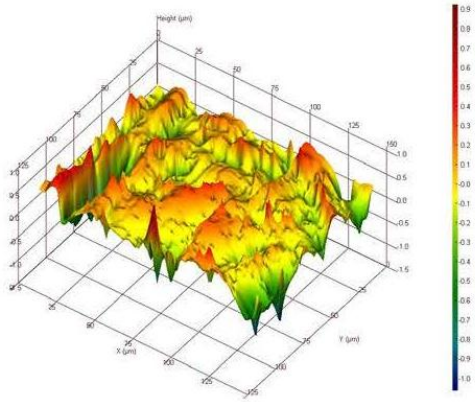

Fig. 3. Example of a surface with relatively low surface roughness. (0.141 µm)

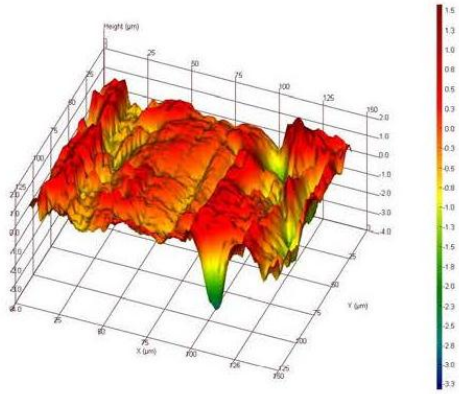

Fig. 4. Example of a surface with relatively average surface roughness. (0.335 µm)

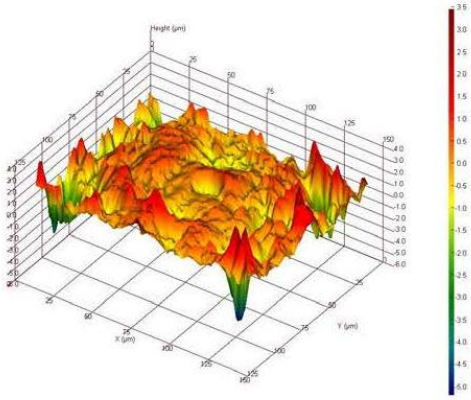

Fig. 5. Example of a surface with relatively high surface roughness. (0.552 µm)

Table 1. 3D Surface roughness parameters

Parameters	Name	Definition	Comments
Sa	Average Roughness	$S_a = \frac{1}{MN}\sum_{m=1}^{M}\sum_{n=1}^{N}\lvert z_{mn} - \bar{z}\rvert$	Average distance to mean
Sq	Root-mean-square roughness	$S_q = \sqrt{\frac{1}{MN}\sum_{m=1}^{M}\sum_{n=1}^{N}(z_{mn} - \bar{z})^2}$	Standard deviation of the surface
Ssk	Skewness	$S_{sk} = \frac{1}{MNS_q}\sum_{m=1}^{M}\sum_{n=1}^{N}(z_{mn} - \bar{z})^3$	Asymetry of the height distribution. Rsk<0 for a surface with holes, Rsk>0 for a surface with peaks.
Sku	Kurtosis	$S_{ku} = \frac{1}{MNS_q^4}\sum_{m=1}^{M}\sum_{n=1}^{N}(z_{mn} - \bar{z})^4$	Width of the height distribution. Rku=3.0 corresponds to Gaussian distribution
Sv	Valley depth	$S_v = \lvert\min(z_{mn})\rvert$	Depth of deepest valley
Sp	Peak height	$S_p = \lvert\max(z_{mn})\rvert$	Height of highest peak
St	Total roughness	$S_t = S_v + S_p$	Distance from the deepest valley to the highest peak, evaluated over entire surface
Sz	Averaged total roughness	$S_z = \langle S_v + S_p \rangle_{eval.surf}$	Distance from the deepest valley to the highest peak evaluated over base surface and averaged

4. RESULTS

The results of measurements and the calculated 3D roughness parameters are listed in Table 2. Sequential coating of first Ti, then TiN, then TiCN, and finally DLC was applied on all the specimens that were tested. A total of 7 samples were analyzed. The 7th sample was selected to have two kinds of geometries, one flat and one round, with different uncoated surface roughness values, in order to see the effect of initial surface roughness on the final surface. Sample 1 was only coated with TiN sub-layers for studying the effect of nitrogen content on roughness.

Samples 2 and 3 were coated until the 3rd sub-layer, which is TiCN, to see how the carbon content affects roughness. Samples 4 through 7 were all coated with DLC. As can be seen in Table 2, it is possible to obtain all the 3D surface roughness parameters with this measuring method. For the scope of this study, only the average 3D surface roughness (*Sa*) was compared between the samples. The reason for not using the other parameters is to avoid the effect of some impurities on the surface from the machining process, such as some local holes on the original surface. For example if the total roughness (*St*) value was used, the holes that are not produced by the DLC process were going to increase the calculated roughness of a coated surface. Using the average roughness minimizes this effect. In order to have a better comparison of the observations, the 10 *Sa* values were averaged as the major roughness indicating value for coated or uncoated analysis of each sample. The results can be seen in the graph presented in Figure 6. The grey columns represent the uncoated surfaces, sample one (yellow column) represents TiN coating, Samples 2 and 3 (purple columns) represent TiCN coating, and the rest of samples (black columns) represent DLC coating.

Table 2. Experimental Data

		Sample 1	Sample 2	Sample 3	Sample 4	Sample 5	Sample 6	Sample 7 (Flat)	Sample 7 (Round)
3D roughness parameters before coating	Sa (µm)	0.2729	0.4875	0.3834	0.384	0.3845	0.4223	0.2939	0.3688
	Sq (µm)	0.3844	0.6965	0.5345	0.5396	0.5704	0.5826	0.4645	0.5513
	Ssk	-0.9125	-0.59923	-0.8694	-0.49116	-0.5569	-0.29615	-1.478	-0.15821
	Sku	9.082	7.854	7.319	9.591	12.142	7.143	21.266	12.595
	Sv (µm)	-2.999	-4.182	-3.669	-3.987	-4.702	-3.875	-4.936	-4.412
	Sp (µm)	2.533	3.765	2.995	3.728	4.106	3.47	3.635	4.795
	St (µm)	5.532	7.949	6.666	7.718	8.807	7.347	8.571	9.206
	Sz (µm)	1.805	2.689	2.393	2.409	2.596	2.814	1.8512	3.001
	Sds (summits /mm2)	32375.43	35938.66	32265.57	19550.88	25558.64	30675.48	23275.24	13504.22
	Sdr (%)	1.1195	2.762	2.115	2.167	2.179	2.985	1.3098	0.69725
	Sci	1.009	1.052	1.05517	0.75787	1.0766	1.19862	0.5271	1.11213
3D roughness parameters after coating	Sa (µm)	0.3448	0.3619	0.2434	0.3433	0.2739	0.2578	0.1835	0.1609
	Sq (µm)	0.4816	0.4876	0.3291	0.4836	0.3772	0.3679	0.2871	0.2204
	Ssk	-0.8513	-0.2346	-0.57915	-0.55309	-0.52677	-1.0984	-0.7872	-0.7551
	Sku	6.736	4.849	5.496	7.133	5.984	10.826	14.441	6.441
	Sv (µm)	-3.062	-2.481	-1.813	-3.168	-2.0999	-2.9	-2.774	-1.5637
	Sp (µm)	2.112	2.312	1.389	2.592	1.7575	1.975	2.307	1.1609
	St (µm)	5.175	4.792	3.202	5.763	3.858	4.874	5.076	2.724
	Sz (µm)	2.017	2.065	1.354	2.237	1.5821	1.724	1.773	1.0915
	Sds (summits /mm2)	31900.28	41393.95	27231.28	19091.84	26391.56	21927.05	3701.605	15986.47
	Sdr (%)	1.5186	1.939	0.635	1.747	1.072	1.041	0.203784	0.4388
	Sci	1.075	1.1097	1.318	1.298	1.205	0.8927	0.687	1.071

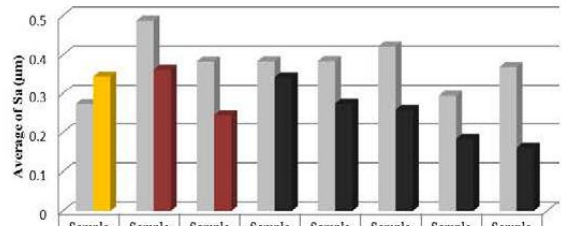

	Sample 1	Sample 2	Sample 3	Sample 4	Sample 5	Sample 6	Sample 7 (Flat)	Sample 7 (Round)
Uncoated	0.2729	0.4875	0.3834	0.384	0.3845	0.4223	0.2939	0.3688
Coated	0.3448	0.3619	0.2434	0.3433	0.2739	0.2578	0.1835	0.1609

Fig. 6. 3D average surface roughness values of samples. The grey columns represent the uncoated surfaces, sample one represents TiN coating, Samples 2 and 3 represent TiCN coating, and the rest of samples represent DLC coating.

The change in surface roughness values of each sample are summarized in Table 3. Estimation of the coating thickness, including sub-layers and DLC coating are also shown, in order to see the effect of thickness of the coatings on roughness. The coating thickness is estimated by considering the growth rate of the coating based on the process parameters and the actual measured coating time.

Table 3: Coating time and change in roughness

Sample	Total coating thickness (µm)	Percent change in average roughness (Sa)
1	0.5	26.3% increase
2	0.5	25.8% decrease
3	0.5	36.5% decrease
4	0.8	10.6% decrease
5	1.2	37.1% decrease
6	1.2	39% decrease
7 (Flat)	2	37.57% decrease
7 (Round)	2	56.4% decrease

5. DISCUSSION

In the light of the results that were presented in the previous section, it can be stated that DLC coating reduces the roughness of a surface by 30% in average. By looking at the results, the main criteria for the amount of reduction in roughness is found to be the thickness of the DLC coating, or similarly, the time that DLC coating is applied on the specimen. It can be seen in Table 3 that when the estimated DLC thickness is only 0.8 µm, only 10.6% decrease in roughness observed; whereas with an estimated DLC coating thickness of 2 µm, the reduction reached 56.4%. This proved the studies that have been done before by Salvadori et al. (2006) and Huang et al. (2004) on the relation with DLC and roughness with different roughness measurement methods.

Apart from the effect of DLC coating on roughness of the surface, the sub-layers were also found do have effect on the properties of the final surface. Sample 1, which was coated with only TiN sub-layer, although, creates good adhesion for the following carbon atoms, showed a 26.3% increase in roughness compared to the original part. However, samples 2 and 3 that which were coated with TiCN had 25.8% and 36.5% decrease on roughness respectively. This showed that the nitrogen content in the coating resulted in a rougher surface, but when carbon content starts to increase, the roughness started to decrease. This proved the studies done by Saha et al. (2011) and Liu et al. (2003) on different types of metals and with different coating methods and surface roughness measurement methods. This also demonstrates that no matter what coating method is used, nitrogen content increases surface roughness.

The last discussion of this study is the effect of the original surface roughness on the final roughness properties. Sample 7 was the best example for showing this effect. This sample, as discussed in the earlier sections, had two different types of surfaces, one flat surface and one round surface, with different initial roughness values. The flat surface had an uncoated roughness of 0.2939 µm and after coating, this value decreased to 0.1835 µm. On the other hand, the round surface had an uncoated surface roughness of 0.3688 µm which decreased to 0.1609 µm after the coating process. This change is visualized in figure 7. As can be seen from the figure, even though the uncoated roughness values are different, the coated roughness values are approximately the same. The slight difference is found to be caused by the different rate of roughness change on surfaces with different roughness values. This showed that with a coating that is thick enough, approximately same surface roughness can be obtained in parts with different uncoated surface roughness values. Based on this observation, it can be concluded that if a part is going to be coated with DLC, in order to reduce manufacturing costs and time, some finishing processes such as grinding and polishing can be reduced or even eliminated.

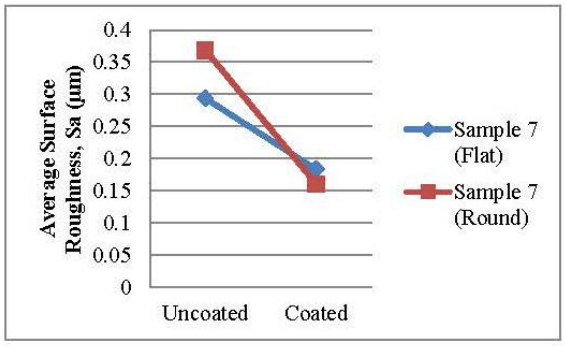

Fig. 7. Reduction in surface roughness of sample 7 with different uncoated surface roughness values.

6. CONCLUSION

The following conclusions can be made based on the findings of this study;

I. DLC coating decreases the surface roughness, and the amount of decrease on surface roughness depends on the thickness of the coating.

II. The nitrogen content in the coating increases the surface roughness, but is a crucial sub layer for the strong adhesion of the DLC coating.

III. No matter what the uncoated surface roughness is, with a thick enough DLC coating, the coated surface roughness values can be approximately the same. This means that expensive and time consuming manufacturing processes for surface finishing such as grinding and polishing can be reduced or even eliminated if the part will go through DLC coating.

7. ACKNOWLEDGEMENTS

The research support provided by the Federal Economic Development Agency for Southern Ontario (FedDev Ontario) and Natural Science and Engineering Research Council of Canada (NSERC) is greatly appreciated.

8. REFERENCES

Barari, A., ElMaraghy, H. A. and Knopf, G. K. (2007) Search- Guided sampling to reduce uncertainty of minimum zone estimation. *Journal of Computing and Information Science in Engineering,* 7(4), 360-371

Gavrilov, N.V., Mamaev, A.S., Plotnikov, S.A., et al. (2010). Comparison testing of diamond-like a-C:H coatings prepared in plasma cathode-based gas discharge and ta-C coatings deposited by vacuum arc. *Surface & coatings technology, 204, 4018-4024.*

Huang, L., Lu, J. and Xu, K. (2003). Investigation of the relation between structure and mechanical properties of hydrogenated diamond-like carbon coatings prepared by PECVD. *Materials science and engineering,* A (373), 45-53.

ISO 25178-2 (2012), Geometrical product specifications (GPS) - Surface texture: Areal -- Part 2: Terms, definitions and surface texture parameters

Liu, D., Benstetter, G., Lodermeier, E. et al. (2003). SPM investigation of diamond-like carbon and carbon nitride films. *Surface and coating technology,* 172, 194-203.

Liu, D., Liu, Y. and Chen, B. (2006). Surface roughness of various diamond-like carbon films. *Plasma science and technology,* 8 (6), 701-707.

Park, S.J., Lee, K.R. and Ko, D.H. (2005). Tribological behaviour of nano-undulated surface of diamond-like carbon films. *Diamond and related materials, 14, 1291-1296.*

Saha, B., Liu, E., Tor, S.B. et al. (2011). Modification of surface properties of silicon micro-molds by nitrogen and silicon doped diamond-like carbon deposited with magnetron co-sputtering. *Vacuum,* 85, 1105-1107.

Salvadori, M.C., Martins, D.R. and Cattani, M. (2006). DLC coating roughness as a function of film thickness. *Surface coatings technology,* 200, 5119-5122.

Sui, J.H., Cai, W., Liu, L.H., et al. (2006). Surface characteristics and electrochemical corrosion behaviour of NiTi coated with diamond-like carbon. *Materials science and engineering,* A (438), 639-642.

Xu, X. and Hu, H. (2009). Development of non-contact surface roughness measurement in last decades. *2009 International conference on measuring technology and mechatronics automation.* Zhangjiajie, Hunan, China 11-12 April 2009. Piscataway, NJ, USA: IEEE.